Stimuli-Responsive Triblock Copolymer Hydrogels for Extrusion-Based Additive Manufacturing

Christopher Fellin

A dissertation

submitted in partial fulfillment of the

requirements for the degree of

Doctor of Philosophy

University of Washington

2021

Reading Committee:

Alshakim Nelson, Chair

Forrest Michael

Christine Luscombe

Program Authorized to Offer Degree:

Department of Chemistry

University of Washington

Abstract

Stimuli-Responsive Triblock Copolymer Hydrogels for Extrusion-Based Additive Manufacturing

Christopher Fellin

Chair of the Supervisory Committee:

Dr. Alshakim Nelson

Department of Chemistry

Additive manufacturing (AM) is a rapidly expanding field that has revolutionized a number of diverse fields including medicine, construction, aerospace, and robotics. The hardware of AM has seen a dramatic improvement over the years, and there currently exists a vast array of technologies with unique advantages for different applications. Extrusion-based printers, specifically direct-ink write (DIW), are one such AM technology that has seen extensive use due to its relatively low cost and fast print speeds. Despite the rapid growth of AM, research has mostly focused on the

adaptation of existing materials for AM applications- leaving material development lagging behind. This has provided an opportunity for materials scientists and engineers to develop novel materials specifically designed for AM applications. Hydrogels are one class of materials that has garnered significant attention for DIW AM. These soft materials mimic the extracellular matrices of cellular environments and have seen extensive use as cell laden inks for 3D bioprinting. Stimuli-responsive hydrogels respond to environmental cues, enabling both effective printing and providing post-print functionality. This thesis focuses on the development of a multi-stimuli-responsive hydrogel platform based on poly(alkyl glycidyl ether) triblock copolymers. Chapter 1 includes an overview of the field of AM and stimuli-responsive hydrogels for extrusion-based AM. Chapter 2 describes the development of the initial temperature- and shear- responsive triblock copolymer hydrogel platform. Chapter 3 further expands this platform through the photo-chemical crosslinking of the hydrogel network and its implementation for the additive manufacturing of catalytically active living materials (AMCALM). Lastly, Chapter 4 continues to advance the functionality the platform through the addition of thiol-reactive monomers for post-functionalization of the hydrogel material.

TABLE OF CONTENTS

LIST OF FIGURES

LIST OF TABLES

LIST OF SCHEMES

ACKNOWLEDGEMENTS

First and foremost, I would also like to thank my graduate advisor, Dr. Alshakim Nelson. You have been a pillar of support and encouragement throughout my years as a graduate student. Your guidance has helped mold me into the scientist I am today. You allowed me to explore my own interests and intuitions, while always providing the necessary grounding to bring me back down to earth. I could not have asked for a better mentor and boss- supportive without being overbearing and hands-off without being unavailable. When the time comes for me to assume the role of mentor, I will strive for the best with you in mind.

Additionally, I could not have done this without the supportive collaboration of the entire Nelson lab. Dylan and Ryan, you were integral to my transition into graduate school, and I always appreciated your patience and willingness to answer any and all questions that popped into my head. Trevor and Amrita, you are the best of lab friends, and I could not have made it through without you. Jenn you have become such a good friend over the last few months, and I know you will do great things. And Pat- we came into grad school together, we lived together, and now we leave together. Cheers.

I would like to thank my committee members Dr. Forrest Michael, Dr. Christine Luscombe, and Dr. Cole DeForest for their support as well as collaborators Dr. Eric Seibel, Dr. Len Nelson, and Shawn Swanson. Working with the UnTape team has been a highlight of my graduate school career and I am blessed to have had the opportunity.

To all my amazing friends: none of this would be possible without you. Some of you I have known for years, others I have only met recently. Ben, Andrew, Trevor, Camille, Ashley, Sarah,

Azra, Maire, Claire, Jarred, all of my friends from home and many many more. All of you helped make my graduate school experience one to remember. Whether it's late-night chemistry socials, learning how to salsa dance, or arguing about fantasy football at 2 in the morning, I will always cherish our experiences together. And a special, special shoutout to Cece Martin. You have made the past six months truly unforgettable.

Last but *definitely* not least, I would like to thank my family. Mom, Dad, Bryan, Eric, and Amanda, this would not be possible without your constant friendship and support. You are the best family I could ask for and I would not be the man I am today without you. Thanks for always giving me a safe place to come home to. Here's to more Fellin family vacations, Harry Potter marathons, and ice cream deserts.

CHAPTER 1: **INTRODUCTION**

1.1 INTRODUCTION TO ADDITIVE MANUFACTURING

Additive manufacturing (AM), also known as 3D printing, is a relatively recent manufacturing technique that utilizes a layer-by-layer process to build complex three-dimensional objects.[1–3] This is in contrast to more traditional subtractive processes where material is removed from a bulk object until the final shape is obtained. AM is advantageous in a number of ways including the ability to rapidly manufacture custom designed prototypes,[4] lower costs and minimal waste,[5] and enhanced object complexity.[6]

There are three main components to additive manufacturing: Software, hardware, and materials. Software programs such as OpenSCAD and Fusion 360 facilitate the development of computer-aided design (CAD) files that create the virtual image of the final printed object. From here, the CAD files are transferred to a printer (the hardware) and the additive manufacturing process begins. The ASTM Standard has identified seven main AM printer technologies: binder jetting, directed energy deposition, material extrusion, material jetting, powder bed fusion, sheet lamination, and vat photopolymerization (Figure 1.1).[7,8] Each technology is unique and suitable for their own targeted applications. Two of the most common printing techniques for polymeric soft materials are material extrusion and vat photopolymerization. Extrusion-based printers such as Fused-Deposition Modeling (FDM) and Direct-Ink Write (DIW) eject material through a nozzle and gradually build the object through layer-by-layer deposition. Vat-photopolymerization methods such as Stereolithography (SLA) and Digital Light Processing (DLP) utilize a light source to selectively cure a photopolymerizable resin until the final print is obtained. Extrusion-based printers are typically cheaper, less time consuming, and offer straightforward opportunities for

multi-material prints.[9] Meanwhile, vat-photopolymerization methods can achieve much better resolution prints but are typically more expensive and time consuming than their extrusion-based counterparts.[10,11] AM hardware is an incredibly innovative field that continues to push the boundaries of AM implementation into ever expanding commercial and academic applications.

The last component of AM is the material used to construct the printed object. Historically, engineers have developed inks by applying existing materials to the field of AM. Engineers have adapted all sorts of common materials such as metals, ceramics, and plastics towards this end.[12] Poly(lactic acid), or PLA, is an excellent example of this phenomenon- first discovered in 1932 and commonly used to manufacture plastic films, bottles, and medical devices, PLA has become one of the most common materials for FDM printing due to its relatively low melting point (130-180 °C) and ease of printing.[13] While this was an adequate approach during the early days of AM, it no longer serves as a suitable model for the development of novel AM inks because many existing materials do not meet the unique rheological requirements necessary for effective printing.[9] Over the past few decades, research has begun to specialize in the development of materials explicitly designed for AM applications.

1.2 Hydrogel Inks for DIW AM

Hydrogels— three dimensional networks of macromolecules held together by chemical or physical crosslinks— are one class of material that has garnered significant research interest for AM applications. These materials have carved out a niche role as cell-laden inks in 3D bioprinting due to their inherently high water content and their ability to replicate some of the chemical and physical attributes of extracellular matrices.[14–16] This has led to groundbreaking advancements in the fields of tissue engineering[17–22] and immobilized-cell bioreactors.[23–25]

The viscoelastic nature of hydrogel materials makes them excellent candidates for extrusion-based AM. For DIW methods, researchers have identified three key viscoelastic parameters that help describe the relative printability of hydrogel inks; viscosity (η),[26] yield stress (σ),[27–30] and tan δ.[31] Ideally, hydrogel inks will possess some form of variable viscosity in order to properly eject from the printhead nozzle.[32,33] This requirement is typically met via shear-thinning behavior wherein the viscosity of the material decreases as shear force increases. These materials are proposed to undergo a "plug-flow" extrusion as the material travels through the high shear environment of the printhead nozzle.[34,35]

Many hydrogel inks are derived from naturally occurring biopolymers such as alginate,[36] gelatin,[37] and chitosan,[38] among others. These materials are advantageous insofar as they are biocompatible, chemically versatile, and inherently functional.[39] However, most biologically derived hydrogels are quite difficult to print and face significant engineering hurdles in order to effectively achieve proper print conditions. Some may require a heating jacket or a cooling bed or must be crosslinked immediately after printing each layer in order to avoid deformation.[40–43] Others require the combination of multiple materials in order to achieve suitable printing properties.[44–46] Synthetic polymers on the other hand, can be specifically designed for AM due to their inherent compositional and architectural control.

1.3 Triblock Copolymer Hydrogels for DIW AM

Our group is interested in developing synthetic triblock copolymer hydrogels for DIW AM. Triblock copolymers are an advantageous platform for hydrogel inks because they can be synthetically designed to exhibit two key stimuli-responsive features necessary for efficient extrusion-based AM: a sol-gel temperature response and shear-thinning behavior. A sol-gel temperature response— wherein the material exists as a non-viscous solution at low temperatures

(5 °C) but returns to its gel morphology at elevated temperatures (25 °C)— allows for homogenization of additives such as cells or drugs and facile loading of the hydrogel ink in the liquid state. Meanwhile, shear-thinning behavior facilitates the extrusion of the material as rod-like filaments and the formation of 3D printed objects.

One of the most utilized hydrogels for DIW methods is an ABA triblock copolymer composed of a central, temperature-responsive poly(propylene oxide) (PPO) 'B' block and two flanking, hydrophilic poly(ethylene oxide) (PEO) 'A' blocks known as Pluronic F127. The hydrophobic nature of the PPO block at ambient temperatures leads to aggregation of the polymer in order to reduce the surface area of the PPO block exposed to the aqueous environment.[47–49] Polymers of this compositional architecture, i.e. central temperature-responsive and flanking hydrophilic blocks, create spherical micelles.[50,51] As the concentration of the polymer increases, the material transitions from a dilute solution of individual micelles into a packed hydrogel network of micelles, held together by weak van der waals forces in a body-centered cubic arrangement. Because these micelles are only held together by physical, transient crosslinks, the material will yield under stress as the network becomes temporarily disrupted.[48,49,52] This manifests itself at the macroscopic level as a shear-thinning behavior. Under ambient conditions, the material exists as a free-standing gel, but upon exposure to shear force the viscosity of the material drops and it begins to flow.

Pluronic F127 hydrogels also demonstrate a sol-gel temperature response. This behavior is governed by a phenomenon unique to amphiphilic polymers known as a lower critical solution temperature, or LCST. Generally, the solubility of a polymer in aqueous solutions is determined by the free energy of mixing, or ΔG_{mix}, as seen in equation 1.1.

Equation 1.1 $\Delta G_{mix} = \Delta H_{mix} - T\Delta S_{mix}$

The hydrophilic regions of the polymer enthalpically favor a mixed state (negative ΔH_{mix}) due to hydrogen bonding between these domains and water molecules. At the same time, it is entropically unfavorable (negative ΔS_{mix}) for water to solvate the PPO block due to the hydrophobic effect.[53–55] This balance between an enthalpically favored mixed state, and an entropically favored demixed state, leads to a temperature dependent solubility. At low temperatures, the enthalpic forces control the system, the ΔG_{mix} is negative, and the polymer is fully solvated. As temperature increases, the positive total entropy change ($-T\Delta S_{mix}$) dominates the system, ΔG_{mix} becomes positive, and phase separation occurs.[56,57] This can be observed macroscopically for F127 by a change in the viscoelastic properties of the material with temperature. At elevated temperatures (25-37 °C), the polymer chains aggregate due to the LCST-like behavior of the polymer and the materials exists in the hydrogel state. However, upon exposure to low temperature environments (5 °C), the material assumes a liquid morphology as solvation of the polymer becomes favorable.

Wang and coworkers developed a similar temperature- and shear- responsive triblock polymer hydrogel by utilizing the LCST behavior of poly(*N*-isopropyl acrylamide)- or PNIPAm.[58] Compared to F127, this polymer possesses the inverse compositional architecture; temperature responsive (PNIPAm) 'A' blocks and a central hydrophilic (PEO) 'B' block. Because the temperature responsive blocks are located at the ends of the polymer chains, they self-assemble to form flower-like micelles. This architecture leads to a number of different macro and nanoscale properties. Instead of relying solely on micelle packing to induce hydrogel formation, these polymers bridge individual micelles and require pull-out of the polymer chains to disrupt the

hydrogel network, leading to differences in viscoelasticity and gel formation.[50,51] Additionally, this architectural design positions the ends of the polymer in the central, hydrophobic segment of the micelle. This is contrary to Pluronic F127 micelles, where the chain ends are located on the hydrophilic portion of the polymer and are exposed to aqueous environments. Wang and coworkers took advantage of this property by attaching the hydrogen bonding moiety ureido pyrimidinone (UPy) to the ends of the polymer chains. These polymers self-assemble upon an increase in temperature as the PNIPAm chains dehydrate, creating micelles and a hydrophobic microenvironment for the UPy groups to hydrogen bond together. Thus, the hydrogel is crosslinked both by the hydrophobic association of the PNIPAm chains and by dimerization of the UPy moieties induced by hydrogen bonding. This triblock copolymer hydrogel proved to be extrudable (shear-thinning), self-healable, thermo-reversible, and injectable.

Poly(alkyl glycidyl ethers) are another class of temperature-responsive polymers that have recently been incorporated into triblock copolymer hydrogels. Watanabe and coworkers first investigated the LCST behavior of various poly(alkyl glycidyl ether) homopolymers.[59] Methyl, ethyl, and ethoxy ethyl glycidyl ether monomers were polymerized using anionic ring opening polymerization (AROP) methods and the LCST of the resulting polymers were determined via cloud point measurement. In dilute solutions (1 wt%) and low temperatures, amphiphilic homopolymers exist as fully solvated coils. As the temperature increases and the ΔG_{mix} becomes positive, the polymer chains phase separate completely into hydrophobic globules (Figure 1.2).[7,53,55,56]

This phase separation behavior can be observed and quantified as the cloud point temperature (T_{cp}) using UV-Vis spectroscopy to monitor a change in absorbance values. Watanabe and coworkers correlated increasing T_{cp} with a decrease in hydrophobicity of the polymer side

chains i.e. poly(methyl glycidyl ether) > poly(ethoxy ethyl glycidyl ether) > poly(ethyl glycidyl ether). Nelson and coworkers exploited the temperature dependent behavior of poly(alkyl glycidyl ether)s to develop a novel triblock copolymer platform for DIW AM.[60] Similar to the design by Wang and coworkers, these triblocks contained a central PEO hydrophilic block, and two temperature-responsive poly(isopropyl glycidyl ether) 'A' blocks. The resulting triblock copolymer was capable of forming thermo-reversible, shear-thinning hydrogels that were utilized as inks for DIW AM.

The temperature- and shear- thinning response of these triblock copolymer hydrogels make them ideal inks for DIW AM; the sol-gel temperature response allows for facile loading and the dispersion of additives in the liquid state while the shear-thinning response facilitates the formation of hydrogel filaments. However, the same property that enable these behaviors, i.e. the physical crosslinking of polymer chains, make them poor hydrogels for many post-print applications. The shear response that facilitates extrusion also leaves the printed constructs vulnerable to deformation, with objects often unable to withstand physical touch. Additionally, these polymers will tend to become diluted over time in aqueous media, leading to dissolution of the hydrogel over short periods of time. This leaves the hydrogel unsuitable for biomedical applications such as tissue engineering, where the printed construct must be submerged in media in order to sustain cell growth and proliferation.

With this in mind, Nelson and coworkers developed a modified Pluronic F127 based hydrogel that enabled post-print curing of the printed structure in order to create a robust hydrogel able to withstand dissolution and deformation.[29,61] In this work, Pluronic F127 was functionalized with methacrylate end groups- a common moiety used in free radical polymerizations. The resulting hydrogel retained both the temperature- and shear- responsive properties that enable

loading and extrusion of the material. Upon exposure to 365 nm UV-light, the modified polymer could undergo photo-chemical crosslinking induced by free radical polymerization of the methacrylate end groups. The physical, transient polymer crosslinks became permanent, chemical ones, leading to a much more robust material. This platform was utilized in a number of biomedical applications including the tissue engineering of 3D printed vascular tubes and the creation of immobilized cell bioreactors.[62–64]

1.4 Developing Stimuli-Responsive Functional Hydrogels for DIW AM

Additive manufacturing also opens the door for the incorporation of functional materials as 3D printed constructs, although the field of triblock copolymer hydrogels has not been thoroughly investigated in this regard. These hydrogels respond to environmental stimuli such as temperature, pH, or small molecules *after* printing, enabling tunable control over behaviors such as swelling and drug release. A great example of this technique was demonstrated by Gracias and coworkers, who developed a dual-gel platform for the 4D printing of bioinspired constructs.[65] By alternating segmental patterns of a temperature responsive PNIPAm hydrogel and an inert polyacrylamide (PAAM) hydrogel, this group was able to take advantage of the differential swelling behavior of each layer to create a range of multi-functional shape-changing structures. Meanwhile, Magdassi and coworkers developed a pH responsive hydrogel for DLP AM.[66] The hydrogel was formulated using an acrylic acid monomer, a poly(ethylene glycol) diacrylate crosslinker, and TPO nanoparticles. Complex three-dimensional objects were printed and demonstrated pH responsive swelling. Sulforhodamine B, a pH independent fluorescent dye, was used to model a small molecule hydrophilic drug. These materials can be utilized to enable drug delivery at specific locations throughout the body where local pH is more basic. Recent work by Howon Lee uses a light responsive hydrogel and multi-material microstereolithography to develop

cephalopod inspired artificial chromatophores.[67] Polydopamine nanoparticles, a common photothermal agent, were incorporated into a PNIPAm hydrogel matrix to induce light-driven contraction as the temperature of the material heats above its LCST. This behavior yielding printed objects capable of individual and independent light sensing and actuation. Lastly, Sanyal and coworkers demonstrated an elegant technique for the modular "catch and release" of proteins and cells using a small molecule sensitive hydrogel.[68] Pyridyl disulfide methacrylate was incorporated into a hydrogel network by copolymerization with poly(ethylene oxide) methyl ether methacrylate and a PEO based crosslinker. The pyridyl disulfide handle is capable of effectively and reversibly conjugating thiol-containing molecules and biomolecules, lending thiol reactive properties to the resulting hydrogel. Micropatterned hydrogel interfaces were fabricated and used to reversibly conjugate, or catch, biomolecules and cells onto their surfaces. These conjugated bonds could be subsequently cleaved, or released, in the presence of dithiothreitol (DTT). Successful conjugation of a biotin containing ligand enabled selective binding of the protein extravidin even in the presence of other proteins such as bovine serum albumin. By conjugating the cell binding protein RGD to the hydrogel surface, the group was able to successfully demonstrate facile cellular attachment with high levels of cell viability (Figure 1.3).

1.5 CONCLUSION

The following chapters will discuss the design and development of a multi-stimuli responsive triblock copolymer hydrogel for DIW AM. Chapter 2 investigates how the structure of the triblock copolymer impacts the temperature- and shear- responsive properties of the hydrogel. Chapter 3 builds on this platform by modifying the polymer with reactive methacrylate chain ends, enabling post-print photo-chemical crosslinking and the adaptation of this platform for the additive manufacturing of catalytically active living materials. Finally, chapter 4 incorporates pyridyl

disulfide monomers into a multi-stimuli responsive hydrogel network for the post-functionalization of 3D printed objects.

1.6 REFERENCES

(1) Tofail, S. A. M.; Koumoulos, E. P.; Bandyopadhyay, A.; Bose, S.; O'Donoghue, L.; Charitidis, C. Additive Manufacturing: Scientific and Technological Challenges, Market Uptake and Opportunities. *Mater. Today* **2018**, *21* (1), 22–37.

(2) Wong, K. V; Hernandez, A. A Review of Additive Manufacturing. *ISRN Mech. Eng.* **2012**, *2012*, 1–10.

(3) Collan, M.; Michelsen, K.-E. Technical , Economic and Societal Effects of Manufacturing 4.0 Automation, Adaption, and Manufacturing in Finland and Beyond; 2020; pp 1–263.

(4) Negi, S.; Dhiman, S.; Sharma, R. K. Basics and Applications of Rapid Prototyping Medical Models. *Rapid Prototyp. J.* **2014**, *20* (3), 256–267.

(5) Huang, R.; Riddle, M.; Graziano, D.; Warren, J.; Das, S.; Nimbalkar, S.; Cresko, J.; Masanet, E. Energy and Emissions Saving Potential of Additive Manufacturing: The Case of Lightweight Aircraft Components. *J. Clean. Prod.* **2016**, *135*, 1559–1570.

(6) Bandyopadhyay, A.; Gualtieri, T.; Bose, S. Global Engineering and Additive Manufacturing. In *Additive Manufacturing*; CRC Press, 2015; pp 1–18.

(7) Zhang, Q.; Weber, C.; Schubert, U. S.; Hoogenboom, R. Thermoresponsive Polymers with Lower Critical Solution Temperature: From Fundamental Aspects and Measuring Techniques to Recommended Turbidimetry Conditions. *Mater. Horizons* **2017**, *4*, 109–116.

(8) ASTM F2792-12a. *Standard Terminology for Additive Manufacturing Technologies*; ASTM International: West Conshohocken, PA, 2013.

(9) Jiang, Z.; Diggle, B.; Tan, M. L.; Viktorova, J.; Bennett, C. W.; Connal, L. A. Extrusion 3D Printing of Polymeric Materials with Advanced Properties. *Adv. Sci.* **2020**, *7* (17).

(10) Appuhamillage, G. A.; Chartrain, N.; Meenakshisundaram, V.; Feller, K. D.; Williams, C. B.; Long, T. E. 110th Anniversary: Vat Photopolymerization-Based Additive Manufacturing: Current Trends and Future Directions in Materials Design. *Ind. Eng. Chem. Res.* **2019**, *58* (33), 15109–15118.

(11) Pagac, M.; Hajnys, J.; Ma, Q. P.; Jancar, L.; Jansa, J.; Stefek, P.; Mesicek, J. A Review of Vat Photopolymerization Technology: Materials, Applications, Challenges, and Future Trends of 3d Printing. *Polymers (Basel).* **2021**, *13* (4), 1–20.

(12) Ngo, T. D.; Kashani, A.; Imbalzano, G.; Nguyen, K. T. Q.; Hui, D. Additive Manufacturing (3D Printing): A Review of Materials, Methods, Applications and

Challenges. *Compos. Part B Eng.* **2018**, *143*, 172–196.

(13) Baran, E.; Erbil, H. Surface Modification of 3D Printed PLA Objects by Fused Deposition Modeling: A Review. *Colloids and Interfaces* **2019**, *3* (2), 43.

(14) Lee, K. Y.; Mooney, D. J. Hydrogels for Tissue Engineering. *Chem. Rev.* **2001**, *101* (7), 1869–1879.

(15) Hoffman, A. S. Hydrogels for Biomedical Applications. *Adv. Drug Deliv. Rev.* **2002**, *54* (1), 3–12.

(16) Lee, J. M.; Yeong, W. Y. Design and Printing Strategies in 3D Bioprinting of Cell-Hydrogels: A Review. *Adv. Healthc. Mater.* **2016**, *5* (22), 2856–2865.

(17) Jia, W.; Gungor-Ozkerim, P. S.; Zhang, Y. S.; Yue, K.; Zhu, K.; Liu, W.; Pi, Q.; Byambaa, B.; Dokmeci, M. R.; Shin, S. R.; Khademhosseini, A. Direct 3D Bioprinting of Perfusable Vascular Constructs Using a Blend Bioink. *Biomaterials* **2016**, *106*, 58–68.

(18) Laronda, M. M.; Rutz, A. L.; Xiao, S.; Whelan, K. A.; Duncan, F. E.; Roth, E. W.; Woodruff, T. K.; Shah, R. N. A Bioprosthetic Ovary Created Using 3D Printed Microporous Scaffolds Restores Ovarian Function in Sterilized Mice. *Nat. Commun.* **2017**, *8* (1), 1–10.

(19) Huang, J.; Fu, H.; Wang, Z.; Meng, Q.; Liu, S.; Wang, H.; Zheng, X.; Dai, J.; Zhang, Z. BMSCs-Laden Gelatin/Sodium Alginate/Carboxymethyl Chitosan Hydrogel for 3D Bioprinting. *RSC Adv.* **2016**, *6* (110), 108423–108430.

(20) Rhee, S.; Puetzer, J. L.; Mason, B. N.; Reinhart-King, C. A.; Bonassar, L. J. 3D Bioprinting of Spatially Heterogeneous Collagen Constructs for Cartilage Tissue Engineering. *ACS Biomater. Sci. Eng.* **2016**, *2* (10), 1800–1805.

(21) Markstedt, K.; Mantas, A.; Tournier, I.; Martínez Ávila, H.; Hägg, D.; Gatenholm, P. 3D Bioprinting Human Chondrocytes with Nanocellulose-Alginate Bioink for Cartilage Tissue Engineering Applications. *Biomacromolecules* **2015**, *16* (5), 1489–1496.

(22) Axpe, E.; Oyen, M. L. Applications of Alginate-Based Bioinks in 3D Bioprinting. *Int. J. Mol. Sci.* **2016**, *17* (12), 1976.

(23) Gona, R. S.; Meyer, A. S. Engineered Proteins and Three-Dimensional Printing of Living Materials. *MRS Bull.* **2020**, *45* (12), 1034–1038.

(24) Johnston, T. G.; Yuan, S. F.; Wagner, J. M.; Yi, X.; Saha, A.; Smith, P.; Nelson, A.; Alper, H. S. Compartmentalized Microbes and Co-Cultures in Hydrogels for on-Demand Bioproduction and Preservation. *Nat. Commun.* **2020**, *11* (1), 1–11.

(25) Schaffner, M.; Rühs, P. A.; Coulter, F.; Kilcher, S.; Studart, A. R. 3D Printing of Bacteria into Functional Complex Materials. *Sci. Adv.* **2017**, *3* (12), eaao6804.

(26) Rastogi, P.; Kandasubramanian, B. Review of Alginate-Based Hydrogel Bioprinting for Application in Tissue Engineering. *Biofabrication* **2019**, *11* (4).

(27) Mouser, V. H. M.; Melchels, F. P. W.; Visser, J.; Dhert, W. J. A.; Gawlitta, D.; Malda, J. Yield Stress Determines Bioprintability of Hydrogels Based on Gelatin-Methacryloyl and Gellan Gum for Cartilage Bioprinting. *Biofabrication* **2016**, *8* (3).

(28) Paxton, N.; Smolan, W.; Böck, T.; Melchels, F.; Groll, J.; Jungst, T. Proposal to Assess Printability of Bioinks for Extrusion-Based Bioprinting and Evaluation of Rheological Properties Governing Bioprintability. *Biofabrication* **2017**, *9* (4).

(29) Smith, P. T.; Basu, A.; Saha, A.; Nelson, A. Chemical Modification and Printability of Shear-Thinning Hydrogel Inks for Direct-Write 3D Printing. *Polymer (Guildf).* **2018**, *152*, 42–50.

(30) Ribeiro, A.; Blokzijl, M. M.; Levato, R.; Visser, C. W.; Castilho, M.; Hennink, W. E.; Vermonden, T.; Malda, J. Assessing Bioink Shape Fidelity to Aid Material Development in 3D Bioprinting. *Biofabrication* **2018**, *10* (1).

(31) Gao, T.; Gillispie, G. J.; Copus, J. S.; Kumar, A. P. R.; Seol, Y. J.; Atala, A.; Yoo, J. J.; Lee, S. J. Optimization of Gelatin-Alginate Composite Bioink Printability Using Rheological Parameters: A Systematic Approach. *Biofabrication* **2018**, *10* (3), 034106.

(32) Jungst, T.; Smolan, W.; Schacht, K.; Scheibel, T.; Groll, J. Strategies and Molecular Design Criteria for 3D Printable Hydrogels. *Chem. Rev.* **2016**, *116* (3), 1496–1539.

(33) He, Y.; Yang, F.; Zhao, H.; Gao, Q.; Xia, B.; Fu, J. Research on the Printability of Hydrogels in 3D Bioprinting. *Sci. Rep.* **2016**, *6* (1), 1–13.

(34) Kraut, G.; Yenchesky, L.; Prieto, F.; Tovar, G. E. M.; Southan, A. Influence of Shear Thinning and Material Flow on Robotic Dispensing of Poly(Ethylene Glycol) Diacrylate/Poloxamer 407 Hydrogels. *J. Appl. Polym. Sci.* **2017**, *134* (29).

(35) Aktas, S.; Kalyon, D. M.; Marín-Santibáñez, B. M.; Pérez-González, J. Shear Viscosity and Wall Slip Behavior of a Viscoplastic Hydrogel. *J. Rheol. (N. Y. N. Y).* **2014**, *58* (2), 513–535.

(36) Rastogi, P.; Kandasubramanian, B. Review of Alginate-Based Hydrogel Bioprinting for Application in Tissue Engineering. *Biofabrication* **2019**, *11* (4).

(37) Wang, X.; Ao, Q.; Tian, X.; Fan, J.; Tong, H.; Hou, W.; Bai, S. Gelatin-Based Hydrogels for Organ 3D Bioprinting. *Polymers (Basel).* **2017**, *9* (401).

(38) Rajabi, M.; McConnell, M.; Cabral, J.; Ali, M. A. Chitosan Hydrogels in 3D Printing for Biomedical Applications. *Carbohydr. Polym.* **2021**, *260*, 117768.

(39) Li, N.; Qiao, D.; Zhao, S.; Lin, Q.; Zhang, B.; Xie, F. 3D Printing to Innovate Biopolymer Materials for Demanding Applications: A Review. *Mater. Today Chem.* **2021**, *20*, 100459.

(40) Hidaka, M.; Kojima, M.; Nakahata, M.; Sakai, S. Visible Light-Curable Chitosan Ink for Extrusion-Based and Vat Polymerization-Based 3d Bioprintings. *Polymers (Basel).* **2021**, *13* (9).

(41) Fischer, B.; Schulz, A.; Gepp, M. M.; Neubauer, J.; Gentile, L.; Zimmermann, H. 3D Printing of Hydrogels in a Temperature Controlled Environment with High Spatial Resolution. *Curr. Dir. Biomed. Eng.* **2016**, *2* (1), 109–112.

(42) Kalkandelen, C.; Ozbek, B.; Ergul, N. M.; Akyol, S.; Moukbil, Y.; Oktar, F. N.; Ekren, N.; Kilic, O.; Kilic, B.; Gunduz, O. Effect of Temperature, Viscosity and Surface Tension on Gelatine Structures Produced by Modified 3D Printer. In *IOP Conference Series: Materials Science and Engineering*; 2018; Vol. 293, p 12001.

(43) Landers, R.; Pfister, A.; Hübner, U.; John, H.; Schmelzeisen, R.; Mülhaupt, R. Fabrication of Soft Tissue Engineering Scaffolds by Means of Rapid Prototyping Techniques. *J. Mater. Sci.* **2002**, *37* (15), 3107–3116.

(44) Jin, Y.; Chai, W.; Huang, Y. Printability Study of Hydrogel Solution Extrusion in Nanoclay Yield-Stress Bath during Printing-Then-Gelation Biofabrication. *Mater. Sci. Eng. C* **2017**, *80*, 313–325.

(45) Schütz, K.; Placht, A. M.; Paul, B.; Brüggemeier, S.; Gelinsky, M.; Lode, A. Three-Dimensional Plotting of a Cell-Laden Alginate/Methylcellulose Blend: Towards Biofabrication of Tissue Engineering Constructs with Clinically Relevant Dimensions. *J. Tissue Eng. Regen. Med.* **2017**, *11* (5), 1574–1587.

(46) Schuurman, W.; Levett, P. A.; Pot, M. W.; van Weeren, P. R.; Dhert, W. J. A.; Hutmacher, D. W.; Melchels, F. P. W.; Klein, T. J.; Malda, J. Gelatin-Methacrylamide Hydrogels as Potential Biomaterials for Fabrication of Tissue-Engineered Cartilage Constructs. *Macromol. Biosci.* **2013**, *13* (5), 551–561.

(47) Alexandridis, P.; Holzwarth, J. F.; Hatton, T. A. Micellization of Poly(Ethylene Oxide)-Poly(Propylene Oxide)-Poly(Ethylene Oxide) Triblock Copolymers in Aqueous Solutions: Thermodynamics of Copolymer Association. *Macromolecules* **1994**, *27* (9), 2414–2425.

(48) Mortensen, K. Structural Studies of Aqueous Solutions of PEO-PPO-PEO Triblock Copolymers, Their Micellar Aggregates and Mesophases; a Small-Angle Neutron Scattering Study. *J. Phys. Condens. Matter* **1996**, *8* (25), 103–124.

(49) Prud'homme, R. K.; Wu, G.; Schneider, D. K. Structure and Rheology Studies of Poly(Oxyethylene−oxypropylene−oxyethylene) Aqueous Solution. *Langmuir* **1996**, *12*, 4651–4659.

(50) Nguyen-Misra, M.; Mattice, W. L. Micellization and Gelation of Symmetric Triblock Copolymers with Insoluble End Blocks. *Macromolecules* **1995**, *28*, 1444–1457.

(51) Chu, B.; Liu, T.; Wu, C.; Zhou, Z.; Mark Nace, V. Structures and Properties of Block Copolymers in Solution. *Macromol. Symp.* **1997**, *118* (1), 221–227.

(52) Mortensenf, K.; Talmon, Y. Cryo-TEM and SANS Microstructural Study of Pluronic Polymer Solutions. *Macromolecules* **1995**, *28*, 8829–8834.

(53) Chandler, D. Interfaces and the Driving Force of Hydrophobic Assembly. *Nature* **2005**, *437* (7059), 640–647.

(54) Southall, N. T.; Dill, K. A.; Haymet, A. D. J. A View of the Hydrophobic Effect. *J. Phys. Chem. B* **2002**, *106*, 521–533.

(55) Lombardo, D.; Kiselev, M. A.; Magazù, S.; Calandra, P. Amphiphiles Self-Assembly: Basic Concepts and Future Perspectives of Supramolecular Approaches. *Adv. Condens. Matter Phys.* **2015**, *2015*.

(56) Aseyev, V.; Tenhu, H.; Winnik, F. M. Non-Ionic Thermoresponsive Polymers in Water. *Adv. Polym. Sci.* **2011**, *242*, 29–89.

(57) Klouda, L.; Mikos, A. G. Thermoresponsive Hydrogels in Biomedical Applications. *Eur. J. Pharm. Biopharm.* **2008**, *68*, 34–45.

(58) Zhang, G.; Chen, Y.; Deng, Y.; Ngai, T.; Wang, C. Dynamic Supramolecular Hydrogels: Regulating Hydrogel Properties through Self-Complementary Quadruple Hydrogen Bonds and Thermo-Switch. *ACS Macro Lett.* **2017**, *6* (7), 641–646.

(59) Aoki, S.; Koide, A.; Imabayashi, S.; Watanabe, M. Novel Thermosensitive Polyethers Prepared by Anionic Ring-Opening Polymerization of Glycidyl Ether Derivatives. *Chem. Lett.* **2002**, *31*, 1128–1129.

(60) Zhang, M.; Vora, A.; Han, W.; Wojtecki, R. J.; Maune, H.; Le, A. B. A.; Thompson, L. E.; McClelland, G. M.; Ribet, F.; Engler, A. C.; Nelson, A. Dual-Responsive Hydrogels for Direct-Write 3D Printing. *Macromolecules* **2015**, *48*, 6482–6488.

(61) Basu, A.; Saha, A.; Goodman, C.; Shafranek, R. T.; Nelson, A. Catalytically Initiated Gel-in-Gel Printing of Composite Hydrogels. *ACS Appl. Mater. Interfaces* **2017**, *9* (46), 40898–40904.

(62) Johnston, T. G.; Yuan, S. F.; Wagner, J. M.; Yi, X.; Saha, A.; Smith, P.; Nelson, A.; Alper, H. S. Compartmentalized Microbes and Co-Cultures in Hydrogels for on-Demand Bioproduction and Preservation. *Nat. Commun.* **2020**, *11* (1), 1–11.

(63) Millik, S. C.; Dostie, A. M.; Karis, D. G.; Smith, P. T.; McKenna, M.; Chan, N.; Curtis, C. D.; Nance, E.; Theberge, A. B.; Nelson, A. 3D Printed Coaxial Nozzles for the Extrusion of Hydrogel Tubes toward Modeling Vascular Endothelium. *Biofabrication* **2019**, *11* (4).

(64) Saha, A.; Johnston, T. G.; Shafranek, R. T.; Goodman, C. J.; Zalatan, J. G.; Storti, D. W.; Ganter, M. A.; Nelson, A. Additive Manufacturing of Catalytically Active Living Materials. *ACS Appl. Mater. Interfaces* **2018**, *10* (16), 13373–13380.

(65) Liu, J.; Erol, O.; Pantula, A.; Liu, W.; Jiang, Z.; Kobayashi, K.; Chatterjee, D.; Hibino, N.; Romer, L. H.; Kang, S. H.; Nguyen, T. D.; Gracias, D. H. Dual-Gel 4D Printing of Bioinspired Tubes. *ACS Appl. Mater. Interfaces* **2019**, *11* (8), 8492–8498.

(66) Larush, L.; Kaner, I.; Fluksman, A.; Tamsut, A.; Pawar, A. A.; Lesnovski, P.; Benny, O.; Magdassi, S. 3D Printing of Responsive Hydrogels for Drug-Delivery Systems. *J. 3D Print. Med.* **2017**, *1* (4), 219–229.

(67) Han, D.; Wang, Y.; Yang, C.; Lee, H. Multimaterial Printing for Cephalopod-Inspired Light-Responsive Artificial Chromatophores. *ACS Appl. Mater. Interfaces* **2021**, *13* (11), 12735–12745.

(68) Gevrek, T. N.; Cosar, M.; Aydin, D.; Kaga, E.; Arslan, M.; Sanyal, R.; Sanyal, A. Facile Fabrication of a Modular "Catch and Release" Hydrogel Interface: Harnessing Thiol-Disulfide Exchange for Reversible Protein Capture and Cell Attachment. *ACS Appl. Mater. Interfaces* **2018**, *10* (17), 14399–14409.

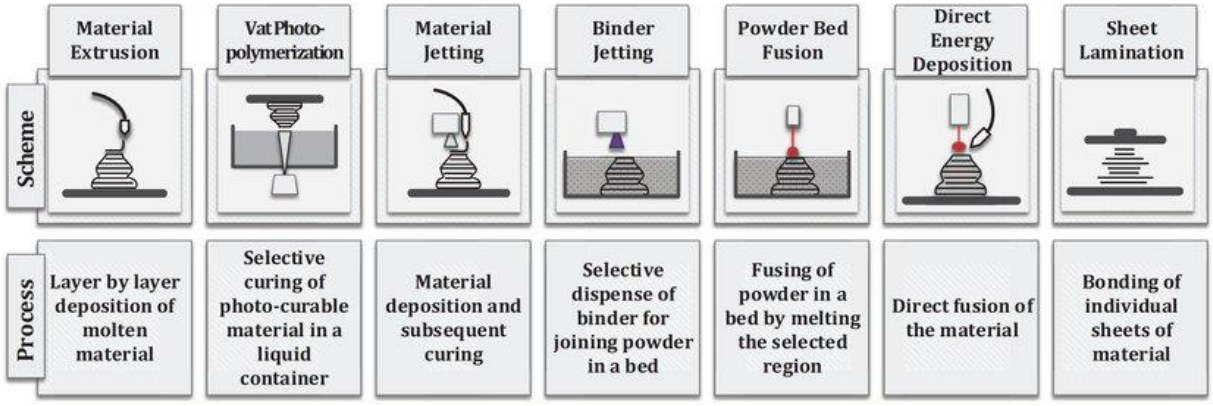

Figure 1.1. Visualization of the seven 3D printing methods according to the ASTM.

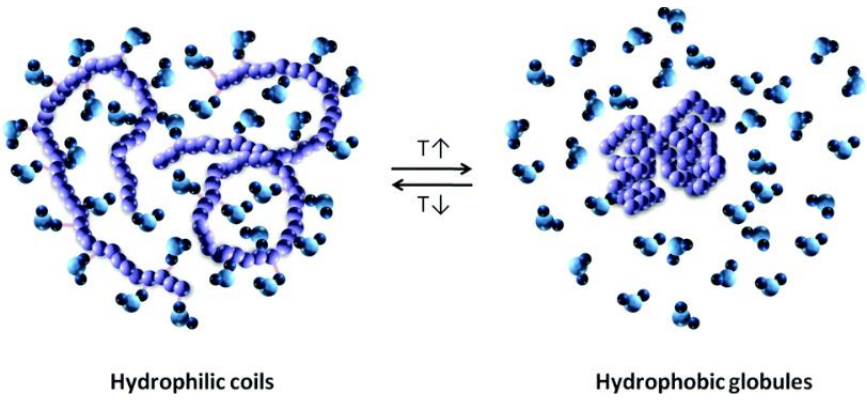

Figure 1.2. Cartoon representation of the fully hydrated coil to collapsed globule transition of amphiphilic homopolymers in dilute solutions (1 wt%) as the ΔG_{mix} becomes positive with increasing temperature

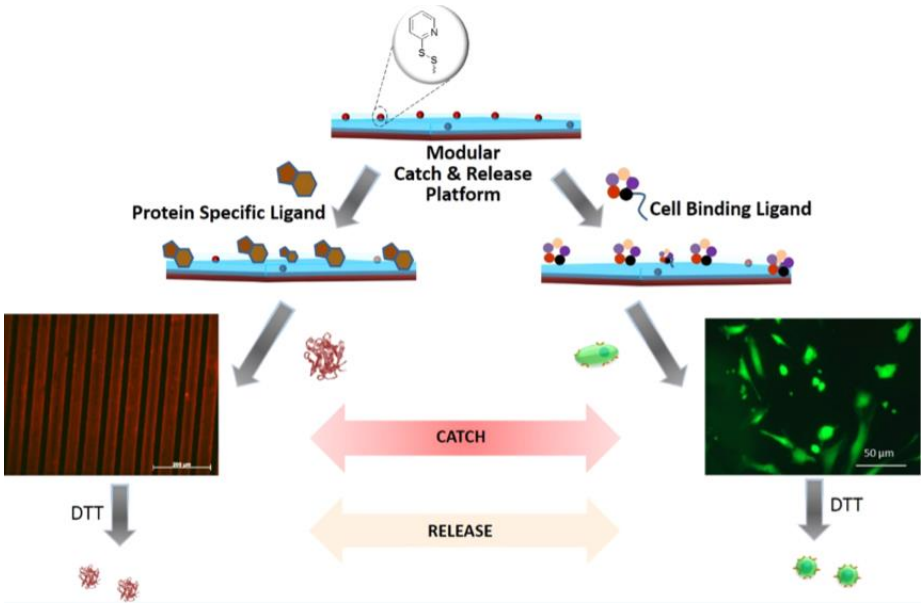

Figure 1.3 Pyridyl disulfide methacrylate was incorporated into a hydrogel network by copolymerization with poly(ethylene oxide) methyl ether methacrylate. The thiol-reactive hydrogel platform was functionalized with biotin and RGD-SH to selectively "catch" Extravidin and attach HUVEC cells, followed by release with DTT.

CHAPTER 2: **TUNABLE TEMPERATURE- AND SHEAR-RESPONSIVE HYDROGELS BASED ON POLY(ALKYL GLYCIDYL ETHER)S**

2.1 ABSTRACT

Herein, we describe the synthesis, characterization, and direct-write 3D printing of triblock copolymer hydrogels that have a tunable response to temperature and shear stress. In aqueous solutions, these polymers utilize the temperature-dependent self-association of poly(alkyl glycidyl ether) 'A' blocks and a central poly(ethylene oxide) (PEO) segment to create a physically cross-linked three-dimensional network. The temperature response of these hydrogels was dependent upon composition, chain length, and concentration of the 'A' block in the copolymer. Rheological experiments confirmed the existence of sol-gel transitions and the shear-thinning behavior of the hydrogel. The temperature- and shear-responsive properties enabled direct-write 3D printing of complex objects with high fidelity. Hydrogel cytocompatibility was also confirmed by incorporating HeLa cells into select hydrogels resulting in high viabilities over 24 h. The tunable temperature response and innate shear-thinning properties of these hydrogels, coupled with encouraging cell viability results, present an attractive opportunity for additive manufacturing and tissue engineering applications.

2.2 INTRODUCTION

Hydrogels are water-swollen, three-dimensional networks of molecules or molecular assemblies that are useful in a range of applications that include drug delivery and tissue engineering.[1–4] These hydrophilic networks are bound by chemical or physical cross-links between the molecules.[5] Stimuli-responsive hydrogels belong to a unique class of materials that adapt to

environmental cues such as pH,[6,7] temperature,[8,9] light,[10,11] and mechanical impetus.[12–14] Temperature and shear stress are examples of two important stimuli responses that enable effective drug delivery,[15–17] additive manufacturing,[18–20] and tissue engineering.[21–23] A thermally reversible sol-gel response—wherein, the hydrogel liquefies upon cooling—allows for facile loading of the hydrogel ink and homogenous dispersion of heat-insensitive drugs or additives in the liquid state.[24] Furthermore, shear-thinning hydrogels facilitate the formation of 3D printed objects and protect encapsulated cells from the damaging shear stress of the syringe nozzle.[25,26] These materials exist in the gel state under ambient conditions, but experience a drop in viscosity when activated by shear stress. The extruded filaments are proposed to undergo a "plug-flow" as the material travels through the nozzle.[27]

Multi-stimuli responsive hydrogels can be formulated from aqueous solutions of amphiphilic ABA triblock copolymers comprised of at least one block that exhibits a temperature-dependent aqueous solubility known as a lower critical solution temperature (LCST). The Lewis group reported the 3D printing of one such hydrogel composed of commercially available Pluronic F127, which is a poly(ethylene oxide)-*block*-poly(propylene oxide)-*block*-poly(ethylene oxide) triblock copolymer.[28] It was demonstrated that the temperature response of Pluronic F127 hydrogels is driven by the LCST of the poly(propylene oxide) (PPO) 'B' block.[29–31]

We have recently reported a similar ABA triblock copolymer that incorporates poly(isopropyl glycidyl ether) (PiPGE) 'A' blocks as hydrogel inks for 3D printing.[32] These poly(isopropyl glycidyl ether)-*block*-poly(ethylene oxide)-*block*-poly(isopropyl glycidyl ether) triblock copolymers utilize the LCST of the PiPGE 'A' blocks to form hydrogels in aqueous solutions. These hydrogels exhibit a similar dual-stimuli response to temperature and shear stress as F127 but require lower polymer concentrations. Based on this research, we envisioned a poly(alkyl

glycidyl ether)-*block*-poly(ethylene oxide)-*block*-poly(alkyl glycidyl ether) triblock copolymer platform with a tunable temperature response. The inherent architectural design of the triblock would retain the temperature- and shear- responsive properties demonstrated in our previous work but enable additional freedom to alter the temperature response through the incorporation of comonomers, adjustment of chain length, and alteration of polymer concentration. We theorize that these triblock copolymers exist as individually solvated unimers at low temperatures, but form networks of physically crosslinked flower micelles at higher temperatures as the solvent becomes increasingly unfavorable for the poly(alkyl glycidyl ether) 'A' blocks.[33–36] The dynamic nature of the physical crosslinks between micelles enable a reversible response to shear stress, facilitating extrusion of these hydrogels from a syringe (Figure 2.1).[37]

In order to further examine the versatility of this platform as temperature- and shear-responsive materials, we investigated a series of poly(alkyl glycidyl ether) homopolymers and poly(alkyl glycidyl ether)-*block*-poly(ethylene oxide)-*block*-poly(alkyl glycidyl ether) triblock copolymers and their corresponding hydrogels. Aqueous solutions of these polymers were examined via UV-Vis spectroscopy to identify trends in cloud point temperature (T_{cp}), while phase diagrams were employed to map the physical state of the triblock copolymers at different concentrations and temperatures. A series of rheological tests were conducted to further characterize the dual-stimuli responsive behavior of these hydrogels. Investigations into the printability and cytocompatibility of the platform indicate a promising potential for use in additive manufacturing and tissue engineering.

2.3 Materials and Methods

2.3.1 Materials

All chemicals and solvents were purchased from Sigma-Aldrich or Fisher Scientific and used without further purification unless noted otherwise. Isopropyl glycidyl ether (iPGE, 98%), ethyl glycidyl ether (EGE, 98%), allyl glycidyl ether (AGE, 99%, Acros), methyl glycidyl ether (MGE, 85%, TCI America), and *n*-propyl glycidyl ether (Synthesis detailed in Supporting Information) were dried over CaH_2 for 24 h, distilled into a flask containing butyl magnesium chloride (2 M in tetrahydrofuran, THF), re-distilled, and stored under N_2 atmosphere. Poly(ethylene oxide) (PEO, M_n 8000 g mol^{-1}) was dried under vacuum overnight prior to use. Dry THF was obtained using neutral alumina using a Pure Process Technology solvent purification system. A potassium naphthalenide solution (1M) was prepared by dissolving naphthalene (3.2 g) in THF (25 mL), adding potassium (0.975 g), and storing under N_2 atmosphere. ^{1}H NMR spectra were obtained on a Bruker Advance 300 or 500 MHz spectrometer. Gel permeation chromatography was performed using a Waters chromatograph equipped with two 10 µm Malvern columns (300 mm x 7.8 mm) connected in series with increasing pore size (1,000, 10,000 Å), using chloroform (Optima, 0.1% v/v trimethylamine) as the eluent, and calibrated with poly(ethylene oxide) standards (400 to 40, 000 g mol^{-1}). The relative molecular weights were measured in chloroform using poly(ethylene oxide) standards and a refractive index detector (flow rate: 1 mL min^{-1}).

2.3.2 Homopolymer Synthesis

All alkyl glycidyl ether homopolymers were synthesized by utilizing the same synthetic procedure with different monomer feed ratios. The following poly(isopropyl glycidyl ether) synthetic scheme will serve as an example. The initiator 4-methyl benzyl alcohol (0.122 g, 1 mmol)

was added to an oven-dried, 100 mL round-bottom flask. Potassium naphthalenide solution (1M in THF) was titrated until a light green paste was formed. The reaction flask was evacuated overnight to drive off the remaining THF. Isopropyl glycidyl ether (6.49 mL, 51.56 mmol) was added to the dried mixture of deprotonated initiator, and the reaction was stirred at 70 °C for 45 h. The polymer solution was quenched using a degassed 1% v/v AcOH in MeOH solution and dialyzed against MeOH for 3 d (3 solvent exchanges) using Spectra/Por regenerated cellulose tubing (MWCO 1.0 kDa) that was pre-soaked in water. The dialyzed polymer solution was concentrated under reduced pressure and dried in a vacuum oven for 24 h to afford a viscous, pale yellow liquid (0.8 g). ^{1}H NMR (500 MHz, $CDCl_3$): δ 1.13-1.14 (m, -O-CH-(CH_3)$_2$), 2.34 (s, -Ph-CH_3), 3.43-3.89 (m, (-O-CH_2-CH(CH_2-O-CH-(CH_3)$_2$)-O-), 4.50 (s, -Ph-CH_2-O-), 7.13-7.14 (d, CH_3-*Ph*-CH_2-, J = 7.5 Hz), 7.21-7.22 (d, CH_3-*Ph*-CH_2-, J = 8 Hz). Molecular weights were determined by ^{1}H NMR spectroscopy by comparing the integration values of the methyl benzylic protons (2.33 ppm) to the alkyl glycidyl ether protons (1.13-1.25 ppm) or the methylene (5.2 ppm) and vinyl (5.9 ppm) protons of allyl glycidyl ether.

2.3.3 Triblock Copolymer Synthesis

ABA triblock copolymers were synthesized via anionic ring-opening polymerization. All copolymers were initiated from PEO (M_n = 8,000 g mol^{-1}). The following procedure for P(iPGE-*stat*-EGE)$_{2.2k}$-*block*-PEO$_{8k}$-*block*-P(iPGE-*stat*-EGE)$_{2.2k}$ (Polymer **9**) will serve as an example for a typical triblock copolymer synthesis. PEO (10 g, 1.25 mmol) was added to the reaction vessel and dried under vacuum overnight. Dry THF (100 mL) was added under an Ar atmosphere and heated to 50 °C to facilitate dissolution of the macroinitiator. Once sufficiently dissolved, a potassium naphthalenide solution (1M in THF) was titrated into the flask until the solution remained a slight green color, indicating full deprotonation of PEO hydroxyl end groups. Isopropyl

glycidyl ether (4.07 g, 35 mmol) and ethyl glycidyl ether (3.57 g, 35 mmol) were added to begin polymerization. The reaction continued for 24 h at 65 °C and was subsequently quenched with a degassed solution of 1% v/v AcOH in MeOH. In the polymerizations with allyl glycidyl ether, reactions were performed at 30 °C to avoid allyl-vinyl isomerization as reported by Lynd and co-workers.[38] The reaction mixture was then precipitated into cold hexane. The polymer was collected via centrifugation (4400 rpm, 10 min) and the supernatant decanted. The product was washed twice with additional hexane and collected again in the same manner. The isolated polymer solution was dried in a vacuum oven for at least 24 h to afford an off-white solid (13.6 g). ^{1}H NMR (500 MHz, $CDCl_3$): δ 1.13-1.15 (m, -O-CH-(C*H*$_3$)$_2$), 1.15-1.19 (t, -O-CH$_2$-C*H*$_3$, *J* = 7.0 Hz), 3.47-3.79 (m -O-C*H*$_2$-C*H*$_2$-O- and -O-C*H*$_2$-C*H*(C*H*$_2$-O-C*H*$_2$-CH$_3$)-O- and -O-C*H*$_2$-C*H*(C*H*$_2$-O-C*H*-(CH$_3$)$_2$)-O-). The method used to calculate the degree of polymerization (DP) can be found in the Supporting Information.

2.3.4 UV-Vis Spectroscopy

Cloud point temperatures (T_{cp}) were determined by UV-Vis spectroscopic measurements on an Agilent 8453 UV Visible Spectrometer. Temperature-dependent absorbance values were acquired every 0.5 °C at λ = 600 nm with a two-minute equilibration time for all samples. The polymers were dissolved in water and equilibrated at 5 °C to afford final sample concentrations of 1 wt%. The T_{cp} was reported as the temperature at 50% of the absorbance increase.

2.3.5 Rheological Measurements

Dynamic oscillatory rheological experiments were performed on a TA Instruments Discovery HR-2 rheometer equipped with a 20 mm parallel-plate geometry unless otherwise specified. Samples were equilibrated in an ice bath for at least 10 min, then carefully loaded onto the Peltier

plate at 5 °C. A pre-shear experiment was applied to ensure bubbles were eliminated from the sample cell. The sample was equilibrated at 21 °C for 8 min. Strain sweep experiments were performed, and all studies were conducted using a strain value in the linear viscoelastic regime. Temperature ramp experiments were performed at 1 Hz from 5 to 50 °C at 2 °C min^{-1}. Cyclic strain tests (frequency 1 Hz) were performed at 21 °C using alternating strains of 1% for 5 minutes and 100% for 3 minutes per cycle. Viscosity versus shear rate experiments were performed at 21 °C. The gel yield stress values were measured under oscillatory strain (frequency: 1 Hz, 21 °C) starting with an initial strain of 0.01% and converted to applied oscillatory stress.

2.3.6 Direct-Write 3D Printing of Hydrogels

A modified pneumatic direct-write 3D printer was assembled based on a Tronxy P802E 3D Printer kit, from Shenzen Tronxy Technology Co. The hydrogel ink was cooled to 5 °C and poured into a Nordson Optimum 10 cc fluid dispensing barrel equipped with a Metcal conical (410 µm inner diameter) precision tip nozzle. The loaded syringe was warmed to ambient temperature and pressurized using nitrogen gas (20 psi) to extrude the gel from the nozzle at 8.0 mm s^{-1}. The printer was controlled with an Arduino using the Marlin firmware. The G-code file was produced with Slic3r software.

2.3.7 Cell Viability Study

Three solutions of polymer 9 (15, 20, and 26.67 wt%) in Dulbecco's Modified Eagle's Medium (DMEM) supplemented with 10% phosphate buffer solution (PBS) and 1% streptomycin/penicillin were equilibrated at 5 °C for 3 d. HeLa cells were grown to confluency at 37 °C. The cells were rinsed with PBS, detached from culture plates using trypsin (0.05%) and EDTA (0.53 mM), and mixed with supplemented DMEM to afford a final concentration of 10 x

10^6 cells/mL. To utilize the thermally reversible gel-to-sol transition, cell media (20 µL) was combined with polymer solution (60 µL) on ice; hydrogels were formed with final concentrations of 11.25, 15, and 20 wt%. The cell/polymer media solution (60 µL) was pipetted onto a culture plate, immersed in supplemented DMEM, and incubated at 37 °C for 24 h. The sample was cooled on an ice block and mixed with a DMEM solution containing LIVE/DEAD® reagents calcein (2 µM) and ethidium homodimer-1 (4 µM). This solution was placed in an incubator for 30 min at 37 °C, imaged on a Leica SP8X Confocal Microscope, and analyzed using the Fiji image processing package.

2.4 Results and Discussions

2.4.1 Synthesis of Homopolymers and Characterization of LCST Response

Living anionic polymerization is an effective method[39–42] for the ring-opening polymerization[43,44] of glycidyl ether derivatives to afford polymers of controlled molecular weight and dispersity. All poly(alkyl glycidyl ether)s in this investigation were synthesized via the initiation from an alcohol using potassium naphthalenide as the base. Watanabe and co-workers[45,46] previously demonstrated that poly(alkyl glycidyl ether)s show LCST behavior in aqueous solutions. Thus, we first synthesized alkyl glycidyl ether homopolymers derived from methyl, ethyl, allyl, isopropyl, or *n*-propyl glycidyl ether monomer (Scheme 2.1) in order to characterize their LCST responses to confirm these results for comparison to the triblock copolymers to be discussed later in this section.

Polymers with molecular weights ranging from 2.1 kg mol^{-1} to 24.5 kg mol^{-1} were synthesized, and 1 wt% aqueous solutions of these polymers were subjected to UV-Vis spectroscopic cloud point measurements to quantify the LCST (Table 2.1, Figure A1). The LCST transition was governed by a change in the system's free energy of mixing, ΔG_{mix}, from negative

to positive upon an increase in temperature.[47,48] This was due to the amphiphilic nature of the polymer in an aqueous environment. The oxygen atoms in the poly(alkyl glycidyl ether)s acted as hydrogen bond acceptors with water that enthalpically favored a mixed state. Meanwhile, the alkyl portions of the polymer contributed to an unfavorable entropic driving force associated with the hydrophobic effect.[49–51] The balance between an enthalpically favored mixed state and an entropically favored demixed state led to a temperature-dependent solubility. At lower temperatures, the enthalpic forces of the polymer dominated the system, which yielded a negative ΔG_{mix} and a transparent solution. As the temperature increased, the negative total entropy change dominated the system and the free energy of mixing became positive. Phase separation occurred as the polymer chains underwent a coil-to-globule transition, and the solution became turbid.[48,49,52]

The T_{cp} values of the poly(alkyl glycidyl ether)s studied were found to abide by these thermodynamic principles and correlated inversely with the number of carbons in the R group. Hydrophilic monomers, wherein R = ethyl and methyl, displayed LCST behavior at approximately 10.8 and 45 °C, respectively. As the number of carbons in the R group increased to three (R = isopropyl, *n*-propyl, and allyl), the large entropy term dominated at all temperatures and yielded water-insoluble polymers. We also observed that the T_{cp} of the alkyl glycidyl ether homopolymers did not show any dependence on molecular weight, remaining nearly constant from 3.0 to 24.5 kg mol^{-1} for poly(ethyl glycidyl ether) (PEGE). These values were consistent with the results of Satoh and Watanabe et al.[46,53] However, we noted a difference in the T_{cp} observed for poly(methyl glycidyl ether) compared to a previous report by Watanabe and co-workers,[46] which was attributed to the hydrophobicity of the methyl benzyl end group that had a significant effect upon the solubility of the homopolymer as a consequence of its low molecular weight.

2.4.2 Synthesis of Triblock Copolymers and Characterization of LCST Response

The incorporation of different alkyl glycidyl ethers into an ABA triblock copolymer comprised of poly(alkyl glycidyl ether) 'A' blocks and a PEO 'B' block afforded a platform of polymers with a tunable temperature response. Poly(alkyl glycidyl ether)-*block*-PEO-*block*-poly(alkyl glycidyl ether) triblock copolymers were synthesized via anionic ring opening polymerization in THF using PEO as the macroinitiator (M_n = 8,000 g mol^{-1}) and potassium naphthalenide as a base (Scheme 2.2).

The block length of each glycidyl ether segment was controlled by varying the molar ratio of monomer to PEO macroinitiator. Statistical copolymers were afforded by the addition of two different alkyl glycidyl ether monomers simultaneously. Specifically, EGE and AGE were co-polymerized to form polymer 4, while EGE and iPGE were co-polymerized to form polymers 5-10. The degree of polymerization (DP) was less than the theoretical value, which suggested that homopolymer impurities or unreacted monomers were present in the reaction mixture but were removed during purification. The low dispersity values ($\leq$ 1.16) of all synthesized triblock copolymers were consistent with controlled ring-opening polymerizations. The LCSTs of these polymers (Table 2.2) were quantified in a manner similar to the homopolymers discussed previously in this section (Figures A2 and A3).

The thermodynamic principles that governed the LCST response of the homopolymers was also applicable to the triblock copolymers. However, the temperature-dependent aqueous solubility of the copolymer as a whole must be taken into consideration, as opposed to the solubility of the individual blocks.[53–57] Although the AGE and the iPGE homopolymers (Table 2.1) did not exhibit LCST behavior, the ABA triblock copolymers containing poly(allyl glycidyl ether) (PAGE) 'A' blocks (polymer 2) or PiPGE 'A' blocks (polymer 3) had T_{cp} values of 29.7 °C

and 24.2 °C, respectively. Polymer 1, which had PEGE 'A' blocks, exhibited a T_{cp} at 60.0 °C. The statistical co-polymerization of EGE and iPGE enabled further tuning of the LCST behavior. We successfully decreased the T_{cp} of the copolymer from 60.0 °C (polymer 1) to 46.2 °C (polymer 5), 40.3 °C (polymer 8), and 32.4 °C (polymer 6) by replacing EGE units in the 'A' blocks with more hydrophobic iPGE monomers (at similar molecular weights).

In addition to molecular composition, the molecular weight of the 'A' blocks can also be exploited to tune the LCST response of the copolymer platform. To probe this relationship, the phase transition temperature of polymers 7-10, with approximately a 1:1 ratio between EGE and iPGE—and with molecular weights of 1.4k, 1.8k, 2.2k, and 2.8k, respectively—were investigated. We observed that the T_{cp} of the triblock copolymer and chain length of the glycidyl ether blocks were inversely related, as the hydrophobic character of the polymer increased with the molecular weight of the poly(alkyl glycidyl ether) segments. We successfully tuned the temperature response of the triblock copolymer in water from 49.3 °C (polymer 7) to 24.1 °C (polymer 10) by changing the molecular weight of the A block.

2.4.3 Triblock Copolymer Phase Diagrams

At low concentrations (1-5 wt%), the triblock copolymer solutions became turbid as the temperature increased, due to the cloud point transition of these polymers. However, as the polymer concentration increased (≥ 5 wt%), this phase separation mechanism gave way to the formation of a three-dimensional hydrogel network and a sol-gel transition. To better understand the role of temperature, polymer concentration, chain length, and composition in the formation of the polymer hydrogels, qualitative phase diagrams were produced for each triblock copolymer. Polymer solutions (2-30 wt%) were prepared and incubated at temperatures that ranged from 5 to 50 °C. Their physical states were determined using the vial inversion method and recorded as a

transparent/opaque liquid, viscous solution, or gel. Transparent formulations were clear, with no turbidity present, whereas opaque solutions were turbid and optically cloudy in appearance.

In the same manner that the hydrophobicity of the copolymers was utilized to tune the LCST response, we exploited the inherent differences in hydrophobic character of the alkyl glycidyl ether monomers to alter the sol-gel transition temperature. Polymer 1 afforded solutions that only became a gel at temperatures >50 °C and concentrations >30 wt% as a consequence of the hydrophilicity of the PEGE block. Relative to polymer 1, polymers 5, 8, 6, and 3 had a greater hydrophobic character due to the presence of iPGE units in the copolymer. We successfully formulated solutions of polymers 5, 8, 6, and 3 that gelled at progressively lower temperatures and concentrations relative to polymer 1 (Figure 2.2).

For example, 20 wt% solutions of polymers 5, 8, 6, and 3 exhibited a sol-gel transition at 45, 30, 25, and 10 °C, respectively. The solubility of polymer 3 (with PiPGE 'A' blocks) significantly decreased, such that it was not fully soluble at 30 wt%. The AGE-containing polymers afforded brittle hydrogels (Figure A4) and were not further investigated.

The sol-gel transition of these polymers in aqueous solution was also affected by molecular weight and polymer concentration. The sol-gel transition temperature was tuned by altering the molecular weight of the glycidyl ether 'A' blocks (Figure 2.3). As the polymer chain length increased, the hydrophobicity of the polymer also increased. For polymers 7-10 at identical concentrations in water (20 wt%), the sol-gel transition temperature decreased as the molecular weight was increased (40, 30, 20, and 15 °C, respectively). Thus, a 25 °C range in gelation temperature was accomplished with the inclusion of 12.5 additional glycidyl ether repeat units per block. The polymer concentration also served an important role in the tunability of the gelation temperature. The sol-gel transition of each hydrogel decreased as the polymer concentration

increased (Figure 2.3). For example, the sol-gel transition temperature of polymer 7 was altered from 40 °C to 25 °C as the concentration was increased from 20 to 30 wt%.

Although the gelation temperature of these solutions cannot be directly predicted by the T_{cp} values, we observed that they were dictated by the polymer composition, molecular weight, and concentration in aqueous media. These results are consistent with that reported by Georgiou and co-workers, whom obtained[58–61] similar results for their thermo-responsive methacrylate-based terpolymers. Similarly, Pluronic F127 has a reported[62] sol-gel transition (14-40 °C) that is dependent upon concentration, but has a T_{cp} above 100 °C.[63] These findings stand in contrast to the PNiPAAm-*block*-PEO-*block*-PNiPAAm triblock copolymers studied by Teodorescu and coworkers, wherein the cloud point measurements and the vial inversion gelation temperatures occurred at similar temperatures.[64,65]

2.4.4 Triblock Copolymer Hydrogel Rheology

Temperature- and shear- responsive hydrogels are useful for direct-write 3D printing as fugitive inks[66,67] and in the fabrication of composites hydrogels.[68] Rheometric characterization of the viscoelastic behaviors of hydrogels can serve as a screening protocol for the suitability of the hydrogels as inks for direct-write 3D printing.[28,69] Specifically, yield stress values can be used to compare the relative extrudability of hydrogels from a nozzle during the printing process. The hydrogel ink maintains a gel state below its yield stress, but the gel network is broken at stresses above this value causing the ink to flow and a steep drop in modulus. The phase diagrams in Figures 2.2 and 2.3 were utilized to identify the optimal hydrogels to investigate as inks for direct-write 3D printing. The selected hydrogels were gels at ambient temperature but reversibly transformed into the ‘liquid’ or ‘viscous solution’ state upon cooling.

Oscillatory stress ramp experiments (Figure 2.4a) were used to determine the yield stress of these select hydrogel formulations. The 20 wt% solutions of polymers 9, 10, and 3 had yield stress values of 569, 1200, and 1252 Pa, respectively. Hydrogels derived from polymer 9 were found to be particularly well-suited for direct-write 3D printing, whereas the yield stress for hydrogels of polymers 10 and 3 were too high and the materials were more difficult to extrude. Thus, a 20 wt% formulation of polymer 9 was chosen for all further rheological experiments, as well as the direct-write 3D printing of the structures presented later in this section.

Temperature-dependent sol-gel transitions in hydrogel inks is advantageous for the addition and homogeneous distribution of additives and the transfer of these inks into the printer cartridge (syringe). The temperature-dependent viscoelastic characterization (Figure 2.4b) confirmed the presence of a sol-gel transition as defined by the intersection of elastic (G') and viscous (G") moduli (the rheometrical gelation temperature (T_{gel}) = 18.72 °C). At temperatures below the T_{gel}, the G" exceeded the G' and the polymer solution was free-flowing; above the T_{gel}, the G' exceeded the G" and the solution became a gel with a maximum G' of 33.3 kPa. Additional rheological characterization demonstrated the shear-thinning and self-healing properties of these hydrogels governed by the physical cross-linking of the low-T_g poly(alkyl glycidyl ether) blocks. The shear-thinning behavior was reflected by the decrease in viscosity with increasing shear rate (Figure 2.4c). A dynamic oscillatory strain experiment (Figure 2.4d) revealed a rapid and reversible response of the hydrogel G' and G" moduli to consecutive cycles of high (100%) and low (1%) strain. During periods of high strain, the G" was greater than the G', which indicated that the material was able to flow. Whereas the sample was a gel when subjected to periods of low strain, as indicated by the larger value for G' relative to G". Also, G' was nearly fully recovered after every cycle with a low degree of mechanical hysteresis.

2.4.5 Direct-Write 3D Printing

As a demonstration printability of our hydrogel platform, a hydrogel ink comprised of 20 wt% polymer 9 was extruded by a direct-write 3D printer. The hydrogel was loaded into the printer syringe in its liquid state at 5 °C and was then warmed to ambient temperature. The hydrogel ink was extruded through a 0.41 mm inner diameter nozzle at 20 psi and an 8.0 mm s^{-1} print speed. During the direct-write 3D printing process, multiple layers are sequentially printed in a layer-by-layer manner. The printed objects shown in Figure 2.5 had 15 layers and exhibited excellent shape fidelity with no sagging or deformation of the individual layers.

2.4.6 Cell Viability

The cytocompatibility of hydrogels based on poly(alkyl glycidyl ether) block copolymers were investigated using HeLa cells. Hydrogels derived from polymer 9 were formulated using DMEM supplemented with 10% FBS and 1% streptomycin/penicillin. The hydrogels in media exhibited a temperature-dependent sol-gel transition—wherein the sample became liquid upon cooling in an ice bath. This temperature-responsive feature enabled the uniform incorporation and distribution of HeLa cells in the liquid state prior to warming the solution to its gel state. The HeLa-embedded hydrogels were incubated at 37 °C for 24 h at final polymer concentrations of 11.25, 15, and 20 wt%. Cell viability was quantified via LIVE/DEAD® assay and confocal microscopy (Figure 2.6). These tests were performed in triplicate (Figure A5-A8) and afforded viabilities of 91% (± 4.10%), 93% (± 6.27%), and 84% (± 18.24%), respectively. The results of these experiments indicate acceptable cell viability at all concentrations tested and demonstrate a promising potential for use in cell encapsulation applications such as cell therapeutics and tissue engineering.

2.5 Conclusion

In summary, we have developed a highly tunable, biocompatible ABA triblock copolymer platform that utilized the hydrophobic self-association of poly(alkyl glycidyl ether) 'A' blocks in aqueous solutions to form three-dimensional networks composed of flower micelles that responded to both thermal and shear stimuli. The identity of the alkyl side-chain (ethyl, isopropyl, *n*-propyl, and allyl) on the poly(alkyl glycidyl ether) block played a significant role in the temperature-responsive behaviors. Interestingly, the 3-carbon alkyl groups afforded homopolymers that did not exhibit any temperature response, but yielded ABA triblock copolymers which clearly exhibited temperature-dependent gelation. Copolymers comprised of ethyl and isopropyl glycidyl ethers were investigated to further tune the temperature response. The gelation temperature of this platform can be readily tuned between 10 and 45 °C by altering the molecular composition, molecular weight, and concentration of the polymer. The temperature and shear-responsive nature of the triblock copolymer hydrogels were characterized via phase diagrams and rheology. We also demonstrated that these polymers were suitable as inks for direct-write 3D printing to afford free-standing, multi-layered 3D constructs. These stimuli-responsive hydrogels represent a promising platform to develop new materials for additive manufacturing and tissue engineering.

2.6 REFERENCES

(1) Malmsten, M. Soft Drug Delivery Systems. *Soft Matter* **2006**, *2*, 760.

(2) Alvarado-Velez, M.; Pai, S. B.; Bellamkonda, R. V. Hydrogels as Carriers for Stem Cell Transplantation. *IEEE Trans. Biomed. Eng.* **2014**, *61*, 1474–1481.

(3) Nicodemus, G. D.; Bryant, S. J. Cell Encapsulation in Biodegradable Hydrogels for Tissue Engineering Applications. *Tissue Eng. Part B. Rev.* **2008**, *14*, 149–165.

(4) DeForest, C. A.; Anseth, K. S. Advances in Bioactive Hydrogels to Probe and Direct Cell Fate. *Annu. Rev. Chem. Biomol. Eng.* **2012**, *3* (1), 421–444.

(5) Peppas, N. A.; Hilt, J. Z.; Khademhosseini, A.; Langer, R. Hydrogels in Biology and Medicine: From Molecular Principles to Bionanotechnology. *Adv. Mater.* **2006**, *18*, 1345–1360.

(6) Suhag, D.; Bhatia, R.; Das, S.; Shakeel, A.; Ghosh, A.; Singh, A.; Sinha, O. P.; Chakrabarti, S.; Mukherjee, M. Physically Cross-Linked PH-Responsive Hydrogels with Tunable Formulations for Controlled Drug Delivery. *RSC Adv.* **2015**, *5*, 53963–53972.

(7) Hibbins, A. R.; Kumar, P.; Choonara, Y. E.; Kondiah, P. P. D.; Marimuthu, T.; du Toit, L. C.; Pillay, V. Design of a Versatile PH-Responsive Hydrogel for Potential Oral Delivery of Gastric-Sensitive Bioactives. *Polymers (Basel).* **2017**, *9*, 474.

(8) Hatefi, A.; Amsden, B. Biodegradable Injectable in Situ Forming Drug Delivery Systems. *J. Control. Release* **2002**, *80*, 9–28.

(9) Huang, X.; Lowe, T. L. Biodegradable Thermoresponsive Hydrogels for Aqueous Encapsulation and Controlled Release of Hydrophilic Model Drugs. *Biomacromolecules* **2005**, *6*, 2131–2139.

(10) Zhao, Y.-L.; Stoddart, J. F. Azobenzene-Based Light-Responsive Hydrogel System †. *Langmuir* **2009**, *25*, 8442–8446.

(11) Ter Schiphorst, J.; Coleman, S.; Stumpel, J. E.; Ben Azouz, A.; Diamond, D.; Schenning, A. P. H. J. Molecular Design of Light-Responsive Hydrogels, for in Situ Generation of Fast and Reversible Valves for Microfluidic Applications. *Chem. Mater.* **2015**, *27*, 5925–5931.

(12) Yesilyurt, V.; Webber, M. J.; Appel, E. A.; Godwin, C.; Langer, R.; Anderson, D. G. Injectable Self-Healing Glucose-Responsive Hydrogels with PH-Regulated Mechanical Properties. *Adv. Mater.* **2016**, *28*, 86–91.

(13) Jaspers, M.; Dennison, M.; Mabesoone, M. F. J.; MacKintosh, F. C.; Rowan, A. E.; Kouwer, P. H. J. Ultra-Responsive Soft Matter from Strain-Stiffening Hydrogels. *Nat. Commun.* **2014**, *5*, 5808.

(14) Badeau, B. A.; Comerford, M. P.; Arakawa, C. K.; Shadish, J. A.; Deforest, C. A. Engineered Modular Biomaterial Logic Gates for Environmentally Triggered Therapeutic Delivery. *Nat. Chem.* **2018**, *10* (3), 251–258.

(15) Gupta, D.; Tator, C. H.; Shoichet, M. S. Fast-Gelling Injectable Blend of Hyaluronan and Methylcellulose for Intrathecal, Localized Delivery to the Injured Spinal Cord. *Biomaterials* **2006**, *27*, 2370–2379.

(16) Li, J.; Loh, X. J. Cyclodextrin-Based Supramolecular Architectures: Syntheses, Structures, and Applications for Drug and Gene Delivery. *Adv. Drug Deliv. Rev.* **2008**, *60*, 1000–1017.

(17) Wang, Q.; Wang, J.; Lu, Q.; Detamore, M. S.; Berkland, C. Injectable PLGA Based Colloidal Gels for Zero-Order Dexamethasone Release in Cranial Defects. *Biomaterials* **2010**, *31*, 4980–4986.

(18) Celikkin, N.; Simó Padial, J.; Costantini, M.; Hendrikse, H.; Cohn, R.; Wilson, C.; Rowan, A.; Święszkowski, W. 3D Printing of Thermoresponsive Polyisocyanide (PIC) Hydrogels as Bioink and Fugitive Material for Tissue Engineering. *Polymers (Basel).* **2018**, *10*, 555.

(19) Highley, C. B.; Rodell, C. B.; Burdick, J. A. Direct 3D Printing of Shear-Thinning Hydrogels into Self-Healing Hydrogels. *Adv. Mater.* **2015**, *27*, 5075–5079.

(20) Censi, R.; Schuurman, W.; Malda, J.; di Dato, G.; Burgisser, P. E.; Dhert, W. J. A.; van Nostrum, C. F.; di Martino, P.; Vermonden, T.; Hennink, W. E. A Printable Photopolymerizable Thermosensitive p(HPMAm-Lactate)-PEG Hydrogel for Tissue Engineering. *Adv. Funct. Mater.* **2011**, *21*, 1833–1842.

(21) Chenite, A.; Chaput, C.; Wang, D.; Combes, C.; Buschmann, M. .; Hoemann, C. .; Leroux, J. .; Atkinson, B. .; Binette, F.; Selmani, A. Novel Injectable Neutral Solutions of Chitosan Form Biodegradable Gels in Situ. *Biomaterials* **2000**, *21*, 2155–2161.

(22) Garty, S.; Kimelman-Bleich, N.; Hayouka, Z.; Cohn, D.; Friedler, A.; Pelled, G.; Gazit, D. Peptide-Modified "Smart" Hydrogels and Genetically Engineered Stem Cells for Skeletal Tissue Engineering. *Biomacromolecules* **2010**, *11*, 1516–1526.

(23) Wang, Q.; Wang, L.; Detamore, M. S.; Berkland, C. Biodegradable Colloidal Gels as Moldable Tissue Engineering Scaffolds. *Adv. Mater.* **2008**, *20*, 236–239.

(24) Jones, M.-C.; Leroux, J.-C. Polymeric Micelles – a New Generation of Colloidal Drug Carriers. *Eur. J. Pharm. Biopharm.* **1999**, *48*, 101–111.

(25) Aguado, B. A.; Mulyasasmita, W.; Su, J.; Lampe, K. J.; Heilshorn, S. C. Improving Viability of Stem Cells during Syringe Needle Flow through the Design of Hydrogel Cell Carriers. *Tissue Eng. Part A* **2012**, *18*, 806–815.

(26) Yan, C.; Altunbas, A.; Yucel, T.; Nagarkar, R. P.; Schneider, J. P.; Pochan, D. J. Injectable Solid Hydrogel: Mechanism of Shear-Thinning and Immediate Recovery of Injectable β-Hairpin Peptide Hydrogels. *Soft Matter* **2010**, *6*, 5143.

(27) Wang, S.; Lee, J. M.; Yeong, W. Y. Smart Hydrogels for 3D Bioprinting. *Int. J. Bioprinting* **2015**, *1*, 3–14.

(28) Kolesky, D. B.; Truby, R. L.; Gladman, A. S.; Busbee, T. A.; Homan, K. A.; Lewis, J. A. 3D Bioprinting of Vascularized, Heterogeneous Cell-Laden Tissue Constructs. *Adv. Mater.* **2014**, *26*, 3124–3130.

(29) Mortensen, K. Structural Studies of Aqueous Solutions of PEO - PPO - PEO Triblock Copolymers, Their Micellar Aggregates and Mesophases; a Small-Angle Neutron Scattering Study. *J. Phys. Condens. Matter* **1999**, *8*, A103–A124.

(30) Prud'homme, R. K.; Wu, G.; Schneider, D. K. Structure and Rheology Studies of Poly(Oxyethylene−oxypropylene−oxyethylene) Aqueous Solution. *Langmuir* **1996**, *12*, 4651–4659.

(31) Alexandridis, P.; Holzwarthf, J. F.; Hatton, T. A. Micellization of Poly (Ethy1ene Oxide) -Poly (Propy1ene Oxide) -Poly (Ethy1ene Oxide) Triblock Copolymers in Aqueous Solutions : Thermodynamics of Copolymer Association. *Macromolecules* **1994**, *27*, 2414–2425.

(32) Zhang, M.; Vora, A.; Han, W.; Wojtecki, R. J.; Maune, H.; Le, A. B. A.; Thompson, L. E.; McClelland, G. M.; Ribet, F.; Engler, A. C.; Nelson, A. Dual-Responsive Hydrogels for Direct-Write 3D Printing. *Macromolecules* **2015**, *48*, 6482–6488.

(33) Chu, B.; Liu, T.; Wu, C.; Zhou, Z.; Mark Nace, V. Structures and Properties of Block Copolymers in Solution. *Macromol. Symp.* **1997**, *118* (1), 221–227.

(34) Nguyen-Misra, M.; Mattice, W. L. Micellization and Gelation of Symmetric Triblock Copolymers with Insoluble End Blocks. *Macromolecules* **1995**, *28*, 1444–1457.

(35) Baleara, N. P.; Tirrell, M.; Lodge, T. P. Micelle Formation of BAB Triblock Copolymers in Solvents That Preferentially Dissolve the A Block. *Macromolecules* **1991**, *24*, 1975–1986.

(36) Kumi, B. C.; Hammouda, B.; Greer, S. C. Self-Assembly of the Triblock Copolymer 17R4 Poly(Propylene Oxide)-Poly(Ethylene Oxide)-Poly(Propylene Oxide) in D2O. *J. Colloid Interface Sci.* **2014**, *434*, 201–207.

(37) Guvendiren, M.; Lu, H. D.; Burdick, J. A. Shear-Thinning Hydrogels for Biomedical Applications. *Soft Matter* **2012**, *8* (2), 260–272.

(38) Rodriguez, C. G.; Ferrier, R. C.; Helenic, A.; Lynd, N. A. Ring-Opening Polymerization of Epoxides: Facile Pathway to Functional Polyethers via a Versatile Organoaluminum Initiator. *Macromolecules* **2017**, *50*, 3121–3130.

(39) Lee, B. F.; Wolffs, M.; Delaney, K. T.; Sprafke, J. K.; Leibfarth, F. A.; Hawker, C. J.; Lynd, N. A. Reactivity Ratios and Mechanistic Insight for Anionic Ring-Opening Copolymerization of Epoxides. *Macromolecules* **2012**, *45*, 3722–3731.

(40) Satoh, Y.; Miyachi, K.; Matsuno, H.; Isono, T.; Tajima, K.; Kakuchi, T.; Satoh, T.

Synthesis of Well-Defined Amphiphilic Star-Block and Miktoarm Star Copolyethers via t-Bu-P4-Catalyzed Ring-Opening Polymerization of Glycidyl Ethers. *Macromolecules* **2016**, *49*, 499–509.

(41) Lee, B. F.; Kade, M. J.; Chute, J. A.; Gupta, N.; Campos, L. M.; Fredrickson, G. H.; Kramer, E. J.; Lynd, N. A.; Hawker, C. J. Poly(Allyl Glycidyl Ether)-A Versatile and Functional Polyether Platform. *J. Polym. Sci. Part A Polym. Chem.* **2011**, *49*, 4498–4504.

(42) Herzberger, J.; Niederer, K.; Pohlit, H.; Seiwert, J.; Worm, M.; Wurm, F. R.; Frey, H. Polymerization of Ethylene Oxide, Propylene Oxide, and Other Alkylene Oxides: Synthesis, Novel Polymer Architectures, and Bioconjugation. *Chem. Rev.* **2016**, *116*, 2170–2243.

(43) Yahiaoui, A.; Hachemaoui, A.; Belbachir, M. Cationic Polymerization of Ethylene Oxide with Maghnite-H as a Clay Catalyst in the Presence of Ethylene Glycol. *J. Appl. Polym. Sci.* **2009**, *113*, 535–540.

(44) Rodriguez, C. G.; Ferrier, R. C.; Helenic, A.; Lynd, N. A. Ring-Opening Polymerization of Epoxides: Facile Pathway to Functional Polyethers via a Versatile Organoaluminum Initiator. *Macromolecules* **2017**, *50*, 3121–3130.

(45) Ogura, M.; Tokuda, H.; Imabayashi, S. I.; Watanabe, M. Preparation and Solution Behavior of a Thermoresponsive Diblock Copolymer of Poly(Ethyl Glycidyl Ether) and Poly(Ethylene Oxide). *Langmuir* **2007**, *23*, 9429–9434.

(46) Aoki, S.; Koide, A.; Imabayashi, S.; Watanabe, M. Novel Thermosensitive Polyethers Prepared by Anionic Ring-Opening Polymerization of Glycidyl Ether Derivatives. *Chem. Lett.* **2002**, *31*, 1128–1129.

(47) Klouda, L.; Mikos, A. G. Thermoresponsive Hydrogels in Biomedical Applications. *Eur. J. Pharm. Biopharm.* **2008**, *68*, 34–45.

(48) Aseyev, V.; Tenhu, H.; Winnik, F. M. Non-Ionic Thermoresponsive Polymers in Water. *Adv. Polym. Sci.* **2011**, *242*, 29–89.

(49) Southall, N. T.; Dill, K. A.; Haymet, A. D. J. A View of the Hydrophobic Effect. *J. Phys. Chem. B* **2002**, *106*, 521–533.

(50) Chandler, D. Interfaces and the Driving Force of Hydrophobic Assembly. *Nature* **2005**, *437* (7059), 640–647.

(51) Magenau, A. J. D.; Richards, J. A.; Pasquinelli, M. A.; Savin, D. A.; Mathers, R. T. Systematic Insights from Medicinal Chemistry To Discern the Nature of Polymer Hydrophobicity. *Macromolecules* **2015**, *48* (19), 7230–7236.

(52) Schild, H. G. Poly(N-Isopropylacrylamide): Experiment, Theory, and Application. *Prog. Polym. Sci* **1992**, *17*, 163–249.

(53) Isono, T.; Miyachi, K.; Satoh, Y.; Sato, S.; Kakuchi, T.; Satoh, T. Design and Synthesis

of Thermoresponsive Aliphatic Polyethers with a Tunable Phase Transition Temperature. *Polym. Chem.* **2017**, *8*, 5698–5707.

(54) Halacheva, S.; Rangelov, S.; Tsvetanov, C. Poly(Glycidol)-Based Analogues to Pluronic Block Copolymers. Synthesis and Aqueous Solution Properties. *Macromolecules* **2006**, *39*, 6845–6852.

(55) Lutz, J. F.; Hoth, A. Preparation of Ideal PEG Analogues with a Tunable Thermosensitivity by Controlled Radical Copolymerization of 2-(2-Methoxyethoxy)Ethyl Methacrylate and Oligo(Ethylene Glycol) Methacrylate. *Macromolecules* **2006**, *39*, 893–896.

(56) Reinicke, S.; Schmelz, J.; Lapp, A.; Karg, M.; Hellweg, T.; Schmalz, H. Smart Hydrogels Based on Double Responsive Triblock Terpolymers. *Soft Matter* **2009**, *5*, 2648–2657.

(57) Schilli, C. M.; Zhang, M.; Rizzardo, E.; Thang, S. H.; Chong, Y. K.; Edwards, K.; Karlsson, G.; Müller, A. H. E. A New Double-Responsive Block Copolymer Synthesized via RAFT Polymerization: Poly(N-Isopropylacrylamide)-Block-Poly(Acrylic Acid). *Macromolecules* **2004**, *37*, 7861–7866.

(58) Ward, M. A.; Georgiou, T. K. Thermoresponsive Terpolymers Based on Methacrylate Monomers: Effect of Architecture and Composition. *J. Polym. Sci. Part A Polym. Chem.* **2010**, *48*, 775–783.

(59) Ward, M. A.; Georgiou, T. K. Thermoresponsive Triblock Copolymers Based on Methacrylate Monomers: Effect of Molecular Weight and Composition. *Soft Matter* **2012**, *8*, 2737–2745.

(60) Constantinou, A. P.; Georgiou, T. K. Thermoresponsive Gels Based on ABC Triblock Copolymers: Effect of the Length of the PEG Side Group. *Polym. Chem.* **2016**, *7*, 2045–2056.

(61) Ward, M. A.; Georgiou, T. K. Multicompartment Thermoresponsive Gels: Does the Length of the Hydrophobic Side Group Matter? *Polym. Chem.* **2013**, *4*, 1893–1902.

(62) Geng, H.; Song, H.; Qi, J.; Cui, D. Sustained Release of VEGF from PLGA Nanoparticles Embedded Thermo-Sensitive Hydrogel in Full-Thickness Porcine Bladder Acellular Matrix. *Nanoscale Res. Lett.* **2011**, *6*, 312.

(63) Alexandridis, P.; Alan Hatton, T. Poly(Ethylene Oxide)-Poly(Propylene Oxide)-Poly(Ethylene Oxide) Block Copolymer Surfactants in Aqueous Solutions and at Interfaces: Thermodynamics, Structure, Dynamics, and Modeling. *Colloids Surfaces A Physicochem. Eng. Asp.* **1995**, *96*, 1–46.

(64) Teodorescu, M.; Negru, I.; Stanescu, P. O.; Drghici, C.; Lungu, A.; Sârbu, A. Thermogelation Properties of Poly(N-Isopropylacrylamide)-Block- Poly(Ethylene Glycol)-Block-Poly(N-Isopropylacrylamide) Triblock Copolymer Aqueous Solutions. *React. Funct. Polym.* **2010**, *70*, 790–797.

(65) Negru, I.; Teodorescu, M.; Stçănescu, P. O.; Drăghici, C.; Lungu, A.; Sârbu, A. Poly(N-Isopropylacrylamide-Co-N-t-Butylacrylamide)-Block-Poly(Ethylene Glycol)-Block-Poly(N-Isopropylacrylamide-Co-N-t-Butylacrylamide) Triblock Copolymers: Synthesis and Thermogelation Properties of Aqueous Solutions. *Colloid Polym. Sci.* **2013**, *291*, 2523–2532.

(66) Homan, K. A.; Kolesky, D. B.; Skylar-Scott, M. A.; Herrmann, J.; Obuobi, H.; Moisan, A.; Lewis, J. A. Bioprinting of 3D Convoluted Renal Proximal Tubules on Perfusable Chips. *Sci. Rep.* **2016**, *6*, 34845.

(67) Kolesky, D. B.; Homan, K. A.; Skylar-Scott, M. A.; Lewis, J. A. Three-Dimensional Bioprinting of Thick Vascularized Tissues. *Proc. Natl. Acad. Sci.* **2016**, *113*, 3179–3184.

(68) Basu, A.; Saha, A.; Goodman, C.; Shafranek, R. T.; Nelson, A. Catalytically Initiated Gel-in-Gel Printing of Composite Hydrogels. *ACS Appl. Mater. Interfaces* **2017**, *9*, 40898–40904.

(69) Smith, P. T.; Basu, A.; Saha, A.; Nelson, A. Chemical Modification and Printability of Shear-Thinning Hydrogel Inks for Direct-Write 3D Printing. *Polymer (Guildf).* **2018**, *152*, 42–50.

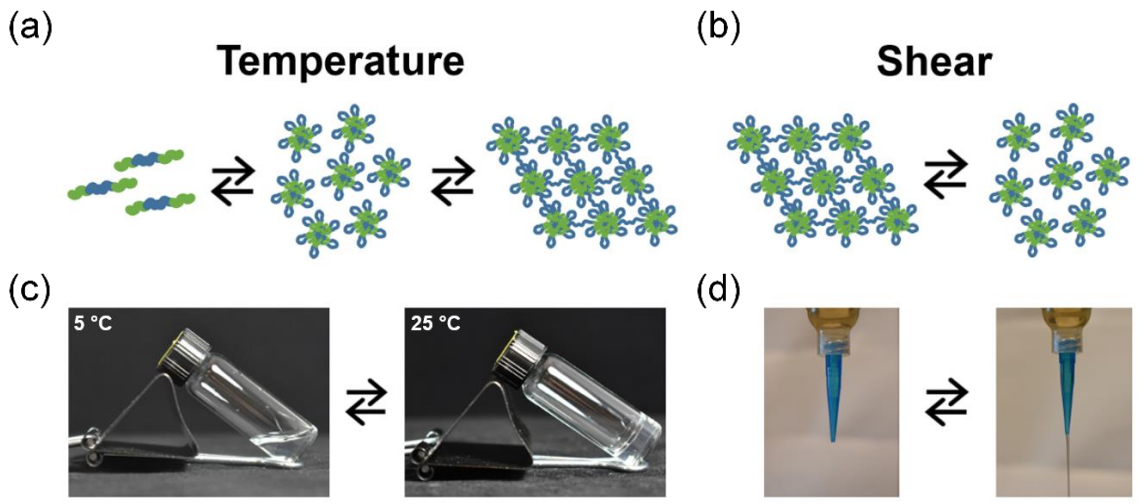

Figure 2.1 Graphical representations of (a) the temperature-dependent equilibrium between unimers (low temperature) and a flower micelle network (high temperature) and (b) the shear stress-induced breaking of physical crosslinks for the poly(alkyl glycidyl ether)-*block*-poly(ethylene oxide)-*block*-poly(alkyl glycidyl ether) triblock copolymer platform. Representative photographs that demonstrate the macroscale (c) thermo-responsive sol (5 °C) to gel (25 °C) transition and (d) extrusion activated shear-responsive properties of a 20 wt% hydrogel of polymer 9 (0.41 mm inner diameter nozzle).

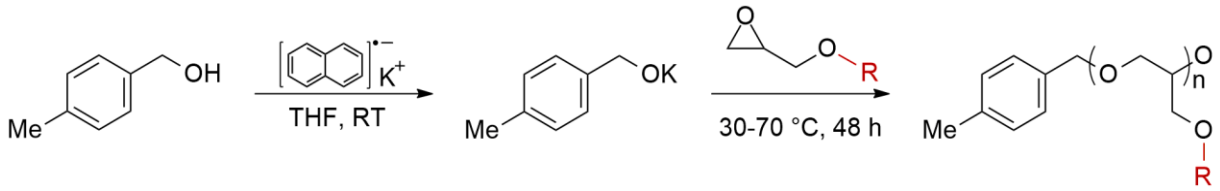

Scheme 2.1 Synthesis of poly(alkyl glycidyl ether)s wherein R represents methyl, ethyl, allyl, isopropyl, or n-propyl groups.

Table 2.1 Characteristics of poly(alkyl glycidyl ether) homopolymers

R Group	M_n (g mol^{-1})[a]	Đ[b]	T_{cp} (°C)[c]
Methyl	2.1k	1.14	45.0
Ethyl	3.0k	1.09	10.0
Ethyl	9.5k	1.12	11.1
Ethyl	24.5k	1.14	10.8
Allyl	3.3k	1.18	—[d]
Allyl	5.8k	1.10	—[d]
Allyl	11.7k	1.15	—[d]
Isopropyl	4.0k	1.08	—[d]
Isopropyl	7.7k	1.11	—[d]
Isopropyl	16.0k	1.22	—[d]
n-propyl	3.2k	1.16	—[d]
n-propyl	8.0k	1.16	—[d]

[a]Number average molecular weight (M_n) was determined by ^{1}H NMR Spectroscopy. [b]Dispersity (Đ) was determined by GPC. [c]Cloud point temperatures (T_{cp}) was determined by UV-Vis Spectroscopy. [d]The T_{cp} of these homopolymers could not be determined due to aqueous insolubility at all temperatures.

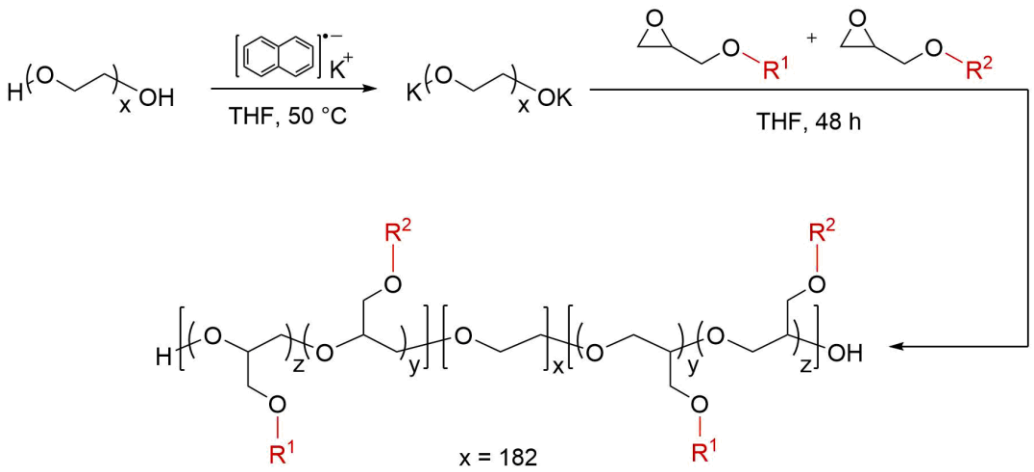

Scheme 2.2 Synthesis of ABA Triblock Copolymers, wherein R represents ethyl, allyl, and isopropyl groups

Table 2.2 Characteristics of poly(alkyl glycidyl ether)-*block*-PEO-*block*-poly(alkyl glycidyl ether) triblock copolymers

	Side Chain (R_1/R_2)	M_n (g mol^{-1})[a]	DP (z/y)[a]	Đ[b]	T_{cp} (°C)[c]
Polymer **1**	Ethyl	1.5k-*b*-8k-*b*-1.5k	14.8	1.10	60.0
Polymer **2**	Allyl	1.4k-*b*-8k-*b*-1.4k	12.4	1.11	29.7
Polymer **3**	Isopropyl	1.8k-*b*-8k-*b*-1.8k	15.2	1.16	24.2
Polymer **4**	Ethyl/Allyl	1.7k-*b*-8k-*b*-1.7k	5.6/9.6 (15.2)	1.11	43.1
Polymer **5**	Ethyl/Isopropyl	1.7k-*b*-8k-*b*-1.7k	10.6/5.0 (15.6)	1.11	46.2
Polymer **6**	Ethyl/Isopropyl	1.7k-*b*-8k-*b*-1.7k	5.4/10.2 (15.6)	1.16	32.4
Polymer **7**	Ethyl/Isopropyl	1.4k-*b*-8k-*b*-1.4k	6.5/6.3 (12.8)	1.15	49.3
Polymer **8**	Ethyl/Isopropyl	1.8k-*b*-8k-*b*-1.8k	8.2/7.9 (16.1)	1.12	40.3
Polymer **9**	Ethyl/Isopropyl	2.2k-*b*-8k-*b*-2.2k	9.8/9.9 (19.7)	1.11	31.3
Polymer **10**	Ethyl/Isopropyl	2.8k-*b*-8k-*b*-2.8k	12.6/12.7 (25.3)	1.14	24.1

[a]Number average molecular weight (M_n) and degree of polymerization (DP) were determined by ^{1}H NMR Spectroscopy. [b]Dispersity (Đ) was determined by GPC. [c]Cloud point temperature (T_{cp}) was determined by UV-Vis Spectroscopy.

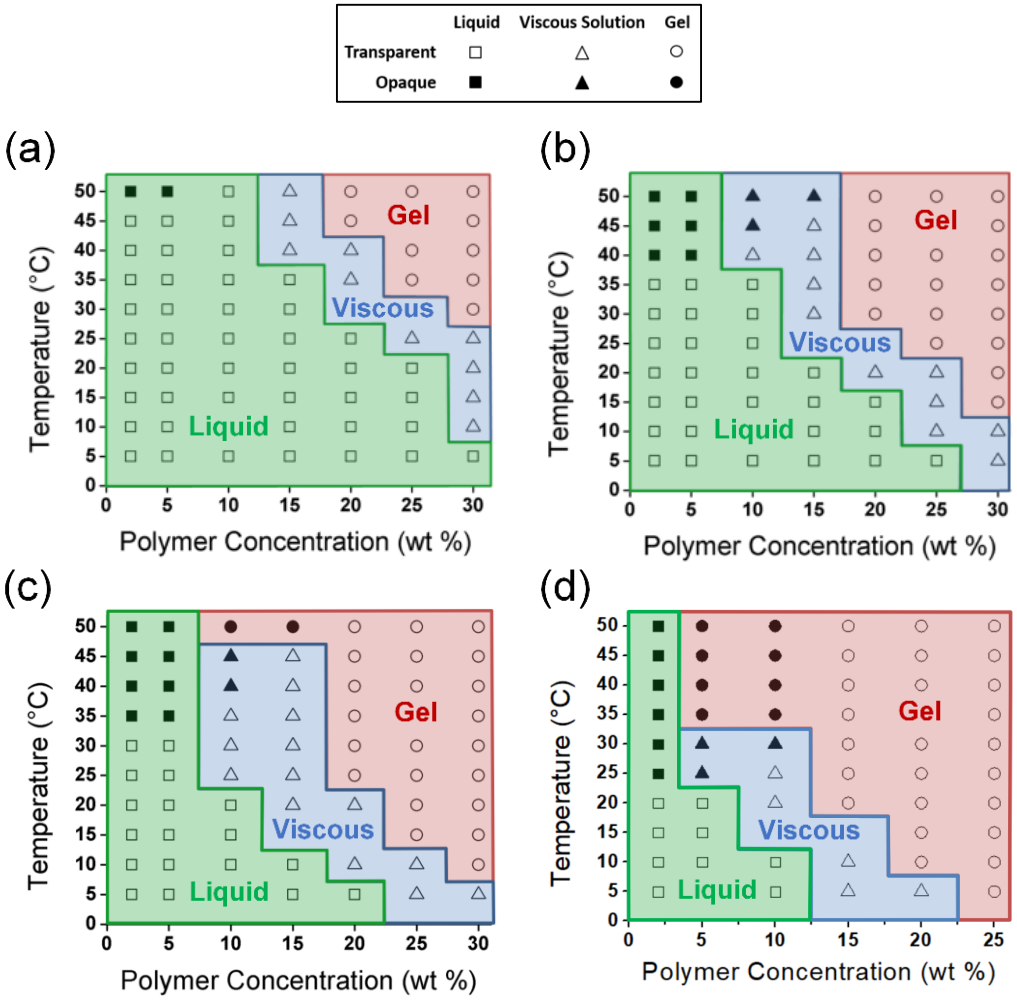

Figure 2.2 Temperature-concentration phase diagrams summarizing the solution and hydrogel states of triblock copolymers of the same total block length containing (a) 5.0 iPGE units (polymer 5), (b) 7.9 iPGE units (polymer 8), (c) 10.2 iPGE units (polymer 6), and (d) 15.2 iPGE units (polymer 3). The green/blue/red shaded areas indicate formulations existing as transparent/opaque liquids (□/■), viscous solutions (△/▲), and gels (○/●), respectively. Transparent formulations are clear with no turbidity. Opaque formulations are turbid and optically cloudy. Their physical states were determined using the vial inversion method.

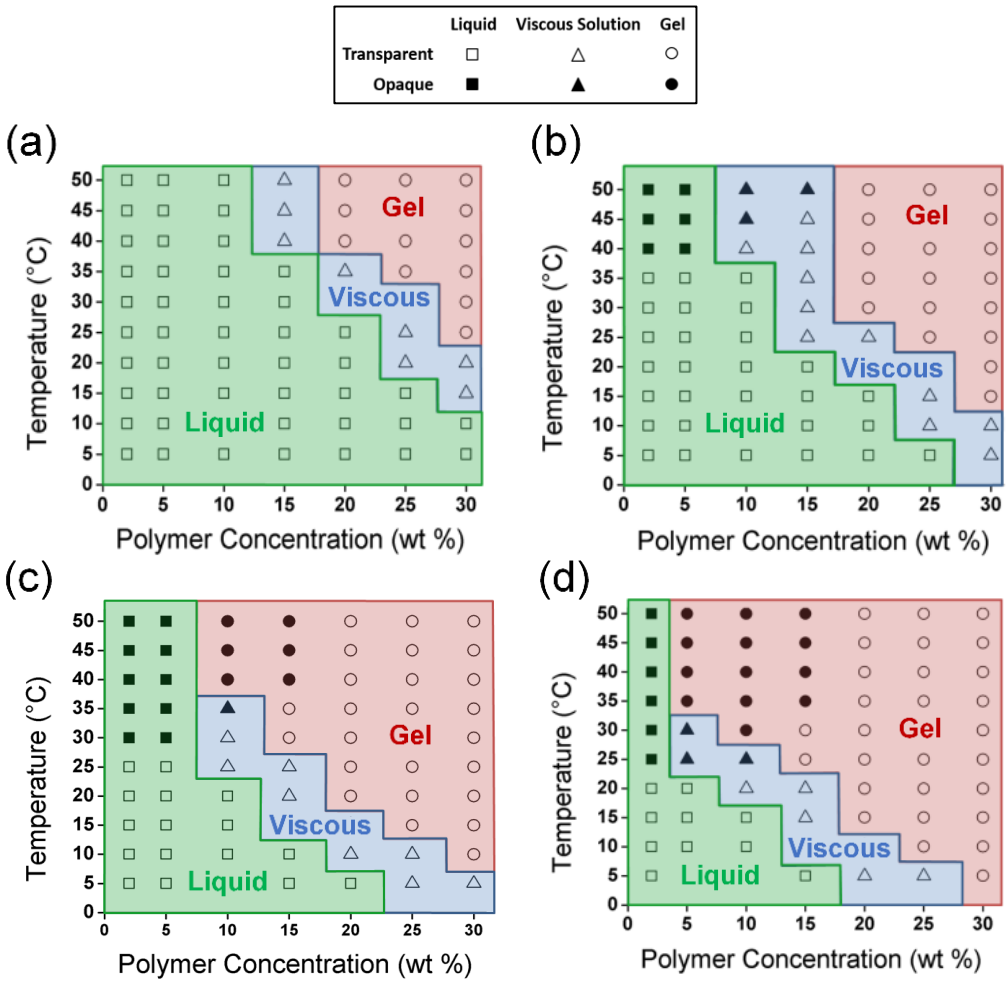

Figure 2.3 Temperature-concentration phase diagrams summarizing the solution and hydrogel states of triblock copolymers with increasing DP (a) 12.8 (polymer 7), (b) 16.1 (polymer 8), (c) 19.7 (polymer 9), and (d) 25.3 (polymer 10). The green/blue/red shaded areas indicate transparent/opaque liquids (□/■), viscous solutions (△/▲), and gels (○/●), respectively. Transparent formulations are clear with no turbidity. Opaque formulations are turbid and optically cloudy. Their physical states were determined using the vial inversion method.

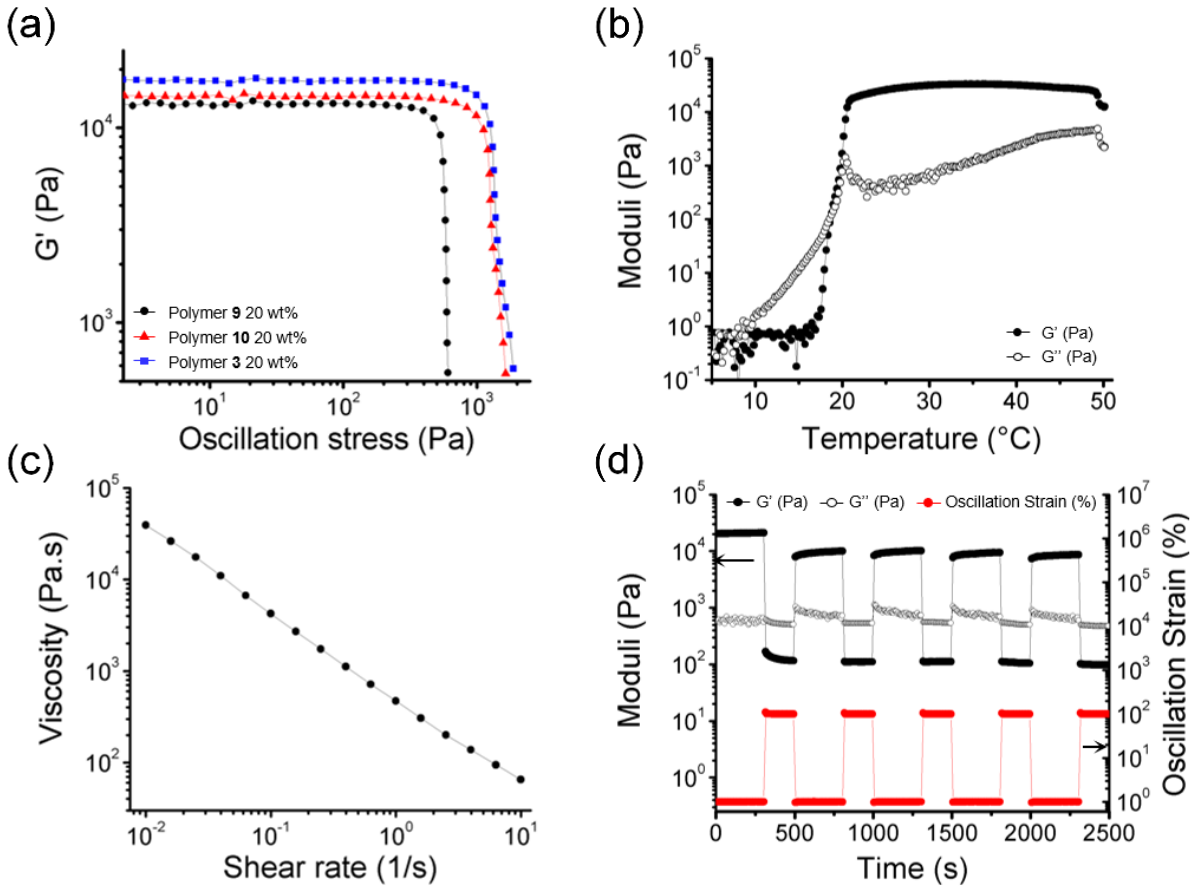

Figure 2.4 Rheological experiments (a) Oscillatory stress experiment indicating yield stress. Yield stress values = 569, 1200, and 1252 for 20 wt% solutions of polymer 9, 10, and 3, respectively. (b) Dynamic oscillatory temperature ramp displaying elastic (G', filled) and viscous (G'', open) moduli. T_{gel} = 18.72 °C (c) Viscosity vs shear rate experiment depicting shear-thinning behavior by a decrease in viscosity with increasing shear rate and (d) Cyclic strain experiment demonstrating rapid recovery of hydrogel elastic modulus (black circles) from periods of high (100%) to low (1%) oscillatory strain (red circles). Arrows indicate reference axis; elastic/viscous moduli (left axis) and oscillatory strain (right axis).

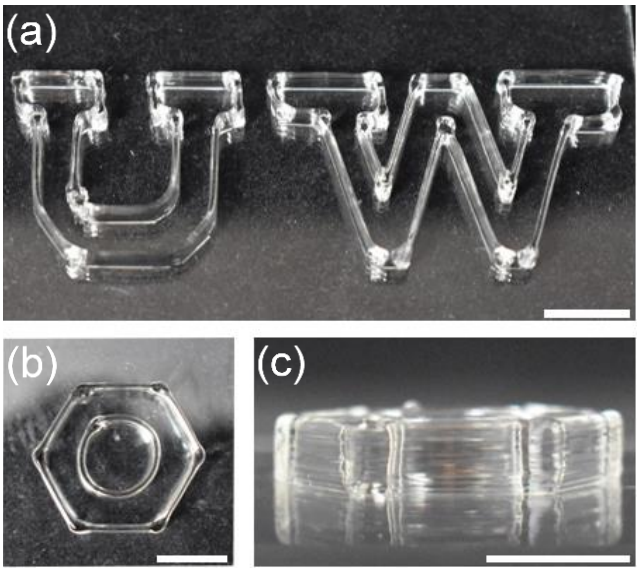

Figure 2.5 3D printed structures of a 15-layer (a) University of Washington initials and (b-c) benzene ring with a 0.41 mm inner diameter nozzle at 8.0 mm s^{-1}. This structure was printed with a formulation of polymer 9 at 20 wt% using a pneumatic direct-write 3D printer (scale bars: 1 cm).

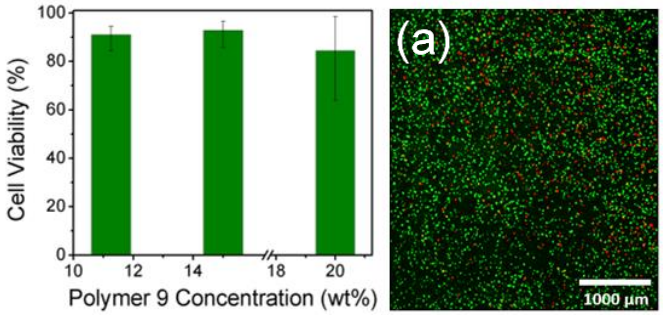

Figure 2.6 Evaluation of a LIVE/DEAD® assay performed on three polymer 9 hydrogels at different concentrations (11.25, 15, 20 wt%). (a) Composite channel confocal microscopy image of encapsulated HeLa cells (11.25 wt%) (scale bar: 1000 µm).

CHAPTER 3: **POLY(ALKYL GLYCIDYL ETHER) HYDROGELS FOR HARNESSING THE BIOACTIVITY OF ENGINEERED MICROBES**

3.1 ABSTRACT

Herein, we describe a method to produce yeast-laden hydrogel inks for direct-write 3D printing cuboidal lattices for immobilized whole-cell catalysis. A poly(alkyl glycidyl ether)-based triblock copolymer was designed to have three important features for this application: (1) a temperature response which allowed for facile processing of the material; (2) the shear response which facilitated the extrusion of the material through a nozzle; and (3) a UV-light induced polymerization which enabled the post extrusion chemical crosslinking of network chains, and the fabrication of robust printed objects. These three key stimuli responses were confirmed via rheometrical characterization. A genetically engineered yeast strain with an upregulated α-factor production pathway was incorporated into the hydrogel ink and 3D printed. The immobilized yeast cells exhibited adequate viability of 87.5% within the hydrogel. The production of the up-regulated α-factor was detected using a detecting yeast strain and quantified at 268 nM (s = 34.6 nM) over 72 h. The reusability of these bioreactors was demonstrated by immersion of the yeast-laden hydrogel lattice in fresh SC media and confirmed by the detection of similar amounts of up-regulated α-factor 259 nM (s = 45.1 nM). These yeast-laden materials represent an attractive opportunity for whole-cell catalysis of other high-value products in a sustainable and continuous manner.

3.2 INTRODUCTION

Whole-cell biocatalysis is a standard practice across a wide range of industries wherein cells are used to transform molecular precursors into a product of interest (antibiotics, drugs, vitamins, insulin, vaccines, etc.). These reactions are generally employed as a batch process wherein the cells and the necessary molecular precursors are combined into a single reaction vessel, stirred for several days, and then the product is isolated from the complex mixture.[1–10] However, batch cell reactors are costly and time consuming because they require sterile conditions, can have low yields, and purification protocols are labor and cost intensive. Immobilized-cell bioreactors, wherein metabolically active cells are trapped within a material such as a hydrogel, offer an alternative method that can simplify the isolation of the product, minimize product inhibition or toxicity, and allow recycling of the cells.[11]

We have previously reported additive manufactured catalytically active living materials (AMCALM) as a platform for immobilized-cell bioreactors.[12] In contrast to previous reports wherein calcium alginate beads[13–16] or electrospun fibers[17–19] were used to encapsulate microbes for fermentation, our approach utilized customized lattices of yeast-laden hydrogels that were printed using a direct-write 3D printer. Additive manufacturing (or 3D printing) is a fabrication process that utilizes layer-by-layer material deposition to construct three-dimensional geometries according to a computer-aided design (CAD) model.[20–27] As such, 3D printing is well-suited for manufacturing living materials[28–33] with spatial and geometrical organization of cells. Hydrogel-based materials are particularly attractive as cell-laden inks for direct-write 3D printing because these materials can recapitulate some of the chemical and physical attributes of the extracellular matrix that exists in biofilms, living tissue, and other naturally occurring microenvironments.[31,34–

[36] These features could include the presence of ligands or functional groups,[37–40] or the stiffness of the hydrogel.[41,42]

There were three important features of the yeast-laden hydrogel ink that were developed for AMCALMs: (1) a temperature response, wherein the material exhibited a reversible gel-to-sol transition upon cooling, that enabled homogeneous dispersion of the yeast cells within the gel and facile loading of the hydrogel into a syringe; (2) a shear-thinning response that facilitated the extrusion of the hydrogel ink from a nozzle to enable the layer-by-layer formation of three-dimensional objects; and (3) an irreversible photo-response wherein polymerizable groups chemically cross-linked the hydrogel into a robust structure. Yeast-laden hydrogel lattices were printed and then utilized in a continuous batch process for the fermentation of glucose to produce ethanol.

Herein, we demonstrate a new polymer hydrogel for the encapsulation and direct-write 3D printing of yeast-laden hydrogel lattices that can be used for the production of a polypeptide. The poly(glycidyl ether)-based ABA triblock copolymer (polymer 2) has similar features (temperature-, shear-, and photo-responses, Figure 3.1) to the Pluronic-based triblock copolymer that was reported previously.[12] Furthermore, a genetically-engineered yeast strain with an upregulated α-factor production pathway was incorporated into the hydrogel to demonstrate the production of an extracellularly excreted polypeptide from the yeast-laden hydrogel. While α-factor is a yeast hormone that does not have any known therapeutic effects, the polypeptide is commonly utilized in the expression and recovery of recombinant proteins.[43,44] When the α-factor leader sequence is appended to the genetic code for an engineered protein, the yeast cell utilizes its native cellular machinery to secrete the protein beyond the cell membrane.[45–50] In our experiments, we not only

demonstrate that the secreted α-factor can be detected in the liquid media surrounding the hydrogel lattice, but also the reusability of the yeast-laden hydrogel lattices.

3.3 Materials and Methods

3.3.1 Materials

All chemicals and solvents were purchased from Sigma-Aldrich or Fisher Scientific and used without further purification unless noted otherwise. Isopropyl glycidyl ether (iPGE, 98%) and ethyl glycidyl ether (EGE, 98%) were dried over CaH_2 for 24 h, distilled into a flask containing butyl magnesium chloride (2 M in tetrahydrofuran, THF), re-distilled, and stored under N_2 atmosphere. Poly(ethylene oxide) (PEO, M_n 8000 g mol^{-1}) was dried under vacuum overnight prior to use. Dry THF was obtained using neutral alumina using a Pure Process Technology solvent purification system. A potassium naphthalenide solution (1M) was prepared by dissolving naphthalene (3.2 g) in THF (25 mL), adding potassium (0.975 g), and storing under N_2 atmosphere. ^{1}H NMR spectra were obtained on a Bruker Advance 300 or 500 MHz spectrometer. Gel permeation chromatography was performed using a Waters chromatograph equipped with two 10 μm Malvern columns (300 mm x 7.8 mm) connected in series with increasing pore size (1,000, 10,000 Å), using chloroform (Optima, 0.1% v/v trimethylamine) as the eluent, and calibrated with poly(ethylene oxide) standards (400 to 40, 000 g mol^{-1}). The relative molecular weights were measured in chloroform using poly(ethylene oxide) standards and a refractive index detector (flow rate: 1 mL min^{-1}). Drop-out Mix Complete without Yeast Nitrogen Base D9515) and Yeast Nitrogen Base (Y2025) were purchased from US Biological Life Sciences. Sytox Green nucleic acid strain (5 mM solution in DMSO; Invitrogen) was purchased from Thermo Fisher Scientific.

3.3.2 Yeast Strains

For microscopy and live/dead viability tests, the strain yJS001 was used (genotype SO992 mfa2::pTEF1_mCherry(kanR)). This strain constitutively expressed mCherry protein, which facilitated characterization using fluorescence microscopy. *Saccharomyces cerevisiae* strain SO992 was used as the control strain in the α-factor production experiments. This strain is a derivative of W303 (genotype MATa ura3 leu2 trp1 his3 can1R ade).

As the α factor-producing strain, we employed a genetically modified MAT-α yeast strain ('secreting strain') expressing the *S. cerevisiae* gene MFα1 (YPL187W) on a constitutively-expressed promoter pGPD (natively expressing YPL197W). The MFα1 gene expresses 3 copies of the α-factor peptide, a 13-amino acid peptide natively used as mating hormone from the MAT-α to the MAT-A strains.

To quantify the α-factor secreted from the yeast immobilized in the hydrogels, we employed a genetically modified MAT-A yeast strain that expresses the fluorescence protein yeVenus driven by the pFUS1 promoter, which is downstream the MAPK signaling pathway, activated by α-factor detection ('detecting strain'). The MAT-A native strain was engineered by deleting BAR1 (native α-factor protease) and integrating the POG1 gene on a constitutively-expressed pGPD promoter to avoid α-factor-induced growth arrest.

Yeast transformations were carried out using a standard lithium acetate protocol. Yeast cells were made competent by growing 50 mL cultures in rich media to log growth phase, then spinning down the cells and washing with H20. Next, linearized DNA, salmon sperm donor DNA, 50% polyethylene glycol and 1M LiOAc were combined with 50 mL of competent cells and the mixture was heat shocked at 42 °C for 15 min. The cells were then spun down, supernatant was removed,

and they were resuspended in H2O and then plated on selective agar media. Transformations were done into MATa W303-1A and MATα W303-1B background strains.

3.3.3 Synthesis of Polymer 1

The ABA triblock copolymer was synthesized via anionic ring-opening polymerization. PEO (M_n = 8,000 g mol^{-1}, 20 g, 2.5 mmol) was added to the reaction vessel and dried under vacuum overnight. Dry THF (250 mL) was added under an Ar atmosphere and heated to 50 °C to facilitate dissolution of the macroinitiator. Once sufficiently dissolved, a potassium naphthalenide solution (1M in THF) was titrated into the flask until the solution remained a slight green color, indicating full deprotonation of PEO hydroxyl end groups. Isopropyl glycidyl ether (4.94 g, 42.5 mmol) and ethyl glycidyl ether (4.34 g, 42.5 mmol) were added to begin polymerization. The reaction continued for 24 h at 65 °C and was subsequently quenched with a degassed solution of 1% v/v AcOH in MeOH. The reaction mixture was then precipitated into cold hexane. The polymer was collected via centrifugation (4400 rpm, 10 min) and the supernatant decanted. The product was washed twice with additional hexane and collected again in the same manner. The isolated polymer solution was dried in a vacuum oven for at least 24 h to afford polymer **1** as an off-white solid (27.5 g). ^{1}H NMR (500 MHz, $CDCl_3$): δ = 1.15-1.17 (m, -O-CH-(C$\underline{H}_3$)$_2$), 1.17-1.23 (t, -O-CH$_2$-C$\underline{H}_3$, J = 7.0 Hz), 3.47-3.81 (m -O-C$\underline{H}_2$-C$\underline{H}_2$-O- and -O-C$\underline{H}_2$-C$\underline{H}$(C$\underline{H}_2$-O-C$\underline{H}_2$-CH$_3$)-O- and -O-C$\underline{H}_2$-C$\underline{H}$(C$\underline{H}_2$-O-C$\underline{H}$-(CH$_3$)$_2$)-O-).

3.3.4 Synthesis of Polymer 2

Polymer 1 (20g, 1.81 mmol) was dissolved in dry THF (250 mL) under a nitrogen atmosphere until complete dissolution of the polymer. Triethylamine (2.45 mL, 18.1 mmol) was added to increase the reactivity of the polymer hydroxyl chain ends and the mixture was heated at 65 °C for

30 min. Methacrylic anhydride (26.9 mL, 181 mmol) was then added and the reaction mixture was stirred for 16 h at 65 °C. After this time, the reaction was quenched with a degassed solution of 1% v/v AcOH in MeOH. The reaction mixture was then precipitated into cold ether. The polymer was collected via centrifugation (4400 rpm, 10 min) and the supernatant decanted. The product was washed twice with additional ether, once with hexane, and collected again by centrifugation. The isolated polymer was dried in a vacuum oven for 24 h to afford polymer 2 as an off-white solid (16.7g). The degree of functionalization (f_n) was determined by comparing the integrations of the methacrylate vinyl (6.12 and 5.55 ppm) and methyl (1.94 ppm) protons, as well as the PEO chain-end methylene protons (5.08-5.15 ppm), to their theoretical values. For example, 1.99 (vinyl, actual)/2 (vinyl, theoretical) X 100 ≈ 100% functionalization of chain ends. These integration values were referenced to the total alkyl glycidyl ether protons for each polymer chain (1.12-1.20 ppm, 121 H). ^{1}H NMR (300 MHz, $CDCl_3$): δ = 1.12-1.20 (m, -O-CH-(C$\underline{H}_3$)$_2$) and -O-CH$_2$-C$\underline{H}_3$), 1.94 (s, C$\underline{H}_3$C(CO$_2$)=CH$_2$), 3.39-3.89 (m, -O-C$\underline{H}_2$-C$\underline{H}_2$-O- and -O-C$\underline{H}_2$-C$\underline{H}$(C$\underline{H}_2$-O-C$\underline{H}_2$-CH$_3$)-O-, and -O-C$\underline{H}_2$-C$\underline{H}$(C$\underline{H}_2$-O-C$\underline{H}$-(CH$_3$)$_2$)-O-), 5.08-5.15 (m, -CH$_2$-C$\underline{H}$-O-(C=O)), 5.48 (s, $\underline{H}$-CH=C), 6.18 (s, $\underline{H}$-CH=C).

3.3.5 Preparation of Synthetic Complete Media

The SC media (1L) was prepared by dissolving drop-out mix (2 g), yeast nitrogen base (6.7 g), and glucose (20 g) in Milli-Q water. The resulting solution was sterilized by filtration through a 0.2 μm nylon filter.

3.3.6 Preparation of Hydrogel Solution

Polymer **2** was dissolved in sterile, deionized water at a concentration of 20 wt % polymer. The resulting polymer solution was cooled overnight at 5 °C to facilitate hydrogel formation via

LCST behavior. After homogenization of the solution at low temperature, the solution was warmed to 21 °C to induce the formation of a gel state. Hydrogels used to print the proof-of-concept models in Figure 3.3 were mixed with the photo-radical initiator 2-hydroxy-2-methylpropiophenone (10 μL) and centrifuged (4400 rpm, 10 min) to remove bubbles.

3.3.7 Preparation of Yeast-Laden Hydrogel Ink

Three To prepare yeast-laden hydrogels, the aforementioned hydrogel solution was cooled to 5 °C in a refrigerator. At this temperature, the hydrogel solution underwent gel-to-sol transition, affording a free-flowing liquid. Yeast cells were added from an overnight liquid culture, at a concentration of 10^7 cells per gram of hydrogel while the gel was in its solution state. The resulting solution was mixed thoroughly and allowed to equilibrate at 5 °C until all of the bubbles present in the solution were removed. Finally, the hydrogel was warmed to 21 °C to undergo a sol to gel transition, resulting in a shear-responsive gel.

3.3.8 Rheometrical Characterization

For rheometrical characterization of the hydrogels, dynamic oscillatory experiments were performed on a TA Instruments Discovery Hybrid Rheometer-2 (DHR-2) equipped with a Peltier temperature controller. The instrument operates by applying a known displacement (strain) and measuring the material's resistance (stress) to the force. Rheometry experiments were conducted by depositing hydrogel between the rheometer base plate and 20 mm parallel plate geometry with a final gap of 1 mm. Samples were equilibrated in an ice bath for at least 30 min and then were carefully loaded onto the Peltier plate at 5 °C and a preshear experiment was applied to eliminate the bubbles from the sample. The sample was equilibrated at 21 °C for 8 min before each run. The gel yield stress values were measured under oscillatory strain (frequency: 1 Hz, 21 °C) starting

with an initial strain of 0.01% and converted to applied oscillatory stress. Viscosity versus shear rate experiments were performed in the range of shear rates between 0.01 and 100 Hz. Cyclic shear thinning experiments (frequency = 1 Hz) were performed at 21 °C using alternating strains of 1% for 5 min and 100% for 3 min per cycle, to investigate the shear-thinning and recovery behavior of the hydrogels. Temperature ramp experiments were performed at 1 Hz from 5−50 °C at 2 °C min^{-1}. Photocuring was performed using a fully integrated smart swap LED photo curing accessory. A 120 s dwell time (frequency: 1 Hz) elapsed before the UV lamp (365 nm LED with an irradiation intensity of 5 mW cm^{-2}) was turned on for 420 s at a constant oscillatory strain (1%).

3.3.9 Additive Manufacturing (Direct-Write 3D Printing) of a Cuboidal-Lattice

A modified pneumatic direct-write 3D printer was assembled based on a Tronxy P802E 3D Printer kit, from Shenzen Tronxy Technology Co. The printer was controlled with an Arduino using the Marlin firmware. All CAD models were designed in OpenSCAD. G-code commands for the printer were generated using Slic3r. The resulting G-code was modified using Python to introduce required commands for the dispensing of the hydrogel via pneumatic pressure. All printing was performed using a 20 wt % hydrogel ink with an extrusion air pressure of 20 psi, a print speed of 5 mm s^{-1}, and a 0.41 mm inner diameter CML Supply conical nozzle attachment.

The dimensions for the 3D printed lattices are 1.9 cm by 1.9 cm by 1.2 cm and each cube weighed between 1.8 and 2.0 g. Upon completion of the 3D printing, the cubes were irradiated under 365 nm light (at 3.4 mW cm^{-2}) for 3 min to cure and chemically fix the structures.

3.3.10 Microscopy and Imaging

Optical imaging: Images of the 3D-printed hydrogels were captured using an iPhone XS. Confocal imaging: Confocal microscopy images were taken using a Leica TCS SP5 II laser

scanning confocal microscope. All images were taken with a dry 20x objective. MCherry protein fluorescence was excited with a 561 nm laser at 5% laser power, and emission was scanned from 569 to 700 nm. Sytox green viability dye was excited with a 488 nm laser at 5% laser power, and emission was scanned from 500 to 550 nm. Samples were sequentially scanned, and the output images were processed using ImageJ Java software.

3.3.11 Cell Viability Assay

The yeast-laden hydrogel was prepared as described above. This gel was cooled to 5 °C to induce a gel-to-sol transition, which was then poured and spread into a sterile petri dish to produce a thin film (~0.5 mm) of the yeast-laden hydrogel. The sample was irradiated with 365 nm UV light for 3 min. This film was then incubated in fresh SC media at 30 °C, and periodically agitated. The media was exchanged every 24 h to ensure fresh nutrient delivery to the embedded cells. At the imaging intervals described in this work, a small square of the film (5 mm × 5 mm) was cut and removed for staining. Sytox Green stain stock solution was diluted to 5 μM, and 20 μL of the dye solution was exposed to hydrogel sample for 5 min. The sample was then washed with SC media and imaged using a Leica SP5 confocal microscope. Constitutively expressed mCherry protein fluorescence from the yeast cells was measured to indicate live cells, while the Sytox dye fluorescence indicated the presence of dead cells.

3.3.12 α-Factor Production

α-Factor production from 3D printed yeast-laden cuboidal lattices was quantified as follows. A yeast-laden hydrogel ink containing 10^7 yeast cells per gram of hydrogel was direct-write 3D printed and photo-cured (3 min) with 365 nm irradiation. The lattices were then washed with SC media, and placed into 50 mL falcon tubes. The tubes were then filled with 10 mL of SC media

for fermentation and placed in a 30 °C shaker (225 rpm) for incubation. After a period of 72 h, the lattices were removed from the reactors and the media was collected. The fermentation media was filtered with a 0.2 μm nylon filter. The up-regulated yeast strain experiments were performed in triplicate alongside a wild-type yeast-laden lattice.

To determine the reusability of the lattices in subsequent fermentation cycles, the same lattices from the first round of α-factor were again washed individually in sterile SC media. The lattices were then placed into new falcon tubes containing 10 mL of SC media, and incubated at the same conditions for an additional 72 h. After incubation, the samples were collected and prepared for characterization in the same manner as mentioned above.

3.3.13 α-Factor Detection and Quantification

To quantify α-factor synthesis from within the yeast-laden hydrogel, we collected the SC media that was used to submerge the hydrogel sample after 72 h. We collected 9 mL of media for each experimental condition and replicate; each sample was split into six 1.5 mL Eppendorf tube and then dehydrated in a Savant SpeedVac Plus SC110A Concentrator for 12 h at Medium dehydration speed. Subsequently, we added 100 μL of molecular graded water into each dehydrated sample, resuspended, and collected the resulting 600 μL into a single sample. The final sample was run again through the Speed-Vac for 12 h at Medium speed and resuspended into 100 μL of molecular graded water. This process concentrated the initial sample to 90-fold its original concentration.

We experimentally tested for α-factor synthesis using detecting strains with a standard cytometer assay protocol. The detecting strains were grown overnight for 20 h in SC media, then diluted to 30 events/μL again in SC media. After 3 h, we inoculated the concentrated samples from the yeast-laden hydrogels into different vials, plus two extra vials: one kept as control (3 μL of 0.1

M Sodium Acetate) and one was inoculated with 10 μM 98% HPLC-pure α-factor peptide in 0.1 M Sodium Acetate obtained from Zymo Research (Irvine, CA, USA). Samples were collected for cytometer measurement 8 h after induction, and median fluorescence values were computed from the resulting histogram.

Fluorescence intensity of the detecting strain was measured with a BD Accuri C6 flow cytometer equipped with a CSampler plate adapter using excitation wavelengths of 488 and 640 nm and an emission detection filter at 533 nm (FL1 channel). A total of 10,000 events above a 400,000 FSC-H threshold (to exclude debris) were recorded for each sample with and core size of 22 mm using the Accuri C6 CFlow Sampler software. Cytometry data were exported as FCS 3.0 files and processed using custom Python scripts to obtain the median FL1-A value at each data point.

We used a model fitted to data to estimate the amount of α-factor detected by the detecting strain starting from its median fluorescence value response. The model interpolates a titration curve of an α-factor-detecting strain that is equivalent to the one used in this study, except its synthesis yeGFP fluorescent protein instead of yeVenus. The interpolation follows a standard Hill activation function:

$$y = K\frac{u^n}{\varphi + u^n} + y_0$$

where u represents the α-factor input concentration in nM, and y the median fluorescence output. To account for the different fluorescent protein, we used the control and the 10 μM α-factor median fluorescent outputs from this experiment to re-fit K and y_0.

To estimate the amount of α-factor synthesized by our strains in the hydrogel, we inverted the formula above to get:

$$u = \sqrt[n]{\varphi \frac{y - y_0}{K + y_0 - y}}$$

3.4 Results and Discussions

3.4.1 Synthesis and Functionalization of the Triblock Copolymer

ABA triblock copolymers of poly(isopropyl glycidyl ether-*stat*-ethyl glycidyl ether)-*block*-poly(ethylene oxide)-*block*-poly(isopropyl glycidyl ether-*stat*-ethyl glycidyl ether) afford shear-thinning hydrogels that have a tunable sol-gel transition temperature based on the ratio of ethyl and isopropyl glycidyl ether monomers (EGE and iPGE, respectively), 'A' block chain length, and concentration.[51] When these polymers were dissolved in aqueous media, flower-like micelles[52] were expected to form based on the design of this ABA triblock copolymer--hydrophobic 'A' blocks flanking a hydrophilic 'B' block. Hydrogels based on this ABA triblock copolymer platform (20 wt%) were suitable inks for direct-write 3D printing and were able to create self-supporting hydrogel structures.[52] However, the physical cross-links present in this system were insufficient to maintain the integrity of the 3D printed object when subjected to either excess aqueous media or to mechanical loads. Thus, chemically cross-linked hydrogels are necessary to improve the robustness of the 3D printed objects.

Polymer 1 was synthesized (Scheme 3.1) via living anionic ring-opening polymerization[53–56] from a poly(ethylene oxide) (PEO) macroinitiator (M_n = 8,000 g mol^{-1}) with an EGE:iPGE ratio of 1.15:1 to afford triblock copolymers with narrow dispersity (Đ = 1.11). Polymerizable methacrylate groups were introduced onto the chain-ends of polymer 1 to afford polymer 2 (Scheme 3.1). We hypothesized that the resulting polymer hydrogel would maintain its thermal-

and shear-responses pre-extrusion, and then photochemically cross-link post-extrusion. The degree of chain-end functionalization (f_n) was determined by comparing the integrations of the methacrylate vinyl (6.12 and 5.55 ppm) and methyl (1.94 ppm) protons, as well as the PEO chain-end methylene protons (5.08-5.15 ppm), to their theoretical values and was found to be quantitative. The polymer was dissolved water (20 wt %) and 2-hydroxy-2-methylpropiophenone was added as the photo-radical initiator (0.1 wt%) for polymerization of the methacrylate groups.

3.4.2 Rheology of the Functionalized Triblock Copolymer Hydrogel

The viscoelastic properties of a 20 wt% solution of polymer 2 in water were characterized using a rheometer. The temperature-dependent viscoelastic behavior of the gel was confirmed by the presence of a sol-gel transition as defined by the intersection of the elastic (G') and viscous (G") moduli (15.61 °C, Figure 3.2a). The solution maintained a non-viscous, liquid-like morphology at 5 °C and became a self-supporting hydrogel network by 21 °C. The temperature-dependent sol-gel transition was also confirmed visually as shown in the photographs in Figure B1.

Hydrogels based on polymer 2 also exhibited shear-thinning behavior. The viscosity of the material decreased with increasing applied shear rate, which is indicative of a shear thinning hydrogel. An oscillatory strain sweep experiment afforded a yield stress value of 1.33 kPa (Figure B2-B3). A dynamic oscillatory strain experiment (Figure 3.2b) demonstrated the strain dependent viscoelastic behavior of the gel upon repeated cycles of high (100%) and low (1%) strain. Initially under low strain, the material exhibited a gel-like morphology as indicated by greater values for G' relative to G". During periods of high strain, G" exceeded G', which indicated that the gel had a higher viscous character consistent with the material in its sol state. The material rapidly

recovered to its gel state when the strain was reduced to 1% and exhibited very little mechanical hysteresis.

The post-extrusion UV cure of the gel was simulated under constant strain (1%) and frequency (1 Hz). After 120 s of equilibration time, the hydrogel was subjected to 5 mW cm^{-2} of 365 nm UV light for 420 s. The G' of the hydrogel increased from 21.56 kPa to 94.23 kPa within 75 s of UV exposure, and the G" decreased from 1.88 kPa to 0.47 kPa in the same time frame. These changes to the G' and G" were indicative of a rapid chemical crosslinking of the hydrogel network via photo-induced radical polymerization of the methacrylated chain ends (Figure 3.3a).

3.4.3 Direct-Write 3D Printing of Triblock Copolymer Dimethacrylate Hydrogels

Utilizing these three stimuli responses, a proof of concept cuboidal lattice was 3D printed using a pneumatic direct write 3D printer at 5 mm s^{-1} and 20 psi with a 0.41 mm inner diameter conical nozzle. The temperature response allowed for facile processing of the hydrogel into the syringe at 5 °C in its liquid state. The hydrogel was then warmed to ambient temperature and extruded. The shear-response facilitated the extrusion of the hydrogel as rod-like filaments. A cuboidal lattice structure, with dimensions of 1.9 cm by 1.9 cm by 1.2 cm, was cured post-extrusion using a custom-made UV box equipped with two 365 nm A19 UV lamps for 180 s at 3.4 mW cm^{-2} (Figure 3.3b-c).

3.4.4 Incorporation of Yeast Cells and Cell Viability

To ensure the viability of encapsulated yeast cells within the polymer 2 hydrogel, *Saccharomyces cerevisiae* constitutively expressing mCherry fluorescent protein was inoculated into a solution of polymer 2 at 5 °C and mixed to make a homogenous mixture. A film of the resulting yeast-laden solution was cast at the same temperature, subsequently warmed to 21 °C to

induce gelation, and cured to create a physically robust hydrogel film. This yeast-laden film appeared transparent after processing due to the relatively low loading concentration of yeast cells. A small sample of the yeast-laden hydrogel film was extracted, stained, and imaged periodically over seven days. Sytox green staining results showed that cells remained 87.5% viable within the cast hydrogel at the end of the week of imaging, as seen in Figures 3.4a and Figures B4-B6. Significant cell colony growth was observed by both confocal microscopy and optical imaging. This growth was also observed visually, as indicated by the opacity of the 3D-printed hydrogel structure in Figure 3.4b-c. These results suggest that the poly(alkyl glycidyl ether)-based hydrogels are comparable in their ability to house and promote yeast cell viability over time to our previously employed[12] F127-based hydrogels.

3.4.5 α-Factor Production with 3D Printed AMCALMs

An engineered yeast strain with upregulated α-factor production was used to demonstrate AMCALM lattices that produced a polypeptide. The pGPD promoter present in the secreting yeast strain allowed the constitutive expression of the MFα1 gene, and thus, continuous production of the α-factor polypeptide. After the reaction, the aqueous reaction media was exposed to the detecting strain that fluoresced in the presence of α-factor.

These lattices were incubated in SC media for a period of 72 h (Figure 3.5), producing an average of 268 nM (s = 34.6 nM) of α-factor (Figure 3.6). The induced fluorescence response from the cuboidal lattice with the secreting strain was 4.40 times greater that of the control strain cuboidal lattice (without upregulated α-factor), which indicated that the up-regulation of the α-factor pathway was successful in the secreting strain. These results provide evidence that AMCALMs were suitable for the production of polypeptides, and that the products could readily diffuse out from the hydrogel matrix into the surrounding media.

One advantage of using an immobilized yeast platform for polypeptide synthesis is the potential to reuse the printed cuboidal lattices. We investigated the reusability of the poly(alkyl glycidyl ether)-based hydrogel living materials for the continued production of α-factor in subsequent batch reactions. When the printed AMCALMs were removed from their first 72 h incubation, and placed into fresh media, they continued to produce an average of 259 nM (s = 45.1 nM) of α-factor after a second 72 h cycle (Figure 3.6). The second batch production was directly comparable to the output achieved during the first batch reaction, which suggests that these immobilized cell bioreactors could be useful for continuous whole-cell catalysis.

3.5 Conclusion

In conclusion, we developed an ABA triblock copolymer based on a poly(alkyl glycidyl ether) that is suitable for 3D printing yeast-laden hydrogels for whole-cell catalysis. These polymer hydrogels exhibit a temperature, shear, and UV-light responsive behaviors that are integral to the preparation of the hydrogel ink and subsequent printing. The post-extrusion, chemical crosslinking of the polymer micelles induced by UV-light is particularly important to fabricate robust forms that do not degrade or dissolve over time.

The poly(alkyl glycidyl ether) based hydrogels also proved to have a negligible effect on the viability and biological activity of the encapsulated yeast cells. The engineered yeast-laden living materials were shown to be capable of producing an average of 263.5 nM of α-factor during two consecutive batch reactions, exhibiting no significant reduction in efficiency between the two cycles.

In this work, we demonstrated that polypeptides can be produced using the AMCALM platform. This result, combined with the prominence of the α-factor leader sequence in

recombinant protein design and production, suggests that that these materials could be employed in the whole-cell catalysis of other higher-value molecules in a sustainable and continuous manner.

3.6 REFERENCES

(1) Zhang, Y.-H. P.; Sun, J.; Ma, Y. Biomanufacturing: History and Perspective. *J. Ind. Microbiol. Biotechnol.* **2017**, *44* (4–5), 773–784.

(2) Li, Y.; Smolke, C. D. Engineering Biosynthesis of the Anticancer Alkaloid Noscapine in Yeast. *Nat. Commun.* **2016**, *7* (1), 12137.

(3) Thodey, K.; Galanie, S.; Smolke, C. D. A Microbial Biomanufacturing Platform for Natural and Semisynthetic Opioids. *Nat. Chem. Biol.* **2014**, *10* (10), 837–844.

(4) Awan, A. R.; Blount, B. A.; Bell, D. J.; Shaw, W. M.; Ho, J. C. H.; McKiernan, R. M.; Ellis, T. Biosynthesis of the Antibiotic Nonribosomal Peptide Penicillin in Baker's Yeast. *Nat. Commun.* **2017**, *8*, 15202.

(5) Gerngross, T. U. Advances in the Production of Human Therapeutic Proteins in Yeasts and Filamentous Fungi. *Nat. Biotechnol.* **2004**, *22* (11), 1409–1414.

(6) Paddon, C. J.; Westfall, P. J.; Pitera, D. J.; Benjamin, K.; Fisher, K.; McPhee, D.; Leavell, M. D.; Tai, A.; Main, A.; Eng, D.; et al. High-Level Semi-Synthetic Production of the Potent Antimalarial Artemisinin. *Nature* **2013**, *496* (7446), 528–532.

(7) DeLoache, W. C.; Russ, Z. N.; Narcross, L.; Gonzales, A. M.; Martin, V. J. J.; Dueber, J. E. An Enzyme-Coupled Biosensor Enables (S)-Reticuline Production in Yeast from Glucose. *Nat. Chem. Biol.* **2015**, *11* (7), 465–471.

(8) Yang, S.; Fei, Q.; Zhang, Y.; Contreras, L. M.; Utturkar, S. M.; Brown, S. D.; Himmel, M. E.; Zhang, M. Zymomonas Mobilis as a Model System for Production of Biofuels and Biochemicals. *Microb. Biotechnol.* **2016**, *9* (6), 699–717.

(9) Davy, A. M.; Kildegaard, H. F.; Andersen, M. R. Cell Factory Engineering. *Cell Syst.* **2017**, *4* (3), 262–275.

(10) Peralta-Yahya, P. P.; Zhang, F.; del Cardayre, S. B.; Keasling, J. D. Microbial Engineering for the Production of Advanced Biofuels. *Nature* **2012**, *488* (7411), 320–328.

(11) Verbelen, P. J.; De Schutter, D. P.; Delvaux, F.; Verstrepen, K. J.; Delvaux, F. R. Immobilized Yeast Cell Systems for Continuous Fermentation Applications. *Biotechnology Letters*. **2006,** 28 (19), 1515–1525.

(12) Saha, A.; Johnston, T. G.; Shafranek, R. T.; Goodman, C. J.; Zalatan, J. G.; Storti, D. W.; Ganter, M. A.; Nelson, A. Additive Manufacturing of Catalytically Active Living Materials. *ACS Appl. Mater. Interfaces* **2018**, *10* (16), 13373–13380.

(13) Cheetham, P. S. J.; Blunt, K. W.; Bocke, C. Physical Studies on Cell Immobilization Using Calcium Alginate Gels. *Biotechnol. Bioeng.* **1979**, *21* (12), 2155–2168.

(14) Nagarajan, S.; Kruckeberg, A. L.; Schmidt, K. H.; Kroll, E.; Hamilton, M.; McInnerney, K.; Summers, R.; Taylor, T.; Rosenzweig, F. Uncoupling Reproduction

from Metabolism Extends Chronological Lifespan in Yeast. *Proc. Natl. Acad. Sci.* **2014**, *111* (15), E1538–E1547.

(15) Lehner, B. A. E.; Schmieden, D. T.; Meyer, A. S. A Straightforward Approach for 3D Bacterial Printing. *ACS Synth. Biol.* **2017**, *6* (7), 1124–1130.

(16) Lode, A.; Krujatz, F.; Brüggemeier, S.; Quade, M.; Schütz, K.; Knaack, S.; Weber, J.; Bley, T.; Gelinsky, M. Green Bioprinting: Fabrication of Photosynthetic Algae-Laden Hydrogel Scaffolds for Biotechnological and Medical Applications. *Eng. Life Sci.* **2015**, *15* (2), 177–183.

(17) Townsend-Nicholson, A.; Jayasinghe, S. N. Cell Electrospinning: A Unique Biotechnique for Encapsulating Living Organisms for Generating Active Biological Microthreads/Scaffolds. *Biomacromolecules* **2006**, *7* (12), 3364–3369.

(18) Liu, Y.; Rafailovich, M. H.; Malal, R.; Cohn, D.; Chidambaram, D. Engineering of Bio-Hybrid Materials by Electrospinning Polymer-Microbe Fibers. *Proc. Natl. Acad. Sci. U. S. A.* **2009**, *106* (34), 14201–14206.

(19) Letnik, I.; Avrahami, R.; Rokem, J. S.; Greiner, A.; Zussman, E.; Greenblatt, C. Living Composites of Electrospun Yeast Cells for Bioremediation and Ethanol Production. *Biomacromolecules* **2015**, *16* (10), 3322–3328.

(20) Brimmo, A.; Goyette, P. A.; Alnemari, R.; Gervais, T.; Qasaimeh, M. A. 3D Printed Microfluidic Probes. *Sci. Rep.* **2018**, *8* (1), 10995.

(21) Dahlberg, T.; Stangner, T.; Zhang, H.; Wiklund, K.; Lundberg, P.; Edman, L.; Andersson, M. 3D Printed Water-Soluble Scaffolds for Rapid Production of PDMS Micro-Fluidic Flow Chambers. *Sci. Rep.* **2018**, *8* (1), 3372.

(22) Mamatha, S.; Biswas, P.; Ramavath, P.; Das, D.; Johnson, R. 3D Printing of Complex Shaped Alumina Parts. *Ceram. Int.* **2018**, *44* (16), 19278–19281.

(23) Melnikova, R.; Ehrmann, A.; Finsterbusch, K. 3D Printing of Textile-Based Structures by Fused Deposition Modelling (FDM) with Different Polymer Materials. *IOP Conf. Ser. Mater. Sci. Eng.* **2014**, *62*, 012018.

(24) Sa, M.-W.; Nguyen, B.-N. B.; Moriarty, R. A.; Kamalitdinov, T.; Fisher, J. P.; Kim, J. Y. Fabrication and Evaluation of 3D Printed BCP Scaffolds Reinforced with ZrO 2 for Bone Tissue Applications. *Biotechnol. Bioeng.* **2018**, *115* (4), 989–999.

(25) Kiran, R. U.; Malferrari, S.; Van Haver, A.; Verstreken, F.; Rath, S. N.; Kalaskar, D. M. Optimization of Extrusion Based Ceramic 3D Printing Process for Complex Bony Designs. *Mater. Des.* **2018**, *162*, 263–270.

(26) Ligon, S. C.; Liska, R.; Stampfl, J.; Gurr, M.; Mülhaupt, R. Polymers for 3D Printing and Customized Additive Manufacturing. *Chem. Rev.* **2017**, *117* (15), 10212–10290.

(27) Kimlinger, M. J.; Martin, R. S. The Use of a 3D-Printed Microfluidic Device and Pressure Mobilization for Integrating Capillary Electrophoresis with Electrochemical

Detection. *Electroanalysis* **2018**, *30* (10), 2241–2249.

(28) Müller, M.; Becher, J.; Schnabelrauch, M.; Zenobi-Wong, M. Nanostructured Pluronic Hydrogels as Bioinks for 3D Bioprinting. *Biofabrication* **2015**, *7* (3), 035006.

(29) Bertassoni, L. E.; Cardoso, J. C.; Manoharan, V.; Cristino, A. L.; Bhise, N. S.; Araujo, W. A.; Zorlutuna, P.; Vrana, N. E.; Ghaemmaghami, A. M.; Dokmeci, M. R.; et al. Direct-Write Bioprinting of Cell-Laden Methacrylated Gelatin Hydrogels. *Biofabrication* **2014**, *6* (2), 024105.

(30) Li, Y.-C.; Zhang, Y. S.; Akpek, A.; Shin, S. R.; Khademhosseini, A. 4D Bioprinting: The next-Generation Technology for Biofabrication Enabled by Stimuli-Responsive Materials. *Biofabrication* **2017**, *9* (1), 012001.

(31) Patra, S.; Young, V. A Review of 3D Printing Techniques and the Future in Biofabrication of Bioprinted Tissue. *Cell Biochem. Biophys.* **2016**, *74* (2), 93–98.

(32) Schaffner, M.; Rühs, P. A.; Coulter, F.; Kilcher, S.; Studart, A. R. 3D Printing of Bacteria into Functional Complex Materials. *Sci. Adv.* **2017**, *3* (12), eaao6804.

(33) Bader, C.; Patrick, W. G.; Kolb, D.; Hays, S. G.; Keating, S.; Sharma, S.; Dikovsky, D.; Belocon, B.; Weaver, J. C.; Silver, P. A.; et al. Grown, Printed, and Biologically Augmented: An Additively Manufactured Microfluidic Wearable, Functionally Templated for Synthetic Microbes. *3D Print. Addit. Manuf.* **2016**, *3* (2), 79–89.

(34) Lee, J. M.; Yeong, W. Y. Design and Printing Strategies in 3D Bioprinting of Cell-Hydrogels: A Review. *Adv. Healthc. Mater.* **2016**, *5* (22), 2856–2865.

(35) Hoffman, A. S. Hydrogels for Biomedical Applications. *Adv. Drug Deliv. Rev.* **2002**, *54* (1), 3–12.

(36) Lee, K. Y.; Mooney, D. J. Hydrogels for Tissue Engineering. *Chem. Rev.* **2001**, *101* (7), 1869–1880.

(37) Smetana, K. Cell Biology of Hydrogels. *Biomaterials* **1993**, *14* (14), 1046–1050.

(38) Smetana, K.; Vacík, J.; Součková, D.; Krčová, Z.; Šulc, J. The Influence of Hydrogel Functional Groups on Cell Behavior. *J. Biomed. Mater. Res.* **1990**, *24* (4), 463–470.

(39) Benoit, D. S. W.; Schwartz, M. P.; Durney, A. R.; Anseth, K. S. Small Functional Groups for Controlled Differentiation of Hydrogel-Encapsulated Human Mesenchymal Stem Cells. *Nat. Mater.* **2008**, *7* (10), 816–823.

(40) Lee, J. H.; Jung, H. W.; Kang, I.-K.; Lee, H. B. Cell Behaviour on Polymer Surfaces with Different Functional Groups. *Biomaterials* **1994**, *15* (9), 705–711.

(41) Discher, D. E.; Janmey, P.; Wang, Y. L. Tissue Cells Feel and Respond to the Stiffness of Their Substrate. *Science*. **2005**, *310* (5751), 1139–1143.

(42) Buxboim, A.; Rajagopal, K.; Brown, A. E. X.; Discher, D. E. How Deeply Cells Feel: Methods for Thin Gels. *J. Phys. Condens. Matter* **2010**, *22* (19), 194116.

(43) Liu, Z.; Tyo, K. E. J.; Martínez, J. L.; Petranovic, D.; Nielsen, J. Different Expression Systems for Production of Recombinant Proteins in Saccharomyces Cerevisiae. *Biotechnol. Bioeng.* **2012**, *109* (5), 1259–1268.

(44) Achstetter, T. Regulation of Alpha-Factor Production in Saccharomyces Cerevisiae: A-Factor Pheromone-Induced Expression of the MF Alpha 1 and STE13 Genes. *Mol. Cell. Biol.* **1989**, *9* (10), 4507–4514.

(45) Baba, E. H.; Berkower, I. Production of a Soluble and Secreted Antigenic Fragment of HBsAg in Yeast. *Biochem. Biophys. Res. Commun.* **1992**, *184* (1), 50–59.

(46) Rakestraw, J. A.; Sazinsky, S. L.; Piatesi, A.; Antipov, E.; Wittrup, K. D. Directed Evolution of a Secretory Leader for the Improved Expression of Heterologous Proteins and Full-Length Antibodies in *Saccharomyces Cerevisiae*. *Biotechnol. Bioeng.* **2009**, *103* (6), 1192–1201.

(47) Robinson, A. S.; Hines, V.; Wittrup, K. D. Protein Disulfide Isomerase Overexpression Increases Secretion of Foreign Proteins in Saccharomyces Cerevisiae. *Nat. Biotechnol.* **1994**, *12* (4), 381–384.

(48) Staniulis, J. Synthesis of Hepatitis B Virus Surface Protein Derivates in Yeast S . Cerevisiae. *Biologija* **2006**, *3* (4), 49–53.

(49) Chigira, Y.; Oka, T.; Okajima, T.; Jigami, Y. Engineering of a Mammalian O-Glycosylation Pathway in the Yeast Saccharomyces Cerevisiae: Production of O-Fucosylated Epidermal Growth Factor Domains. *Glycobiology* **2008**, *18* (4), 303–314.

(50) Kjeldsen, T.; Frost Pettersson, A.; Hach, M. The Role of Leaders in Intracellular Transport and Secretion of the Insulin Precursor in the Yeast Saccharomyces Cerevisiae. *J. Biotechnol.* **1999**, *75* (2–3), 195–208.

(51) Fellin, C. R.; Adelmund, S. M.; Karis, D. G.; Shafranek, R. T.; Ono, R. J.; Martin, C. G.; Johnston, T. G.; DeForest, C. A.; Nelson, A. Tunable Temperature- and Shear-Responsive Hydrogels Based on Poly(Alkyl Glycidyl Ether)S. *Polymer International*. 2019, *68* (7), 1238-1246.

(52) Winnik, M. A.; Yekta, A. Associative Polymers in Aqueous Solution. *Curr. Opin. Colloid Interface Sci.* **1997**, *2* (4), 424–436.

(53) Lee, B. F.; Kade, M. J.; Chute, J. A.; Gupta, N.; Campos, L. M.; Fredrickson, G. H.; Kramer, E. J.; Lynd, N. A.; Hawker, C. J. Poly(Allyl Glycidyl Ether)-A Versatile and Functional Polyether Platform. *J. Polym. Sci. Part A Polym. Chem.* **2011**, *49* (20), 4498–4504.

(54) Heinen, S.; Rackow, S.; Schäfer, A.; Weinhart, M. A Perfect Match: Fast and Truly Random Copolymerization of Glycidyl Ether Monomers to Thermoresponsive Copolymers. *Macromolecules* **2017**, *50* (1), 44–53.

(55) Satoh, Y.; Miyachi, K.; Matsuno, H.; Isono, T.; Tajima, K.; Kakuchi, T.; Satoh, T. Synthesis of Well-Defined Amphiphilic Star-Block and Miktoarm Star Copolyethers

via t-Bu-P4-Catalyzed Ring-Opening Polymerization of Glycidyl Ethers. *Macromolecules* **2016**, *49* (2), 499–509.

(56) Barteau, K. P.; Wolffs, M.; Lynd, N. A.; Fredrickson, G. H.; Kramer, E. J.; Hawker, C. J. Allyl Glycidyl Ether-Based Polymer Electrolytes for Room Temperature Lithium Batteries. *Macromolecules* **2013**, *46* (22), 8988–8994.

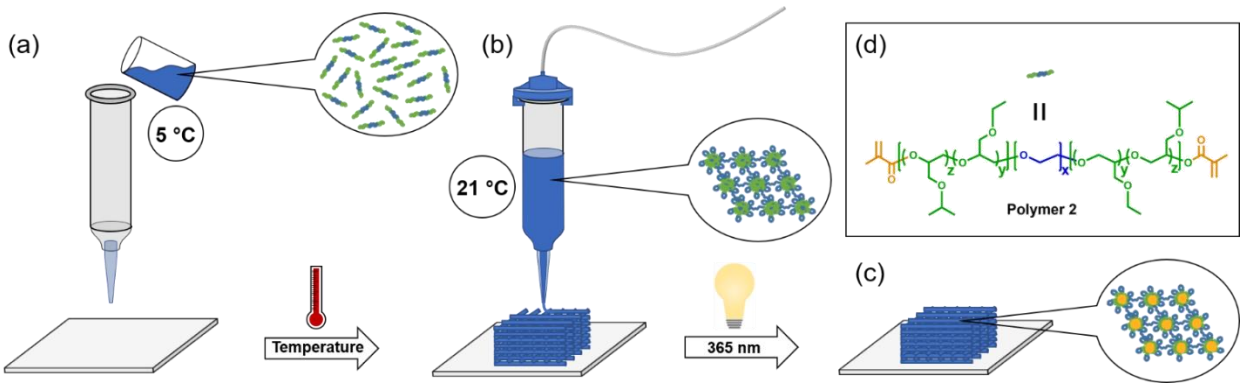

Figure 3.1 A graphical overview of the three key stimuli responses of polymer 2 hydrogels necessary for AMCALM applications. (a) The temperature responsive feature of the hydrogels enabled facile loading of the hydrogel material at 5 °C. (b) The shear-stress response facilitated the formation of complex three-dimensional objects at 21 °C. (c) UV-light (365 nm) initiated the polymerization of the methacrylate end-groups and chemical crosslinking of the polymer 2 hydrogel. (d) The chemical structure of polymer 2. The letter designations (z = 6.4, y = 7.4, x = 182) refer to the average number of isopropyl glycidyl ether, ethyl glycidyl ether, and ethylene oxide repeat units, respectively.

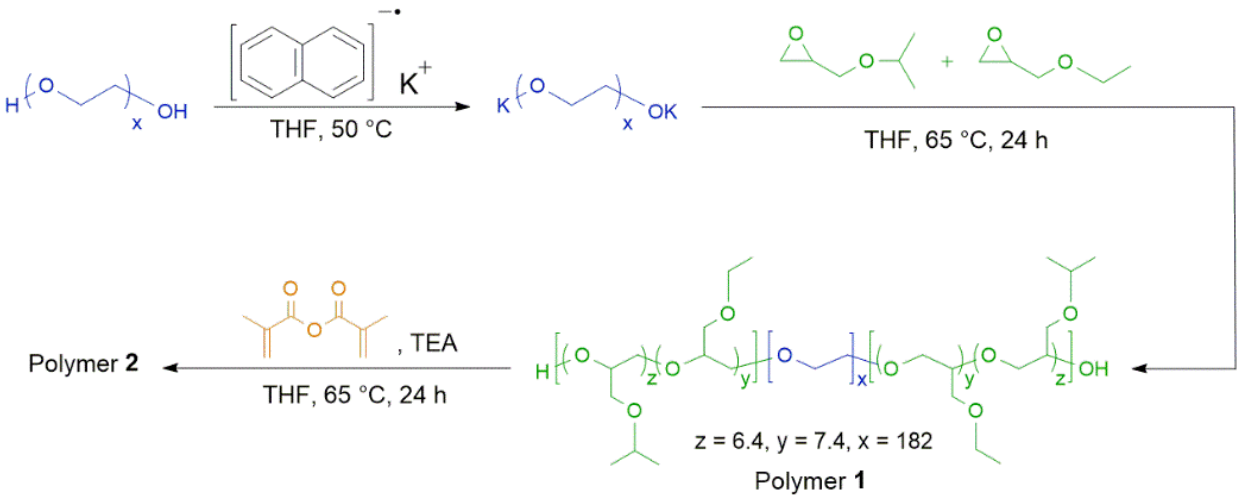

Scheme 3.1 Synthesis of the ABA triblock copolymer (polymer 1) and functionalization with methacrylic anhydride (polymer 2). The letter designations (z = 6.4, y = 7.4, x = 182) refer to degree of polymerization for isopropyl glycidyl ether, ethyl glycidyl ether, and ethylene oxide,

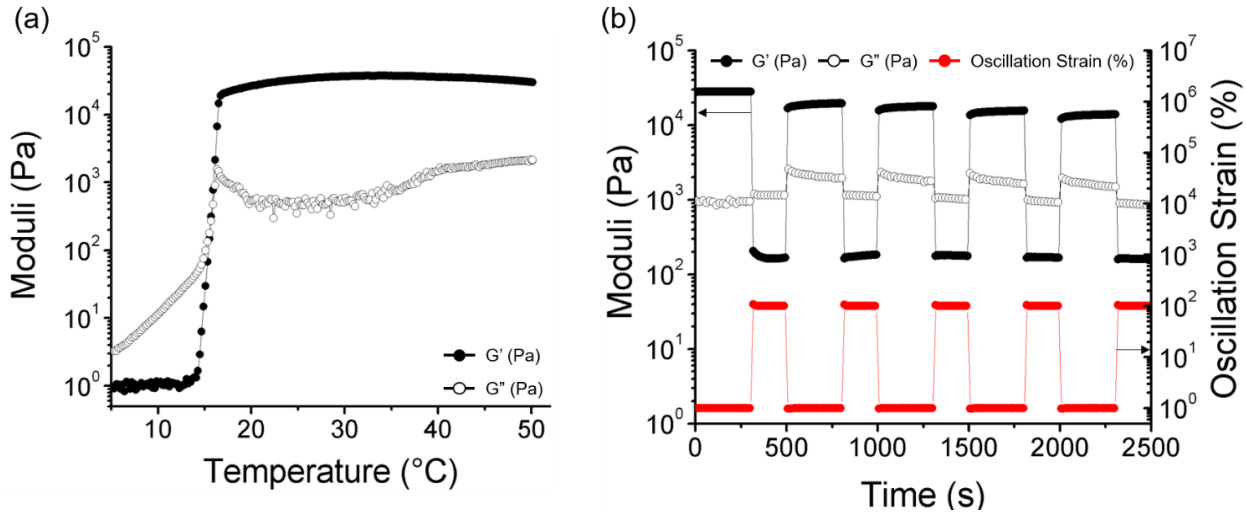

Figure 3.2 Rheometrical experiments for a 20 wt% formulation of polymer 2. (a) Dynamic oscillatory temperature ramp displaying elastic (G', filled) and viscous (G'', open) moduli. T_{gel} = 15.61 °C. (b) Cyclic strain experiment demonstrating rapid recovery of hydrogel elastic modulus (black circles) from periods of high (100%) to low (1%) oscillatory strain (red circles). Arrows indicate reference axis; elastic/viscous moduli (left axis) and oscillatory strain (right axis).

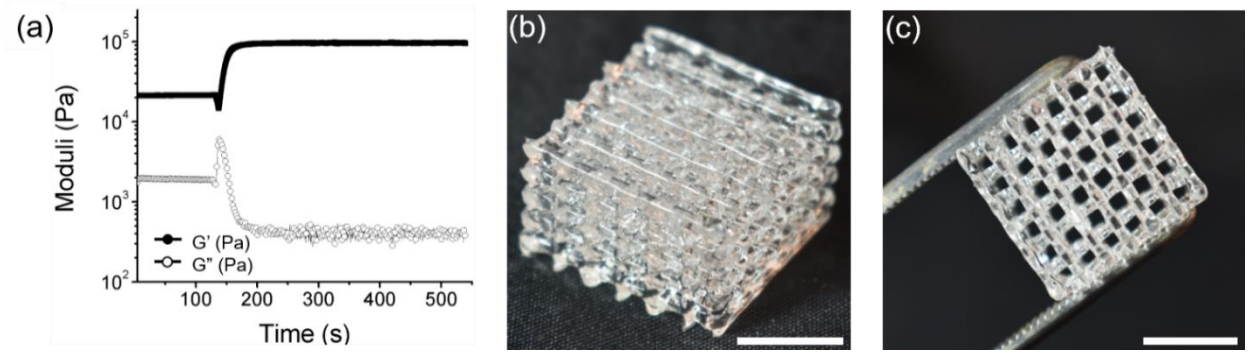

Figure 1.3 (a) A rheological UV-cure experiment using a 20 mm parallel plate geometry. The hydrogel was equilibrated for 120 s before being subjected to 5 mW cm-2 of 365 nm UV light for 420 s at a constant strain (1%) and frequency (1 Hz). (b-c) A 3D printed, proof of concept cuboid structure (1.9 cm by 1.9 cm by 1.2 cm). This structure was printed from a pneumatic direct write 3D printer at 5 mm s-1 and 20 psi using a 0.41 mm inner diameter nozzle (scale bar: 1 cm).

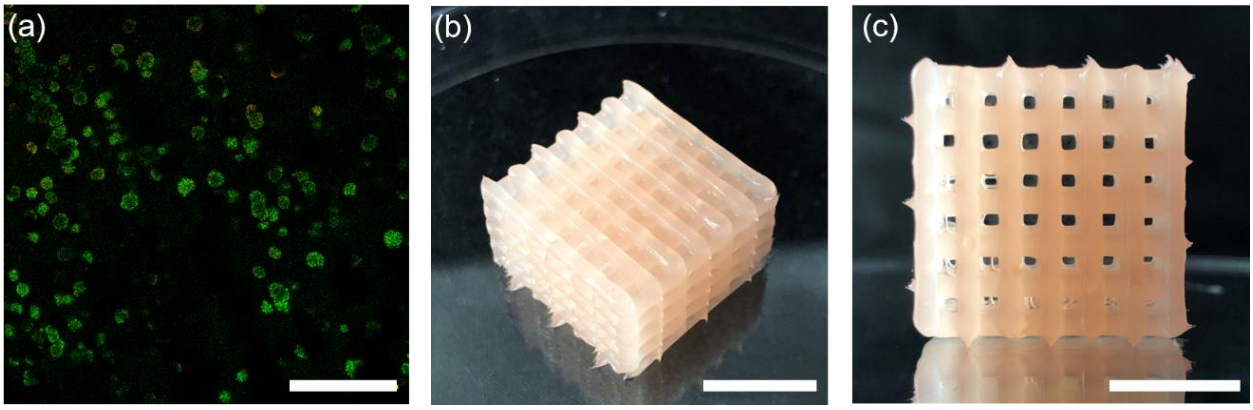

Figure 3.4 (a) A sample composite image of live cells (green channel) and dead cells (red channel) after 7 days of incubation (scale bar: 200 μm). (b) Side and (c) top-down view of the 3D-printed, yeast-laden hydrogel after two rounds of α-factor synthesis in SC media (scale bar 1 cm).

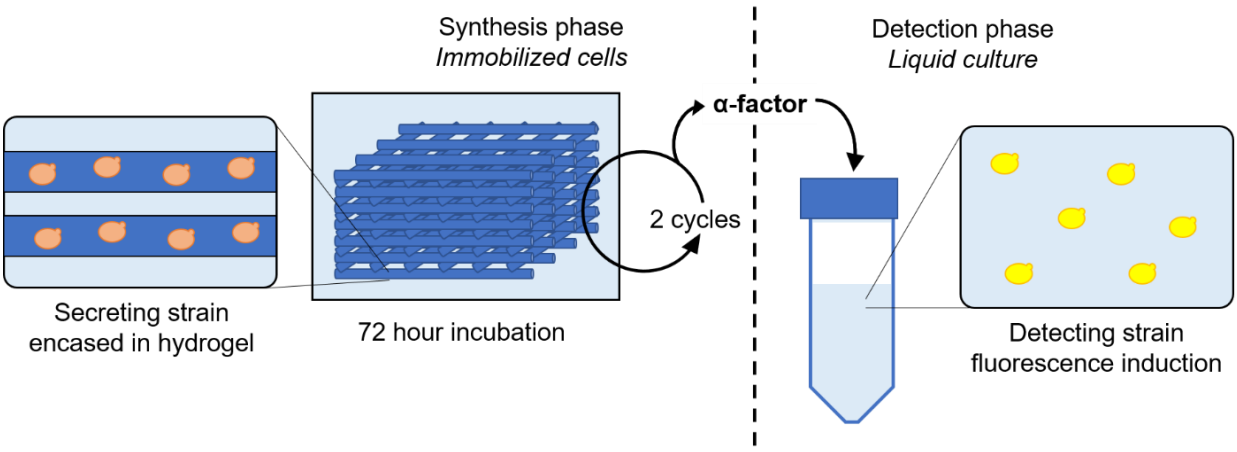

Figure 3.5 Immobilized yeast within the hydrogel matrix were incubated in SC media for 72 h at 30 °C with automated shaker agitation. The media was collected at the end of the incubation period and exposed to the receiver strain in a separate tube, and the resulting fluorescence was measured. The cuboidal lattice was reused in a subsequent incubation with fresh media to produce an additional batch of α-factor.

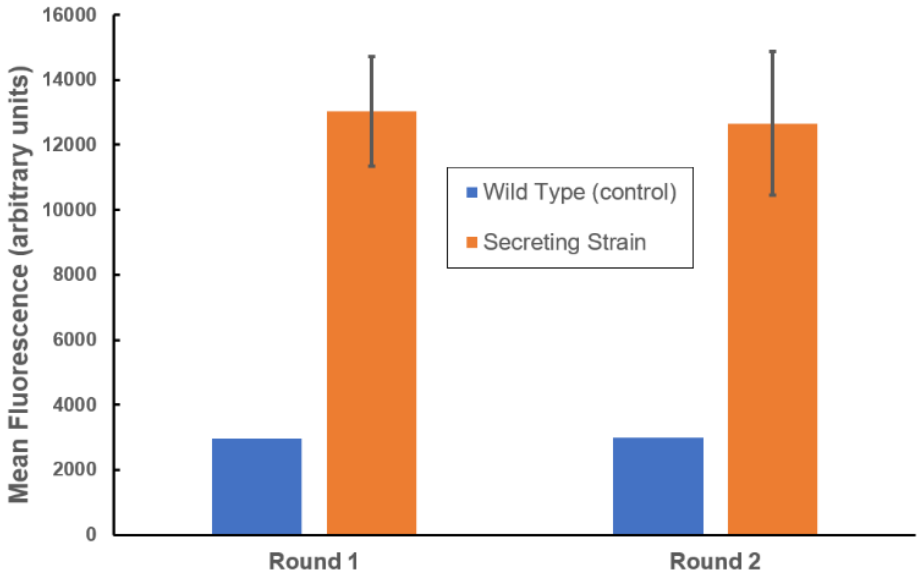

Figure 3.6 Fluorescence values obtained from the quantification of α-factor produced from the wild type (control) AMCALMs and the secreting strain AMCALMs. Round 1 indicates the first incubation period of 72 h, while Round 2 indicates the reemployment of the same printed materials in a second, subsequent 72 h batch reaction in fresh SC media.

CHAPTER 4: **THE POST-FUNCTIONALIZATION OF MULTI-STIMULI-RESPONSIVE HYDROGELS FOR DIRECT-INK WRITE ADDITIVE MANUFACTURING**

4.1 ABSTRACT

Herein, we describe the development of a multi-stimuli-responsive hydrogel platform capable of post-functionalization with thiol-bearing molecules as inks for DIW 3D printing. The poly(alkyl glycidyl ether) methacrylate (PGE-MA) hydrogels maintain three key stimuli-responses necessary for extrusion based additive manufacturing: a sol-gel temperature response, shear-thinning behavior, and the ability to photochemically crosslink. In addition, the chemically crosslinked hydrogels demonstrated a temperature dependent swelling consistent with LCST behavior. Pyridyl disulfide urethane methacrylate (PDS-UM) monomers were introduced to the network as a thiol-reactive handle for post-functionalization of the hydrogel. The reactivity of PGE-MA/PDS-UM hydrogels were investigated at different temperatures (5, 25, 37 °C) and swelling statuses (as cured/preswollen) using glutathione as a reactive probe. To illustrate the versatility of the PGE-MA/PDS-UM platform, a number of additional thiol-containing probes such as proteins, polymers, and small molecules were conjugated to the hydrogel network at various temperatures, pH's, and concentrations. In a final demonstration of the multi-stimuli-responsive hydrogel platform, a customized DIW 3D printer was used to fabricate a robot figurine that was subsequently conjugated with a fluorescent tag and displayed the ability to change in size with environmental temperature.

4.2 INTRODUCTION

Hydrogels are water-swollen networks of macromolecules bound by chemical or physical crosslinks. Their soft nature and inherently high water content (typically 70-99%) mimic the natural environment of living tissues, making them ideal for tissue engineering[1–3] and wound healing applications.[4,5] Stimuli-responsive hydrogels react to environmental cues such as temperature,[6] light,[7] or mechanical stress[8,9] to induce a chemical or physical change in material properties. These hydrogels have recently been adopted in the field of additive manufacturing, a technique that utilizes computer aided hardware and software for the sequential deposition of a material to fabricate three-dimensional objects.[10,11] Direct-ink write (DIW) additive manufacturing is one such method that can use shear-thinning hydrogels to facilitate flow of the material through fine resolution nozzles.[12–15] Certain stimuli-responses, such as shear-thinning behavior, enable effective printing while others create objects with advanced functionality after printing such as actuation,[16–18] shape memory,[19–21] and pH dependent drug release.[22,23]

Stimuli-responsive triblock copolymers can afford versatile gel-based inks for DIW 3D printing.[24–29] Our group has investigated and developed poly(alkyl glycidyl ether)-based hydrogels that exhibit temperature-, shear-, and light-responsive properties.[30–32] The sol-gel temperature response enables facile homogenization of additives while the shear-thinning response facilitates the extrusion of the material from the printhead nozzle and generates the 3D printed object. The material can then be chemically cross-linked using photo-initiated free radical polymerization to create robust objects capable of withstanding dissolution and deformation.

The conjugation of molecules to hydrogel materials under mild conditions with high specificity offers a straightforward method of introducing additional functionality to these systems.[33–38] For instance, the Anseth group developed a PEG/protein hydrogel with orthogonal

alkene functionality for the conjugation of photopatterned biomolecules. Thiol-ene click chemistry was used to modify the existing hydrogel with the cell-adhesion tripeptide motif Arg-Gly-Asp (RGD) for cell attachment with spatial control.[39] Alternatively, azide-alkyne click reactions were utilized by Sanyal and coworkers for the post-functionalization of dendron-polymer conjugate hydrogels. While some of the alkynes were utilized as crosslinking points to form the hydrogel, residual alkyne groups were available for the covalent attachment of additional azide-containing molecules including fluorescent dyes (4-azido-N-ethyl-1,8-naphthalimide and BODIPY) and biotin for protein immobilization.[40] Adapting such techniques to the post-functionalization of 3D printed systems could enable facile modification of hydrogel materials for a multitude of post-print applications.

Pyridyl disulfide is a versatile motif used in a number of applications as a reactive handle for thiol-containing molecules.[41] The efficient thiol-pyridyl disulfide exchange enables conjugation of small-to-large molecule reactants including peptides,[42–44] proteins,[45–47] and even RNA[48–50] with high specificity under mild conditions. Additionally, the 2-pyridothione leaving group has a convenient absorbance spectrum that allows for methodical tracking of conjugation rates by monitoring the evolution of the 343 nm absorbance peak via UV-Vis spectroscopy.

While the utilization of pyridyl disulfides in polymeric systems has been investigated, its use as a reactive functionality towards the post-functionalization of hydrogels has not been thoroughly explored. One recent example includes work by Sanyal and co-workers to post-functionalize PEG hydrogels with thiolated biotin to immobilize TRITC−extravidin proteins and RGD to immobilize HUVEC cells.[51]

Herein, we report the post-functionalization of multi-stimuli-responsive hydrogels for DIW 3D printing. Methacrylated poly(isopropyl-*stat*-ethyl glycidyl ether)$_{1.6k}$-*block*-poly(ethylene

oxide)$_{8.0k}$-*block*-poly(isopropyl-*stat*-ethyl glycidyl ether)$_{1.6k}$ (PGE-MA) based hydrogels demonstrated temperature-dependent equilibrium swelling ratios (ESRs) consistent with lower critical solution temperature (LCST) behavior. Pyridyl disulfide urethane methacrylate (PDS-UM) monomers were successfully incorporated into PGE-MA hydrogels as a platform for post-functionalization with thiol-containing molecules. Glutathione (GSH) was used as a small molecule probe to measure the conjugation kinetics of PGE-MA/PDS-UM hydrogels at different temperatures (5, 25, 37 °C) and swelling states (as cured/preswollen). Other thiol-containing molecules (small molecules, polymer, and protein) were also conjugated onto PGE-MA hydrogels. To demonstrate the potential for these materials, we PGE-MA/PDS-UM hydrogels were DIW 3D printed and post-print functionalized with fluorescein thiol (FITC-SH). The differential swelling in response to environmental temperatures was also confirmed for these printed objects.

4.3 Materials and Methods

4.3.1 Materials

All chemicals and solvents were purchased from Sigma-Aldrich, Fisher Scientific, or Oakwood Chemical and used without further purification unless noted otherwise. CYCLO(ARG-GLY-ASP-D-PHE-CYS) (RGD-SH) was purchased from AstraTech. RGD-PEG-SH was purchased from Biochempeg Scientific. Isopropyl glycidyl ether (iPGE, 98%) and ethyl glycidyl ether (EGE, 98%) were dried over CaH2 for 24 h, distilled into a flask containing butyl magnesium chloride (2 M in tetrahydrofuran, THF), re-distilled, and stored under N2 atmosphere. Poly(ethylene oxide) (PEO, Mn 8000 g mol-1) was dried under vacuum overnight prior to use. Dry THF was obtained using neutral alumina using a Pure Process Technology solvent purification system. A potassium naphthalenide solution (1M) was prepared by dissolving naphthalene (3.2 g) in THF (25 mL), adding potassium (0.975 g), and storing under N2 atmosphere. ^{1}H NMR spectra

were obtained on a Bruker Advance 300 or 500 MHz spectrometer. All absorbance spectra were collected on either a Varian Cary 5000 UV-Vis-NIR or Agilent 8453 UV-Vis spectrophotometer.

4.3.2 Synthesis of HEPDS

Hydroxyethyl pyridyl disulfide was synthesized (Scheme C1) according to literature procedures. Briefly, dipyridyl disulfide (5 g, 23 mmol) and glacial acetic acid (0.6 mL) were dissolved in MeOH (60 mL). A solution of 2-mercaptoethanol (1.41 mL, 20 mmol) in MeOH (25 mL) was added dropwise to the reaction solution at over 30 min and the solution was allowed to stir at RT for 24 h. The solvent was then removed under reduced pressure and the product was redissolved in minimal ethyl acetate. The solution was washed with deionized water (3x), dried with anhydrous sodium sulfate, and filtered. After concentrating again under reduced pressure, the product was purified via silica gel column chromatography using an ethyl acetate/hexane mixture (17:3) as the elution solvent. The product was obtained as a light-yellow oil (1.58 g, 38% yield). ^{1}H NMR (499 MHz, CDCl3): δ = 8.52-8.50 (d, 1H), 7.60-7.57 (t, 1H), 7.42-7.40 (d, 1H), 7.17-7.14 (t, 1H), 3.82-3.80 (t, 2H), 2.97-2.95 (t, 2H).

4.3.3 Synthesis of PDS-UM

Pyridyl disulfide-urethane methacrylate (PDS-UM) was synthesized (Scheme C2) using modified literature procedures[52]. HEPDS (1.58 g, 8.44 mmol) was dissolved in dry THF (5 mL) and added to a flame dried reaction flask. 2-isocyanoethyl methacrylate (1.43 mL, 10.12 mmol) and dibutyltin dilaurate (19.75 μL) were subsequently added under inert N_2 atmosphere and the reaction mixture was allowed to stir at RT for 20 h. The solvent was then removed under reduced pressure. The impure product was redissolved in DCM and was washed with deionized water and brine. The product was purified via silica gel column chromatography using an ethyl

acetate/hexane mixture (2:3) as the elution solvent. The product was obtained as a white powder (2.41 g, 88% yield). ^{1}H NMR (499 MHz, CDCl3): δ = 8.48-8.47 (d, 1H), 7.70-7.62 (m, 2H), 7.11-7.08 (t, 1H), 6.12 (s, 1H), 5.60 (s, 1H), 4.99 (s, 1H), 4.34-4.32 (t, 2H), 4.24-4.21 (t, 2H), 3.51-3.47 (q, 2H), 3.05-3.03 (t, 2h), 1.95 (s, 3H).

4.3.4 Preparation of PGE-MA/PDS-UM Hydrogel Solution

For the formulation of a 5 g batch of hydrogel, PGE-MA was first dissolved in deionized water at a concentration of 20 wt % polymer. The resulting polymer solution was cooled overnight at 5 °C to facilitate complete dissolution of the polymer via LCST behavior. Using the temperature-responsive sol-gel transition of the polymer, a 0.088 M solution of PDS-UM in MeOH (100 μL) and the photo-radical initiator 2-hydroxy-2-methylpropiophenone (5 μL) were added to the sol state at 5 °C and homogenized using a vortex mixer for 30 s. The hydrogel was centrifuged (4400 rpm, 10 min) to remove bubbles.

4.3.5 Hydrogel Sample Preparation

Hydrogel solutions were poured into nine disk molds (r = 5 mm, h = 5 mm) and cured under 365 nm UV light for 15 min. The nine cured disks were washed with water to remove any unreacted polymer from the sample surface.

4.3.6 PGE-MA Swelling Studies

The swelling rates of PGE-MA hydrogels were studied at three different temperatures (5, 25, and 37 °C) and three different swelling states (dry, as cured, and preswollen). Three hydrogel samples were placed in scintillation vials containing deionized water at their respective temperatures and weighed at time points from 0-48 h. The swelling ratio was determined using the following equation:

$$Swelling\ Ratio = \frac{W_t - W_i}{W_i}$$

Where W_t refers to the weight of the hydrogel sample at time point *t* and W_i refers to the weight of the initial dried or as cured sample. Swelling reversibility studies were conducted in a similar manner. Three hydrogel samples were placed in scintillation vials containing deionized water in a 37 °C environment. The samples were allowed to equilibrate and weighed after 1 day. The samples were returned to the scintillation vials and placed in a 5 °C environment and weighed again after 1 day. This procedure was repeated five times for a total of 10 days.

4.3.7 2-Pyridothione Calibration

A calibration curve was established by dissolving various concentrations of 2-pyridothione (0.01 – 0.5 mM) in deionized water and measuring the corresponding absorbance values at λ = 343 nm. A linear regression analysis of the absorbance vs concentration plot produced a linear fit with an R^2 value of 0.999.

4.3.8 2-Pyridothione Release Studies

The release rates of PGE-MA/PDS-UM hydrogels were studied at three different temperatures (5, 25, and 37 °C) and three different swelling states (dry, as cured, and preswollen). GSH was chosen as the free-thiol reactant molecule at concentrations typically found in tumor cells (10 mM). Three hydrogel samples were placed in scintillation vials containing a GSH solution (7 mL, 10 mM in deionized water) at their respective temperatures. Periodically over the course of 96 h, aliquots were taken for UV-Vis analysis. The percent release was determined using the absorbance at λ = 343 nm corresponding to the released 2-pyridothione and the following equation:

$$Percent\ release\ (\%) = \frac{Abs_t}{M_c * \frac{0.0006g\ PDS-UM}{1g\ Hydrogel} * \frac{1}{342.44\frac{g}{mol}} * 1000 * \frac{1}{7+\delta\ mL} * 1000 * 5.4776} * 100$$

Where Abs_t refers to the absorbance of the reaction solution at time t and M_c refers to the mass of the as cured samples. Any water added from the hydrogel samples (δ) was taken into account and added to the initial volume (7 mL).

4.3.9. Direct-write 3D Printing of PGE-MA/PDS-UM Hydrogels

A modified pneumatic direct-write 3D printer was assembled based on a Tronxy P802E 3D Printer kit, from Shenzen Tronxy Technology Co. The CAD model was designed on Fusion 360 and the G-code file was produced with Slic3r software. The hydrogel ink was cooled to 5 °C and poured into a Nordson Optimum 10 cc fluid dispensing barrel equipped with a Metcal conical (410 μm inner diameter) precision tip nozzle. The loaded syringe was warmed to ambient temperature and pressurized using nitrogen gas (20 psi) to extrude the gel from the nozzle at 5.0 mm s^{-1}. The printer was controlled with an Arduino using the Marlin firmware.

4.4 Results and Discussion

4.4.1. Temperature Dependent Hydrogel Swelling

PGE-MA triblock copolymers were synthesized via anionic ring-opening polymerization of ethyl or isopropyl glycidyl ether initiated from poly(ethylene glycol) using potassium naphthalenide as a base and functionalized using methacrylic anhydride. The lower critical solution temperature (LCST) driven sol-gel transition is ideal for material processing, while the shear-thinning response enables effective extrusion-based additive manufacturing. Photo-chemical crosslinking of the material through UV-light initiated polymerization of methacrylate chain ends creates robust hydrogels capable of post-print bioreactor applications. However, the permanent fixation of the network removes the sol-gel and shear-thinning response of the material, as the polymer chains are now covalently bound and no longer have the freedom to disassemble at lower

temperatures or under high shear environments. Interestingly, chemically crosslinked polymers such as F127[53–55] or poly(N-isopropyl acrylamide) (PNIPAm)[56–58] are known to exhibit volume phase transitions as a result of LCST behavior. Therefore, we hypothesized that PGE-MA hydrogels would maintain their temperature-responsive behavior after crosslinking in the form of temperature dependent equilibrium swelling ratios (ESR) (Figure 4.1).

To investigate this behavior, crosslinked hydrogel samples (20 wt% PGE-MA in deionized water) were placed in aqueous solutions at 5, 25, and 37 °C and their swelling ratios were recorded periodically over 48 h (Figure 4.2a). At low temperatures (5 °C), the hydrogels experience enhanced swelling, achieving an ESR of 53.0 ± 0.8%. Meanwhile, at room (25 °C) or elevated (37 °C) temperatures, the material reaches an ESR of 28.5 ± 1.3 and 8.6 ± 0.8%, respectively. This is consistent with LCST behavior: As the temperature of the environment decreases, the system absorbs a higher degree of water as the polymer becomes more hydrophilic and the glycidyl ether blocks become fully solvated. With increasing temperatures, the polymer chains contract as they become more hydrophobic, and the material equilibrates at lower swelling ratios. All hydrogel samples reached final ESR values after 24 h of incubation.

Similar to the reported sol-gel transition, the ESR of the crosslinked hydrogel is reversible and showed no loss in mass or change in ESR over 5 cycles of alternating between 5 and 37 °C (Figure 4.2b). Hydrogel samples originally equilibrated at 5 °C experienced a drop in ESR when placed in high (37 °C) temperature environments. Once placed back into low temperature solutions, the hydrogel samples recover back to their highly swollen state.

4.4.2. Formulation and Rheological Characterization of PGE-MA/PDS-UM Hydrogels

PDS-UM monomers were synthesized using a modified procedure[52] and incorporated into PGE-MA hydrogels to create a hydrogel that can be post-functionalized with thiol-containing

molecules (Scheme C1-C2). PDS monomers are naturally hydrophobic and often require fabrication in organic solvents[51,59,60] or functionalization onto hydrophilic polymers[61,62] in order to prepare PDS containing hydrogels. One unique aspect of amphiphilic triblock copolymers such as PGE-MA is their ability to self-assemble into flower-like micelles and encapsulate hydrophobic molecules such as PDS-UM.[63–67] The inherent sol-gel temperature transition of PGE-MA hydrogels was used to efficiently dissolve and homogenize the PDS-UM monomer at a molar ratio of 1:10 (PDS-UM:PGE-MA). The PGE-MA/PDS-UM formulation was optimized by visually comparing different concentration of PDS-UM to ensure maximum loading within the micelles while maintaining good solubility.

Rheological characterization of PGE-MA/PDS-UM hydrogels confirmed that the incorporation of PDS-UM did not negatively impact the temperature-, shear-, or light-responsive properties of the material (Figure C1). The temperature-dependent viscoelastic character of the material was confirmed by the presence of a sol-gel transition (T = 14.32 °C) as defined by the crossover between the solid-like character of the material (storage modulus, G') and the liquid-like character of the material (loss modulus, G") (Figure C1a). The material exhibited shear-thinning behavior as characterized by a negative correlation between viscosity and shear rate, illustrating the shear-induced flow required for extrusion-based printing methods (Figure C1b). A dynamic oscillatory strain experiment demonstrated the rapid and reversible response of the material to periods of high (100%) and low (1%) strain (Figure C1c). At low strain, such as those experienced by the hydrogel before and after printing, the material exists as a gel with G' values greater than G". Under periods of high strain, such as those experienced during extrusion, G" values were greater than G' indicating the material was able to flow. Finally, the photochemical crosslinking of the hydrogel network was confirmed by increasing G' values upon exposure to 365

nm UV light (Figure C1d). This indicates a rapid polymerization of methacrylate chain ends, the formation of chemical crosslinks, and the stiffening of the hydrogel network.

4.4.3. Reactivity of PGE-MA/PDS-UM Hydrogels Toward Thiols

Given the temperature-responsive behavior of PGE-MA/PDS-UM hydrogels, we further investigated the effect of the thermally responsive swelling behavior upon the reactivity of the PDS-UM toward thiols. We hypothesized that the LCST response of the PGE-MA network will afford fully solvated polymer chains at lower temperatures and the exposed PDS-UM monomer would be more reactive. To test this hypothesis, as-cured PGE-MA/PDS-UM hydrogel samples were placed in pre-equilibrated solutions of glutathione (GSH) at 5, 25, and 37 °C. The conjugation of GSH with the PDS-UM monomer can be tracked by monitoring the absorbance peak of released 2-pyridothione at 343 nm. A calibration curve was established by dissolving 2-pyridothione in aqueous solutions at various concentrations (0.1-5 mM, Figure 4.3).

An aliquot of each solution was taken at various time points over the course of 96 h and investigated by UV-Vis spectroscopy. The percent release was calculated relative to the theoretical concentration of 2-pyridothione, assuming complete reaction of all PDS-UM active sites and plotted versus time (Figure 4.4a). Contrary to our hypothesis, the release rates of 2-pyridothione from PGE-MA/PDS-UM hydrogels were *faster* at smaller ESRs and higher temperatures, and the release rates were *slower* at greater ESRs and lower temperatures (Table 4.1). For instance, the percent release of 2-pyridothione at 24 h for samples equilibrated at 37 °C was 10.4 % higher than at 25 °C and 23.8 % higher than at 5 °C. The largest difference in percent release was observed throughout the first 24 h of incubation, with near quantitative release of 2-pyridothione at all temperatures within 96 h.

These results suggest that as-cured PGE-MA/PDS-UM hydrogels do, in fact, exhibit temperature-dependent release profiles, albeit with an inverse correlation between ESR and release rate. Interestingly, when hydrogel samples are preswollen before placement in reactive GSH solutions (Figure 4.4b), the magnitude of 2-pyridothione release is significantly diminished. Not only were percent release values lower during the early stages of release (24 h = 46.2 vs 60.8, 53.0 vs 74.2 and 50.8 vs 84.6 for 5, 25, and 37 °C, respectively) but the final maximum release values never broke 73 %. Additionally, the temperature dependent release profiles observed for as cured samples are minimized, if not entirely removed. For instance, samples equilibrated at 25 °C had the highest percent release of 2-pyridothione at 24 h, 2.2 % greater than samples at 37 °C and 6.8 % more than samples at 5 °C. These results suggest that the active swelling of the hydrogel network has a major impact on the magnitude and temperature dependency of release kinetics for PGE-MA/PDS-UM hydrogels.

4.4.4. Thiol Containing Molecular Library

To demonstrate the versatility of our PGE-MA/PDS-UM platform, a number of different thiol-containing molecules were conjugated to the hydrogels. The percent release of 2-pyridothione after 24 and 96 h for each compound was recorded in Table 4.2. Cysteamine and 2-mercaptoethanol (2-MCE) were chosen as model compounds to demonstrate the ability of our platform to conjugate molecules in the presence of polar hydrogen bonding functionalities (-NH_2 and -OH). RGD-SH and RGD-PEG-SH (M_n = 5,000) were included due to their cell adhesive capabilities as well as to demonstrate the ability to conjugate large polymeric compounds. Similarly, BSA (M_n = 66kD) with a single free cysteine reacted with up to 12.9% of the available PDS-UM sites. The larger macromolecules, BSA and PEG conjugated significantly less (12.9 % and 30.9 %, respectively) than the smaller molecular probes GSH/RGD (97.9 % and 80.4 %,

respectively). This can be attributed to the large increase in molecular weight (1-2 orders of magnitude) for the same number of available thiols (1) per molecule.

Meanwhile, 2,2- (Ethylenedioxy)diethanethiol (EDT) and pentaerythritol tetra(3-mercaptopropionate) (PET) were incorporated to demonstrate the conjugation of multi-functional small molecules. A stoichiometric amount of EDT (2x thiol) and PET (4x thiol) relative to thiol equivalent (0.5 and 0.25 molar equivalents) were added to the reaction solution. Conjugation values of 77.4 and 33.2 % suggest that one molecule of EDT/PET is reacting with multiple PDS-UM reactive sites, as a 1:1 conjugation ratio would yield values of 50 and 25%, respectively. Because EDT and PET are both small molecules and cannot be expected to bridge the gap between multiple micelles, these results further suggest that multiple PDS-UM monomers are located within the hydrophobic core of a single micelle.

Lastly, we investigated the effect of pH upon the reaction of thiols with PGE-MA/PDS-UM. Bagiyan and co-workers previously reported that thiols can undergo spontaneous auto-oxidation in the presence of molecular oxygen in aqueous solutions. According to their results, the rate of auto-oxidation to disulfides is affected by both pH and temperature. For instance, the auto-oxidation rate of cysteamine was reportedly 15 - 20 times larger at a pH of 8.5 - 9.0 than 4 – 5, and 6 times larger at 45 °C compared to 15 °C. It was therefore necessary to modulate both the pH and temperature of our reaction solutions to suppress auto-oxidation of both the conjugating molecule as well as the 2-pyridothione leaving group. GSH, a naturally acidic compound containing two carboxylic acid moieties, undergoes efficient conjugation at pH 3 and 37 °C. Cysteamine hydrochloride, EDT, PET, RGD, and RGD-PEG-SH were reacted in solutions with the pH 5, while BSA and 2-MCE were conjugated in a phosphate buffer solution (1x PBS, pH 7.4). These compounds were therefore incubated at 25 and 5 °C, respectively, to account for the increasing

basicity of the reaction solutions. All molecules were able to achieve efficient conjugation under these reaction conditions.

4.4.4. 3D Printing and Post-Functionalization of PGE-MA/PDS-UM Hydrogels

As a final demonstration, we 3D printed hydrogel objects that were post-print functionalized with a fluorescent dye. A customized DIW 3D printer was used to extrude hydrogel ink in a patternwise manner to create the robot figurine shown in Figure 4.5. The sol-gel temperature response allowed for homogenization of the PDS-UM monomer, as well as facile loading of the material into the printer syringe. The shear-thinning response facilitated the formation of rod-like filaments and enabled effective printing of the material into the computer-generated object. The post-print photochemical crosslinking allowed for handling and swelling of the object without deformation or dissolution. A thiolated fluoresceine dye (FITC-SH) was synthesized according to literature procedures[68] and conjugated to the material via thiol-reactive PDS-UM groups (Figure 4.5). The figure demonstrated high fluorescence intensity with no observable decline after successive equilibrations with fresh buffer solution. And finally, the temperature dependent ESRs allow the printed object to grow/shrink based on environmental conditions. The printed figure achieved an upper limit size of 5.2 x 7.1 cm at 5 °C (Figure 4.5a), and a minimum size of 4.75 x 6.34 cm at 37 °C (Figure 4.5b).

4.5 Conclusion

In conclusion, we developed a multi-stimuli-responsive hydrogel platform capable of post-functionalization with thiol-containing molecules for DIW additive manufacturing. Crosslinked PGE-MA hydrogel samples demonstrated temperature dependent equilibrium swelling ratios consistent with LCST behavior i.e., higher degrees of swelling at lower temperatures. PDS-UM

monomers were incorporated into the network, providing the hydrogel with a thiol-reactive handle for post-functionalization. The reactivity of PGE-MA/PDS-UM hydrogels was investigated at different temperatures (5, 25, 37 °C) and swelling statuses (as cured/preswollen). The conjugation rates were found to increase with temperature and were faster in as cured samples. The versatility of the platform was demonstrated by conjugating a diverse set of thiol-containing probes to the hydrogel including peptides, proteins, polymers, and multi-functional small molecules at various temperatures, pH values, and concentrations. Lastly, the multi-stimuli-responsive properties of the PGE-MA/PDS-UM system were demonstrated by post-functionalizing a 3D printed robot figurine. The sol-gel temperature response, shear-thinning behavior, and photochemical crosslinking properties enabled efficient DIW printing. The printed figurine was post-functionalized with the thiolated fluorescent tag, FITC-SH, and displayed changes in size induced by the temperature dependent swelling of the PGE-MA hydrogel.

4.5 REFERENCES

(1) Spicer, C. D. Hydrogel Scaffolds for Tissue Engineering: The Importance of Polymer Choice. *Polym. Chem.* **2020**, *11* (2), 184–219.

(2) Hunt, J. A.; Chen, R.; Van Veen, T.; Bryan, N. Hydrogels for Tissue Engineering and Regenerative Medicine. *J. Mater. Chem. B* **2014**, *2* (33), 5319–5338.

(3) El-Sherbiny, I. M.; Yacoub, M. H. Hydrogel Scaffolds for Tissue Engineering: Progress and Challenges. *Glob. Cardiol. Sci. Pract.* **2013**, *2013* (3), 38.

(4) Tavakoli, S.; Klar, A. S. Advanced Hydrogels as Wound Dressings. *Biomolecules* **2020**, *10* (8), 1–20.

(5) Pan, Z.; Ye, H.; Wu, D. Recent Advances on Polymeric Hydrogels as Wound Dressings. *APL Bioeng.* **2021**, *5* (1), 11504.

(6) Jeong, B.; Kim, S. W.; Bae, Y. H. Thermosensitive Sol-Gel Reversible Hydrogels. *Adv. Drug Deliv. Rev.* **2002**, *54* (1), 37–51.

(7) Li, L.; Scheiger, J. M.; Levkin, P. A. Design and Applications of Photoresponsive Hydrogels. *Adv. Mater.* **2019**, *31* (26), 1807333.

(8) Xiao, L.; Zhu, J.; Londono, J. D.; Pochan, D. J.; Jia, X. Mechano-Responsive Hydrogels Crosslinked by Block Copolymer Micelles. *Soft Matter* **2012**, *8* (40), 10233–10237.

(9) Taki, M.; Yamashita, T.; Yatabe, K.; Vogel, V. Mechano-Chromic Protein-Polymer Hybrid Hydrogel to Visualize Mechanical Strain. *Soft Matter* **2019**, *15* (46), 9388–9393.

(10) Wang, S.; Lee, J. M.; Yeong, W. Y. Smart Hydrogels for 3D Bioprinting. *Int. J. Bioprinting* **2015**, *1* (1), 3–14.

(11) Shafranek, R. T.; Millik, S. C.; Smith, P. T.; Lee, C. U.; Boydston, A. J.; Nelson, A. Stimuli-Responsive Materials in Additive Manufacturing. *Progress in Polymer Science*. Elsevier Ltd June 1, 2019, pp 36–67.

(12) Highley, C. B.; Rodell, C. B.; Burdick, J. A. Direct 3D Printing of Shear-Thinning Hydrogels into Self-Healing Hydrogels. *Adv. Mater.* **2015**, *27* (34), 5075–5079.

(13) Ouyang, L.; Highley, C. B.; Rodell, C. B.; Sun, W.; Burdick, J. A. 3D Printing of Shear-Thinning Hyaluronic Acid Hydrogels with Secondary Cross-Linking. *ACS Biomater. Sci. Eng.* **2016**, *2* (10), 1743–1751.

(14) Mccracken, J. M.; Badea, A.; Kandel, M. E.; Gladman, A. S.; Wetzel, D. J.; Popescu, G.; Lewis, J. A.; Nuzzo, R. G. Programming Mechanical and Physicochemical Properties of 3D Hydrogel Cellular Microcultures via Direct Ink Writing. *Adv. Healthc. Mater.* **2016**, *5* (9), 1025–1039.

(15) Robert Barry III, B. A.; Shepherd, R. F.; Hanson, J. N.; Nuzzo, R. G.; Wiltzius, P.; Lewis, J. A.; Lewis, J. A.; Shepherd, R. F.; Barry III, R. A.; Wiltzius, P.; Hanson, J. N.;

Nuzzo, R. G. Direct-Write Assembly of 3D Hydrogel Scaffolds for Guided Cell Growth. *Adv. Mater* **2009**, *21*, 2407–2410.

(16) Naficy, S.; Gately, R.; Gorkin, R.; Xin, H.; Spinks, G. M. 4D Printing of Reversible Shape Morphing Hydrogel Structures. *Macromol. Mater. Eng.* **2017**, *302* (1).

(17) Bakarich, S. E.; Gorkin, R.; Panhuis, M. In Het; Spinks, G. M. 4D Printing with Mechanically Robust, Thermally Actuating Hydrogels. *Macromol. Rapid Commun.* **2015**, *36* (12), 1211–1217.

(18) Odent, J.; Vanderstappen, S.; Toncheva, A.; Pichon, E.; Wallin, T. J.; Wang, K.; Shepherd, R. F.; Dubois, P.; Raquez, J. M. Hierarchical Chemomechanical Encoding of Multi-Responsive Hydrogel Actuators: Via 3D Printing. *J. Mater. Chem. A* **2019**, *7* (25), 15395–15403.

(19) Sanchez-Rexach, E.; Smith, P. T.; Gomez-Lopez, A.; Fernandez, M.; Cortajarena, A. L.; Sardon, H.; Nelson, A. 3D-Printed Bioplastics with Shape-Memory Behavior Based on Native Bovine Serum Albumin. *ACS Appl. Mater. Interfaces* **2021**, *13* (16), 19193–19199.

(20) Wang, Y.; Miao, Y.; Zhang, J.; Wu, J. P.; Kirk, T. B.; Xu, J.; Ma, D.; Xue, W. Three-Dimensional Printing of Shape Memory Hydrogels with Internal Structure for Drug Delivery. *Mater. Sci. Eng. C* **2018**, *84*, 44–51.

(21) Shiblee, M. N. I.; Ahmed, K.; Kawakami, M.; Furukawa, H. 4D Printing of Shape-Memory Hydrogels for Soft-Robotic Functions. *Adv. Mater. Technol.* **2019**, *4* (8).

(22) Li, H.; Go, G.; Ko, S. Y.; Park, J. O.; Park, S. Magnetic Actuated PH-Responsive Hydrogel-Based Soft Micro-Robot for Targeted Drug Delivery. *Smart Mater. Struct.* **2016**, *25* (2), 027001.

(23) Cicuéndez, M.; Doadrio, J. C.; Hernández, A.; Portolés, M. T.; Izquierdo-Barba, I.; Vallet-Regí, M. Multifunctional PH Sensitive 3D Scaffolds for Treatment and Prevention of Bone Infection. *Acta Biomater.* **2018**, *65*, 450–461.

(24) Zhang, M.; Vora, A.; Han, W.; Wojtecki, R. J.; Maune, H.; Le, A. B. A.; Thompson, L. E.; McClelland, G. M.; Ribet, F.; Engler, A. C.; Nelson, A. Dual-Responsive Hydrogels for Direct-Write 3D Printing. *Macromolecules* **2015**, *48*, 6482–6488.

(25) Kolesky, D. B.; Truby, R. L.; Gladman, A. S.; Busbee, T. A.; Homan, K. A.; Lewis, J. A. 3D Bioprinting of Vascularized, Heterogeneous Cell-Laden Tissue Constructs. *Adv. Mater.* **2014**, *26*, 3124–3130.

(26) Wong, J.; Gong, A. T.; Defnet, P. A.; Meabe, L.; Beauchamp, B.; Sweet, R. M.; Sardon, H.; Cobb, C. L.; Nelson, A. 3D Printing Ionogel Auxetic Frameworks for Stretchable Sensors. *Adv. Mater. Technol.* **2019**, 1900452.

(27) Wong, J.; Basu, A.; Wende, M.; Boechler, N.; Nelson, A. Mechano-Activated Objects with Multidirectional Shape Morphing Programmed via 3D Printing. *ACS Appl. Polym. Mater.* **2020**, *2* (7), 2504–2508.

(28) Basu, A.; Saha, A.; Goodman, C.; Shafranek, R. T.; Nelson, A. Catalytically Initiated

Gel-in-Gel Printing of Composite Hydrogels. *ACS Appl. Mater. Interfaces* **2017**, *9* (46), 40898–40904.

(29) Karis, D. G.; Ono, R. J.; Zhang, M.; Vora, A.; Storti, D.; Ganter, M. A.; Nelson, A. Cross-Linkable Multi-Stimuli Responsive Hydrogel Inks for Direct-Write 3D Printing. *Polym. Chem.* **2017**, *8* (29), 4199–4206.

(30) Fellin, C. R.; Adelmund, S. M.; Karis, D. G.; Shafranek, R. T.; Ono, R. J.; Martin, C. G.; Johnston, T. G.; DeForest, C. A.; Nelson, A. Tunable Temperature- and Shear-Responsive Hydrogels Based on Poly(Alkyl Glycidyl Ether)S. *Polym. Int.* **2019**, *68* (7), 1238–1246.

(31) Priks, H.; Butelmann, T.; Illarionov, A.; Johnston, T. G.; Fellin, C.; Tamm, T.; Nelson, A.; Kumar, R.; Lahtvee, P. J. Physical Confinement Impacts Cellular Phenotypes within Living Materials. *ACS Appl. Bio Mater.* **2020**, *3* (7), 4273–4281.

(32) Johnston, T. G.; Fellin, C. R.; Carignano, A.; Nelson, A. Poly(Alkyl Glycidyl Ether) Hydrogels for Harnessing the Bioactivity of Engineered Microbes. *Faraday Discuss.* **2019**, *219*, 58–72.

(33) Smith, M. L.; Heitfeld, K.; Slone, C.; Vaia, R. A. Autonomic Hydrogels through Postfunctionalization of Gelatin. *Chem. Mater.* **2012**, *24* (15), 3074–3080.

(34) Yigit, S.; Sanyal, R.; Sanyal, A. Fabrication and Functionalization of Hydrogels through "Click" Chemistry. *Chemistry - An Asian Journal*. John Wiley & Sons, Ltd October 4, 2011, pp 2648–2659.

(35) Kosif, I.; Park, E. J.; Sanyal, R.; Sanyal, A. Fabrication of Maleimide Containing Thiol Reactive Hydrogels via Diels-Alder/Retro-Diels-Alder Strategy. *Macromolecules* **2010**, *43* (9), 4140–4148.

(36) Wang, L.; Zhu, L.; Hickner, M.; Bai, B. Molecular Engineering Mechanically Programmable Hydrogels with Orthogonal Functionalization. *Chem. Mater* **2017**, *29*, 28.

(37) Iha, R. K.; Wooley, K. L.; Nyström, A. M.; Burked, D. J.; Kade, M. J.; Hawker, C. J. Applications of Orthogonal "Click" Chemistries in the Synthesis of Functional Soft Materials. *Chem. Rev.* **2009**, *109* (11), 5620–5686.

(38) Campos, L. M.; Killops, K. L.; Sakai, R.; Paulusse, J. M. J.; Damiron, D.; Drockenmuller, E.; Messmore, B. W.; Hawker, C. J. Development of Thermal and Photochemical Strategies for Thiol-Ene Click Polymer Functionalization. *Macromolecules* **2008**, *41* (19), 7063–7070.

(39) Deforest, C. A.; Polizzotti, B. D.; Anseth, K. S. Sequential Click Reactions for Synthesizing and Patterning Three-Dimensional Cell Microenvironments. *Nat. Mater.* **2009**, *8* (8), 659–664.

(40) Altin, H.; Kosif, I.; Sanyal, R. Fabrication of "Clickable" Hydrogels via Dendron-Polymer Conjugates. *Macromolecules* **2010**, *43* (8), 3801–3808.

(41) Altinbasak, I.; Arslan, M.; Sanyal, R.; Sanyal, A. Pyridyl Disulfide-Based Thiol-

Disulfide Exchange Reaction: Shaping the Design of Redox-Responsive Polymeric Materials. *Polymer Chemistry*. Royal Society of Chemistry December 28, 2020, pp 7603–7624.

(42) Zugates, G. T.; Anderson, D. G.; Little, S. R.; Lawhorn, I. E. B.; Langer, R. Synthesis of Poly(β-Amino Ester)s with Thiol-Reactive Side Chains for DNA Delivery. *J. Am. Chem. Soc.* **2006**, *128* (39), 12726–12734.

(43) Duvall, C. L.; Convertine, A. J.; Benoit, D. S. W.; Hoffman, A. S.; Stayton, P. S. Intracellular Delivery of a Proapoptotic Peptide via Conjugation to a RAFT Synthesized Endosomolytic Polymer. *Mol. Pharm.* **2010**, *7* (2), 468–476.

(44) Ju, Y.; Zhang, M.; Zhao, H. Poly(ϵ-Caprolactone) with Pendant Natural Peptides: An Old Polymeric Biomaterial with New Properties. *Polym. Chem.* **2017**, *8* (35), 5415–5426.

(45) Keller, S.; T.wilson, J.; Patilea, G. I.; Kern, H. B.; Convertine, A. J.; Stayton, P. S. Neutral Polymer Micelle Carriers with PH-Responsive, Endosome-Releasing Activity Modulate Antigen Trafficking to Enhance CD8+ T Cell Responses. *J. Control. Release* **2014**, *191*, 24–33.

(46) Bontempo, D.; Heredia, K. L.; Fish, B. A.; Maynard, H. D. Cysteine-Reactive Polymers Synthesized by Atom Transfer Radical Polymerization for Conjugation to Proteins. *J. Am. Chem. Soc.* **2004**, *126* (47), 15372–15373.

(47) Matsumoto, N. M.; González-Toro, D. C.; Chacko, R. T.; Maynard, H. D.; Thayumanavan, S. Synthesis of Nanogel-Protein Conjugates. *Polym. Chem.* **2013**, *4* (8), 2464–2469.

(48) Heredia, K. L.; Nguyen, T. H.; Chang, C. W.; Bulmus, V.; Davis, T. P.; Maynard, H. D. Reversible SiRNA-Polymer Conjugates by RAFT Polymerization. *Chem. Commun.* **2008**, No. 28, 3245–3247.

(49) Vázquez-Dorbatt, V.; Tolstyka, Z. P.; Chang, C. W.; Maynard, H. D. Synthesis of a Pyridyl Disulfide End-Functionalized Glycopolymer for Conjugation to Biomolecules and Patterning on Gold Surfaces. *Biomacromolecules* **2009**, *10* (8), 2207–2212.

(50) Gunasekaran, K.; Nguyen, T. H.; Maynard, H. D.; Davis, T. P.; Bulmus, V. Conjugation of SiRNA with Comb-Type PEG Enhances Serum Stability and Gene Silencing Efficiency. *Macromol. Rapid Commun.* **2011**, *32* (8), 654–659.

(51) Gevrek, T. N.; Cosar, M.; Aydin, D.; Kaga, E.; Arslan, M.; Sanyal, R.; Sanyal, A. Facile Fabrication of a Modular "Catch and Release" Hydrogel Interface: Harnessing Thiol-Disulfide Exchange for Reversible Protein Capture and Cell Attachment. *ACS Appl. Mater. Interfaces* **2018**, *10* (17), 14399–14409.

(52) Li, L.; Liu, X.; Xu, J.; Kan, C. Microfluidic Preparation of Thiol-Containing Monodisperse Polymer Microspheres and Their Adsorption of Pb2+ in Water. *Chem. Eng. J.* **2019**, *375*, 122012.

(53) Song, L.; Zhang, B.; Gao, G.; Xiao, C.; Li, G. Single Component Pluronic F127-Lipoic Acid Hydrogels with Self-Healing and Multi-Responsive Properties. *Eur. Polym. J.*

2019, *115*, 346–355.

(54) Zhao, S.; Cao, M.; Wu, J.; Xu, W. Synthesis and Characterization of Biodegradable Thermo- Ad PH-Sensitive Hydrogels Based on Pluronic F127/Poly(ε-Caprolactone) Macromer and Acrylic Acid. *Macromol. Res.* **2009**, *17* (12), 1025–1031.

(55) Zhu, W.; Wang, B.; Zhang, Y.; Ding, J. Preparation of a Thermosensitive and Biodegradable Microgel via Polymerization of Macromonomers Based on Diacrylated Pluronic/Oligoester Copolymers. *Eur. Polym. J.* **2005**, *41* (9), 2161–2170.

(56) Wu, T. Y.; Zrimsek, A. B.; Bykov, S. V.; Jakubek, R. S.; Asher, S. A. Hydrophobic Collapse Initiates the Poly(N -Isopropylacrylamide) Volume Phase Transition Reaction Coordinate. *J. Phys. Chem. B* **2018**, *122* (11), 3008–3014.

(57) Okudan, A.; Altay, A. Investigation of the Effects of Different Hydrophilic and Hydrophobic Comonomers on the Volume Phase Transition Temperatures and Thermal Properties of N-Isopropylacrylamide-Based Hydrogels. *Int. J. Polym. Sci.* **2019**, *2019*.

(58) Xu, X.; Liu, Y.; Fu, W.; Yao, M.; Ding, Z.; Xuan, J.; Li, D.; Wang, S.; Xia, Y.; Cao, M. Poly(N-Isopropylacrylamide)-Based Thermoresponsive Composite Hydrogels for Biomedical Applications. *Polymers*. MDPI AG March 1, 2020, p 580.

(59) Chien, H. W.; Xu, X.; Ella-Menye, J. R.; Tsai, W. B.; Jiang, S. High Viability of Cells Encapsulated in Degradable Poly(Carboxybetaine) Hydrogels. *Langmuir* **2012**, *28* (51), 17778–17784.

(60) Perera, M. M.; Ayres, N. Gelatin Based Dynamic Hydrogels: Via Thiol-Norbornene Reactions. *Polym. Chem.* **2017**, *8* (44), 6741–6749.

(61) Choh, S. Y.; Cross, D.; Wang, C. Facile Synthesis and Characterization of Disulfide-Cross-Linked Hyaluronic Acid Hydrogels for Protein Delivery and Cell Encapsulation. *Biomacromolecules* **2011**, *12* (4), 1126–1136.

(62) Zhang, Y.; Heher, P.; Hilborn, J.; Redl, H.; Ossipov, D. A. Hyaluronic Acid-Fibrin Interpenetrating Double Network Hydrogel Prepared in Situ by Orthogonal Disulfide Cross-Linking Reaction for Biomedical Applications. *Acta Biomater.* **2016**, *38*, 23–32.

(63) Cabral, H.; Miyata, K.; Osada, K.; Kataoka, K. Block Copolymer Micelles in Nanomedicine Applications. *Chemical Reviews*. American Chemical Society July 25, 2018, pp 6844–6892.

(64) Xu, W.; Ling, P.; Zhang, T. Polymeric Micelles, a Promising Drug Delivery System to Enhance Bioavailability of Poorly Water-Soluble Drugs. *J. Drug Deliv.* **2013**, *2013*, 1–15.

(65) Kumi, B. C.; Hammouda, B.; Greer, S. C. Self-Assembly of the Triblock Copolymer 17R4 Poly(Propylene Oxide)-Poly(Ethylene Oxide)-Poly(Propylene Oxide) in D2O. *J. Colloid Interface Sci.* **2014**, *434*, 201–207.

(66) Nguyen-Misra, M.; Mattice, W. L. Micellization and Gelation of Symmetric Triblock Copolymers with Insoluble End Blocks. *Macromolecules* **1995**, *28*, 1444–1457.

(67) Chu, B.; Liu, T.; Wu, C.; Zhou, Z.; Mark Nace, V. Structures and Properties of Block Copolymers in Solution. *Macromol. Symp.* **1997**, *118* (1), 221–227.

(68) Park, S.; Foote, P. K.; Krist, D. T.; Rice, S. E.; Statsyuk, A. V. UbMES and UbFluor: Novel Probes for Ring-between-Ring (RBR) E3 Ubiquitin Ligase PARKIN. *J. Biol. Chem.* **2017**, *292* (40), 16539–16553.

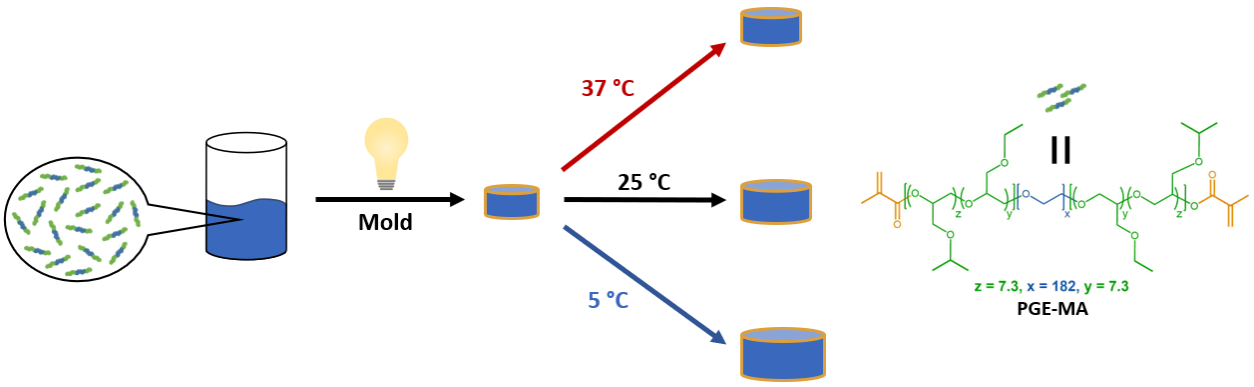

Figure 4.1 A graphical representation of the LCST-driven temperature dependent swelling behavior of PGE-MA hydrogels.

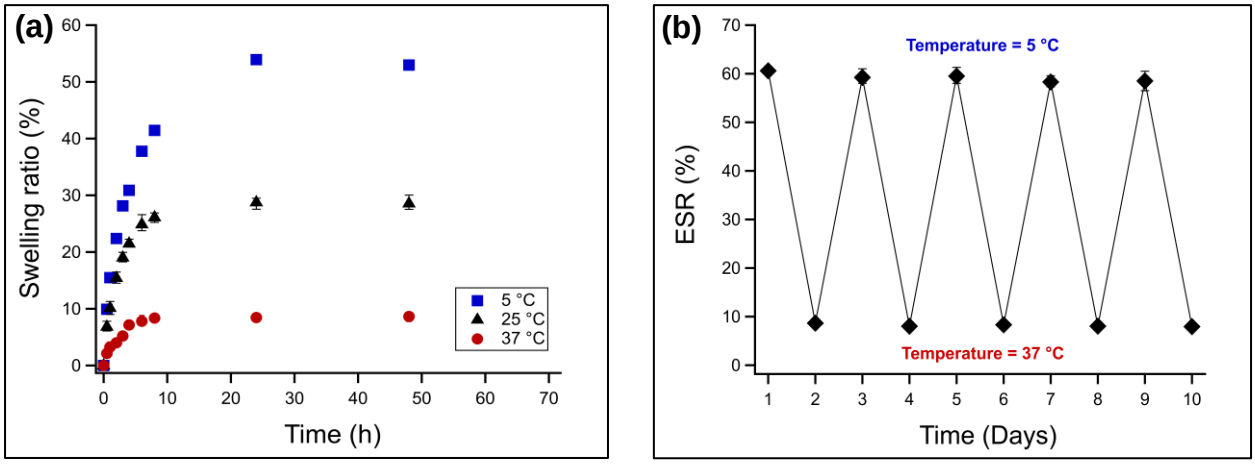

Figure 4.2 (a) Swelling ratio (%) vs Time (h) for PGE-MA/PDS-UM samples at 5 (blue squares), 25 (black triangles), and 37 °C (red circles). (b) Demonstration of reversible swelling from 5 °C to 37 °C over ten days.

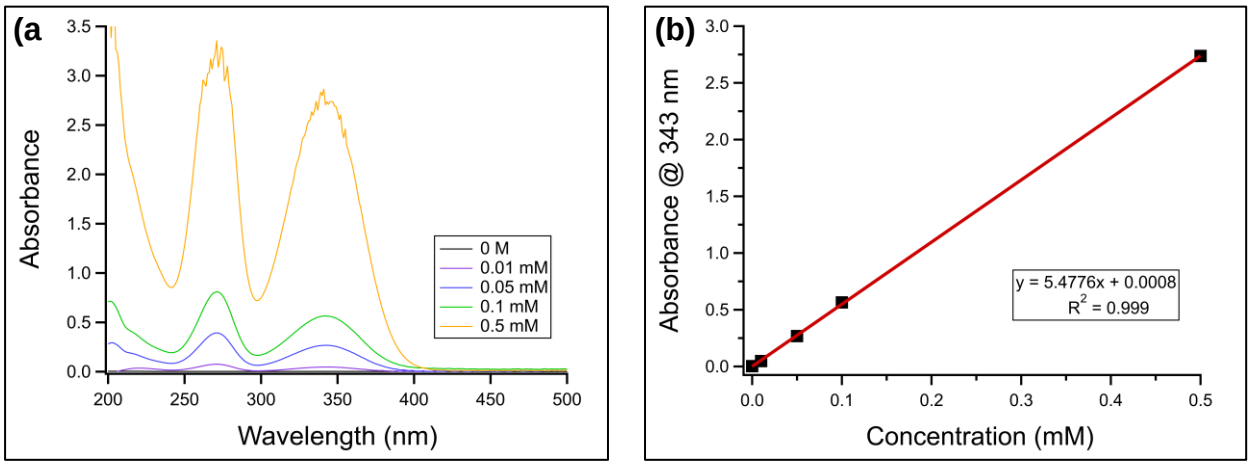

Figure 4.3 (a) Absorbance profiles and (b) calibration curve of 2-pyridothione (0.1-0.5 mM) in deionized water.

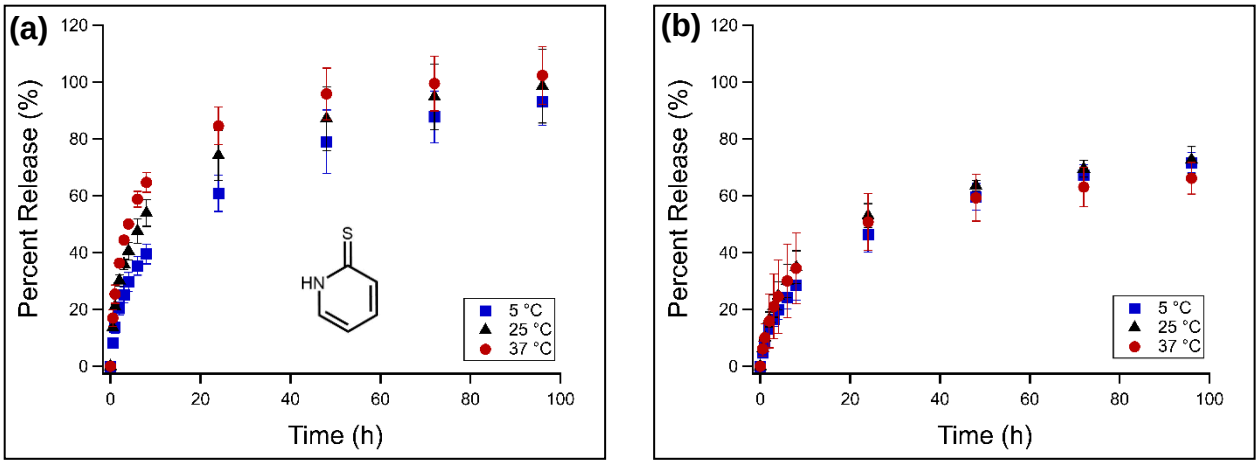

Figure 4.4 Percent release of 2-pyridothione (%) vs time (h) for (a) as-cured and (b) preswollen PGE-MA/PDS-UM samples at 5 (blue squares), 25 (black triangles), and 37 °C (red circles).

Temperature (°C)	Swelling status	24h (%)	96h (%)
5	Preswollen	46.2 ± 6.0	71.6 ± 3.6
5	As cured	60.8 ± 6.4	93.1 ± 8.2
25	Preswollen	53.0 ± 4.2	72.6 ± 4.7
25	As cured	74.2 ± 8.8	98.5 ± 13.0
37	Preswollen	50.8 ± 10.1	66.1 ± 5.5
37	As cured	84.6 ± 6.6	102.3 ± 10.2

Table 4.1 Percent release of 2-pyridothione (%) at different temperatures (5, 25, 37 °C), swelling statuses (as cure/preswollen), and time points (24/96 h).

Molecule	% Release (24 h)	% Release (96 h)	Equivalents	pH	Temperature (°C)
GSH	79.3	97.9	40	3	37
Cysteamine	80.9	77.0	40	5	25
EDT	80.4	77.5	0.5	5	25
PET	30.3	33.2	0.25	5	25
RGD-SH	71.6	80.4	5	5	25
RGD-PEG-SH	24.3	30.9	5	5	25
2-MCE	87.5	90.2	40	7.4	5
BSA	10.1	12.9	1	7.4	5

Table 4.2 Conjugation of thiol-containing molecules to PGE-MA/PDS-UM hydrogels. The percent release of 2-pyridothione was determined via UV-Vis spectroscopy at 24 and 96 h. The pH (3, 5, and 7.4) and temperature (5, 25, 37 °C) were modified to suppress auto-oxidation of the conjugating molecule and the 2-pyridothione leaving group.

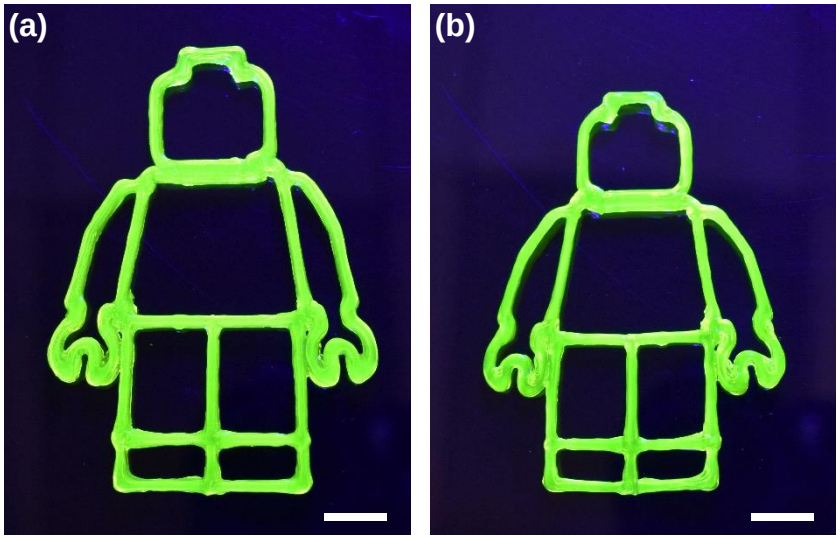

Figure 4.5 A 3D printed robot figurine was printed using a custom made, pneumatic DIW printer with a 0.41mm inner diameter nozzle at 5.0 mm/s. The fluorescent tag FITC-SH was conjugated to the object and the figurine was swelled at (a) 5°C and (b) 37 °C to demonstrate the thiol-reactivity and temperature dependent swelling of the PGE-MA/PDS-UM system (scale bars: 1cm).

APPENDIX A

Tunable Temperature- and Shear-Responsive Hydrogels Based on Poly(alkyl glycidyl Ether)s

***N*-propyl Glycidyl Ether Synthesis:** *N*-propyl glycidyl ether was synthesized according to literature from epichlorohydrin (34.4 mL, 0.44 mol) and 1-propanol (32.9 mL, 0.44 mol) in hexanes at reflux for 6 h. Potassium hydroxide pellets (56.11 g, 1 mol) were used as base with tetrabutylammonium bromide (1.77g, 5.5 mmol) as a phase transfer catalyst. The crude product was filtered, washed three times with brine, concentrated under reduced pressure, and purified via vacuum distillation to afford a yellow oil (15 g, 30% yield). ^{1}H NMR (300 MHz, $CDCl_3$): δ 0.91-0.95 (t, 3H, *J* = 7.5 Hz), 1.55-1.67 (sext, 2H, *J* = 7.5 Hz), 2.60-2.62 (dd, 1H, *J* = 4.5, 8.5 Hz) 2.78-2.81 (dd, 1H, *J* = 7.0, 8.5) 3.12-3.17 (m, 1H) 3.35-3.52 (m, 2H) 3.69-3.74 (dd, 1H, *J* = 5, 19.5)

General synthesis of poly(alkyl glycidyl ethers): All alkyl glycidyl ether homopolymers were synthesized by utilizing the same synthetic procedure with different monomer feed ratios. The following poly(isopropyl glycidyl ether) synthetic scheme will serve as an example. The initiator, 4-methyl benzyl alcohol (0.122 g, 1 mmol) was added to an oven dried, 100 mL round bottom flask. Potassium naphthalenide solution (1M in THF) was titrated until a light green paste was formed. The reaction flask was evacuated overnight to drive off the remaining THF. Isopropyl glycidyl ether (6.49 mL, 51.56 mmol) was added to the dried mixture of deprotonated initiator, and the reaction was stirred at 70 °C for 45 h. The polymer solution was quenched using a degassed 1% v/v AcOH in MeOH solution and dialyzed against MeOH for 3 d (3 solvent exchanges) using Spectra/Por regenerated cellulose tubing (MWCO 1.0 kDa) that was pre-

soaked in water. The dialyzed polymer solution was concentrated under reduced pressure and dried in a vacuum oven for 24 h to afford a viscous, pale yellow liquid (0.8 g).

General synthesis of triblock copolymers: ABA triblock copolymers were synthesized via anionic ring-opening polymerization. All copolymers were initiated from PEO ($M_{n\,=}$ 8,000 g mol^{-1}). The following procedure for (P*i*PGE-*stat*-PEGE)$_{2.2k}$-*b*-PEO$_{8k}$-*b*-(PEGE-*stat*-P*i*PGE)$_{2.2k}$ (Polymer **9**) will serve as an example for a typical triblock copolymer synthesis. PEO (10 g, 1.25 mmol) was added to the reaction vessel and dried under vacuum overnight. Dry THF (100 mL) was added under an argon atomosphere and heated to 50 °C to facilitate dissolution of the macroinitator. Once sufficiently dissolved, a potassium naphthalenide solution (1M in THF) was titrated into the flask until the solution remained a slight green color, indicating full deprotonation of PEO hydroxyl end groups. This was followed by the simultaneous addition of isopropyl glycidyl ether (4.07 g, 35 mmol) and ethyl glycidyl ether (3.57 g, 35 mmol) to begin polymerization. The reaction continued for 24 h at 65 °C and was subsequently quenched with a degassed solution of 1% v/v AcOH in MeOH. In the polymerizations with allyl glycidyl ether, the reactions were performed at 30 °C in order to avoid allyl-vinyl isomerization as reported by Lynd and co-workers.[32] The reaction mixture was then precipitated into cold hexane. The polymer was collected via centrifugation (4400 rpm, 10 min) and the supernatant decanted. The product was washed twice with additional hexane and collected again in the same manner. The isolated polymer solution was dried in a vacuum oven for at least 24 h to afford an off-white solid (13.6 g).

Calculation of Triblock Copolymer M_n

Number average molecular weight was calculated using ^{1}H NMR and an example for a copolymer of PEGE-*stat*-P*i*PGE-*b*-PEG-*b*-PEGE-*stat*-P*i*PGE is given. The M_n of PEG is 8k Da which corresponds to approximately 182 ethylene glycol units per macroinitiator. If we use Polymer **9** and Figure A22 as the example spectrum then the number of ethyl and isopropyl glycidyl ether units can be calculated by finding the PEG to PEGE and PEG to P*i*PGE ratio. The integration for the peaks from 1.16-1.20 ppm correspond to the methyl group on PEGE and is usually set to 3.00. The peaks from 1.13-1.6 ppm corresponding to the P*i*PGE methyl groups integrate to 5.82. The PEG, PEGE, and P*i*PGE ether backbone protons manifest as peaks from 3.2-3.9 ppm and integrate to a value of 48.486. Since the PEGE and P*i*PGE ether backbone peaks overlap in the 3.5 ppm region, their contribution to the overall integration must be subtracted through the following steps.

First it is necessary to calculate the relative integrations of the *i*PGE and EGE methyl protons. The integration values for the methyl groups of *i*PGE and EGE are divided by the number of protons they represent (6 and 3, respectively).

$$\frac{5.82\ Integrated\ \text{i}PGE\ CH_3\ Protons}{6\ Actual\ iPGE\ CH_3\ Protons} = 0.97\ Relative\ \text{i}PGE\ Integration$$

$$\frac{3.00\ Integrated\ EGE\ CH_3\ Protons}{3\ Actual\ EGE\ CH_3\ Protons} = 1.00\ Relative\ EGE\ Integration$$

These values are then used to calculate the number of relative EGE and *i*PGE backbone protons. This is done by multiplying the relative integrations by the number of backbone protons.

$$0.97\ Relative\ \text{i}PGE\ Integration * 6\ \text{i}PGE\ Backbone\ Protons = 5.82\ Relative\ \text{i}PGE\ Backbone\ Protons$$

$$1.00\ Relative\ EGE\ Integration * 7\ EGE\ Backbone\ Protons = 7\ Relative\ EGE\ Backbone\ Protons$$

The contribution of EGE protons can now be subtracted from the total integration, and the corresponding number of repeat units determined, using the calculation shown below.

$$\frac{182\ Ethylene\ Gylcol\ Units}{\frac{(48.486\ Total\ Backbone - 7\ EGE - 5.82\ \mathrm{i}PGE)}{4\ PEG\ CH_2}} * 1.0\ Relative\ EGE\ Integration = 20.4\ EGE\ Repeat\ Units$$

To calculate the number of iPGE repeat units we need only to multiple the EGE repeat units by the relative iPGE integration

$$20.4\ EGE\ Repeat\ Units * 0.97\ Relative\ \mathrm{i}PGE\ Integration = 19.8\ \mathrm{i}PGE\ Repeat\ Units$$

^{1}H NMR annotation for Poly(methyl glycidyl ether) (500 MHz, $CDCl_3$): 2.34 (s, -Ph-C*H*$_3$), 3.35-3.93 (m, (-O-C*H*$_2$-C*H*(C*H*$_2$-O-*CH*$_3$)-O-), 4.50 (s, -Ph-C*H*$_2$-O-), 7.14-7.15 (d, CH$_3$-*Ph*-CH$_2$-, *J* = 7.5 Hz), 7.21-7.22 (d, CH$_3$-*Ph*-CH$_2$-, *J* = 8.0 Hz)

^{1}H NMR annotation for Poly(ethyl glycidyl ether) (500 MHz, $CDCl_3$): δ 1.16-1.20 (t, -O-CH$_2$-C*H*$_3$, *J* = 7.2 Hz), 2.34 (s, -Ph-C*H*$_3$), 3.47-3.63 (m, (-O-C*H*$_2$-C*H*(C*H*$_2$-O-C*H*$_2$-CH$_3$)-O-), 4.50 (s, -Ph-C*H*$_2$-O-), 7.12-7.15 (d, CH$_3$-*Ph*-CH$_2$-, *J* = 8.1 Hz), 7.20-7.23 (d, CH$_3$-*Ph*-CH$_2$-, *J* = 8.1 Hz)

^{1}H NMR annotation for Poly(allyl glycidyl ether (500 MHz, $CDCl_3$): 2.34 (s, -Ph-C*H*$_3$), 3.45-3.83 (m, (-O-C*H*$_2$-C*H*(C*H*$_2$-O-CH$_2$-CH=CH$_2$)-O-), 3.98-3.99 (d, -O-C*H*$_2$-CH=CH$_2$)-O-, *J* = 5.5 Hz) 4.49 (s, -Ph-C*H*$_2$-O-) 5.14-5.16 (d, -O-CH$_2$-CH=C*H*$_2$)-O-, 10.0 Hz) 5.24-5.27 (d, -O-CH$_2$-CH=C*H*$_2$)-O-, *J* = 17.0 Hz) 5.85-5.92 (m, -O-CH$_2$-C*H*=CH$_2$)-O-) 7.13-7.14 (d, CH$_3$-*Ph*-CH$_2$-, 8.0 Hz) 7.20-7.21 (d, CH$_3$-*Ph*-CH$_2$-, 8.0 Hz)

^{1}H NMR annotation for Poly(*n*-propyl glycidyl ether) (500 MHz, $CDCl_3$): δ 0.89-0.92 (t, -O-CH_2-CH_2-C*H*$_3$, *J* = 7.0 Hz), 1.54-1.61 (sext, -O-CH_2-C*H*$_2$-CH_3 *J* = 7.0 Hz), 2.34 (s, -Ph-C*H*$_3$), 3.38-3.93 (m, (-O-C*H*$_2$-C*H*(C*H*$_2$-O-C*H*$_2$-CH_2-CH_3)-O-), 4.50 (s, -Ph-C*H*$_2$-O-), 7.13-7.15 (d, CH_3-*Ph*-CH_2-, *J* = 7.5 Hz), 7.21-7.22 (d, CH_3-*Ph*-CH_2-, *J* = 7.5 Hz)

^{1}H NMR annotation for Polymer 1 (500 MHz, $CDCl_3$): δ 1.17-1.20 (t, -O-CH_2-C*H*$_3$, *J* = 4.2 Hz) 3.47-3.65 (m -O-C*H*$_2$-C*H*$_2$-O- and -O-C*H*$_2$-C*H*(C*H*$_2$-O-C*H*$_2$-CH_3)-O-)

^{1}H NMR annotation for Polymer 2 (500 MHz, $CDCl_3$): 3.47-3.65 (m, -O-C*H*$_2$-C*H*$_2$-O- and -O-C*H*$_2$-C*H*(C*H*$_2$-O-CH_2-CH=CH_2)-O-), 3.99 (s, -O-C*H*$_2$-CH=CH_2)-O-), 5.14-5.16 (d, -O-CH_2-CH=C*H*$_2$)-O-, *J* = 10 Hz), 5.24-5.28 (d, -O-CH_2-CH=C*H*$_2$)-O-, *J* = 17.5 Hz). 5.85-5.92 (m, -O-CH_2-C*H*=CH_2)-O-).

^{1}H NMR annotation for Polymer 3 (500 MHz, $CDCl_3$): δ 1.12-1.15 (m, -O-CH-(C*H*$_3$)$_2$), 3.47-3.65 (m, -O-C*H*$_2$-C*H*$_2$-O- and -O-C*H*$_2$-C*H*(C*H*$_2$-O-C*H*-$(CH_3)_2$)-O-)

^{1}H NMR annotation for Polymer 4 (500 MHz, $CDCl_3$): δ 1.16-1.22 (t, -O-CH_2-C*H*$_3$), 3.48-3.66 (m, -O-C*H*$_2$-C*H*$_2$-O- and -O-C*H*$_2$-C*H*(C*H*$_2$-O-CH_2-CH=CH_2)-O- and -O-C*H*$_2$-C*H*(C*H*$_2$-O-C*H*$_2$-CH_3)-O-), 3.98-3.99 (dd, -O-C*H*$_2$-CH=CH_2)-O-, *J* = 4.0 Hz), 5.14-5.16 (d, -O-CH_2-CH=C*H*$_2$)-O-, *J* = 10 Hz), 5.24-5.28 (d, -O-CH_2-CH=C*H*$_2$)-O-, *J* = 17.5 Hz), 5.85-5.92 (m, -O-CH_2-C*H*=CH_2)-O-)

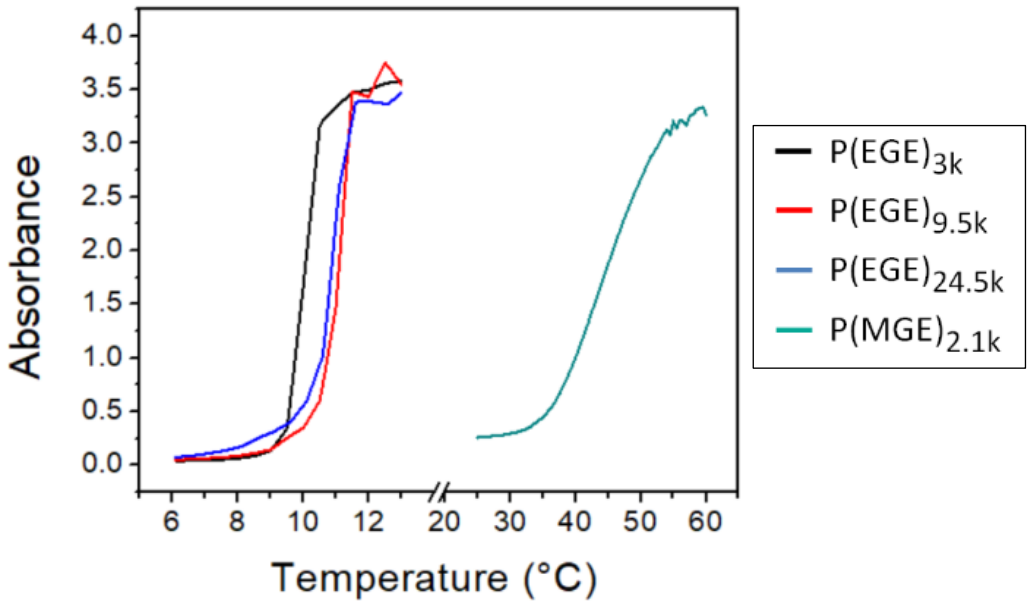

Figure A1. Homopolymer Cloud Point Measurements

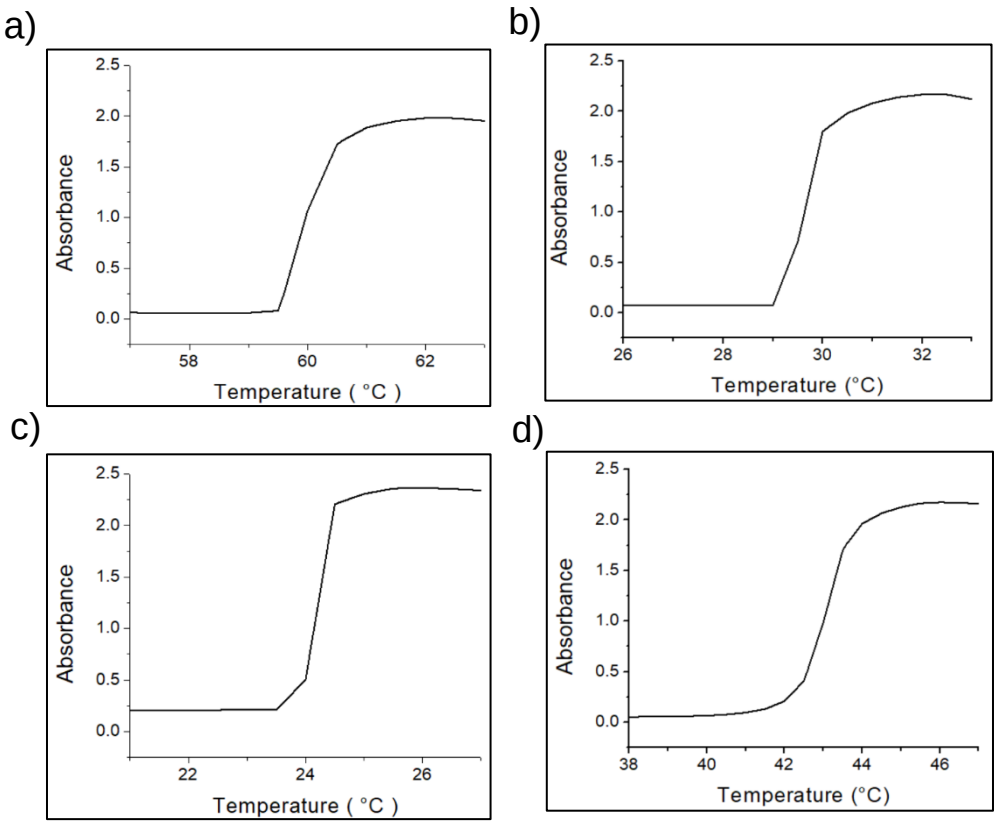

Figure A2. T_{cp} of (a) Polymer **1,** (b) Polymer **2**, (c) Polymer **3**, and (d) Polymer **4**

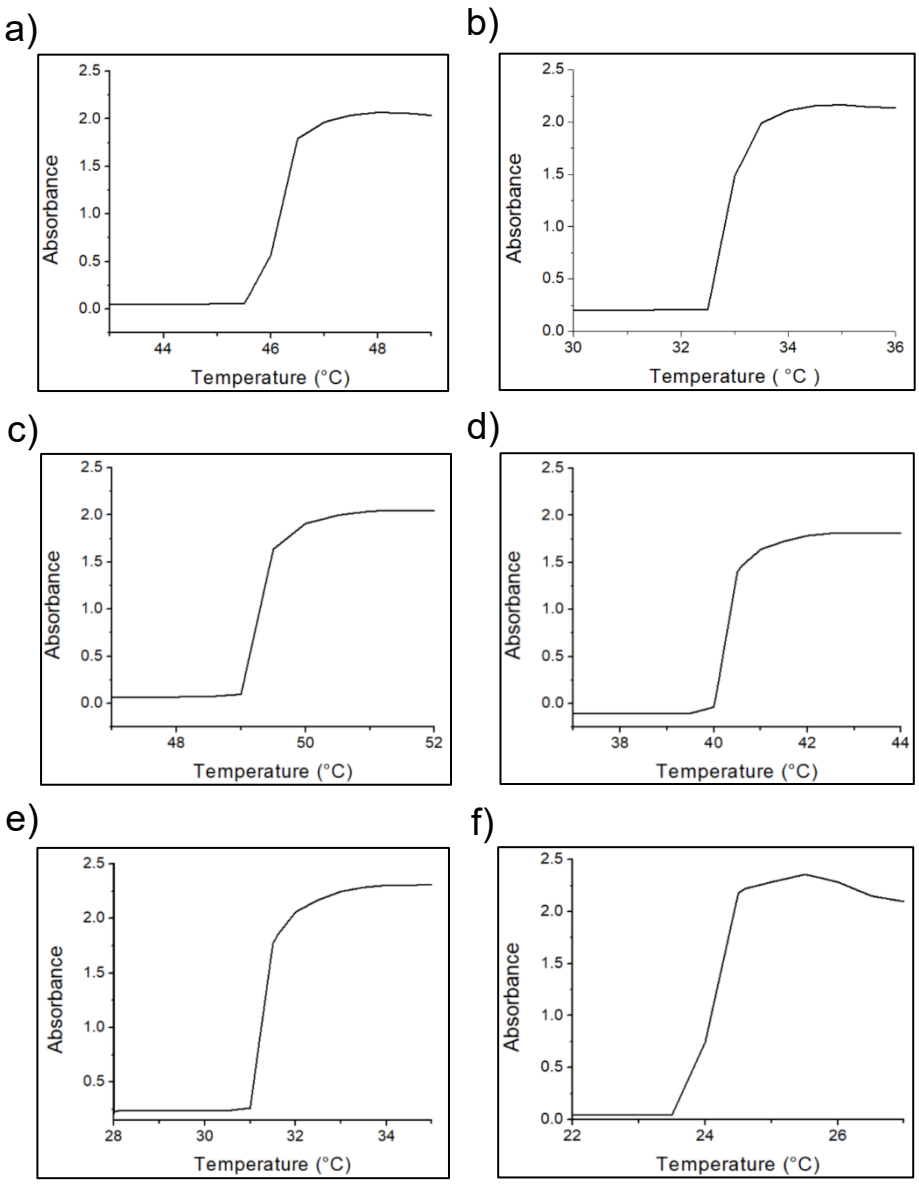

Figure A3. T_{cp} of (a) Polymer **5**, (b) Polymer **6**, (c) Polymer **7**, (d) Polymer **8**, (e) Polymer **9**, and (f) Polymer **10**

Figure A4. Allyl glycidyl ether triblock brittle hydrogel

	11.25 wt%	15 wt%	20 wt%
Trial 1	.936404	.956416	.985594
Trial 2	.944649	.966234	.638673
Trial 3	.90142	.963687	.910025
Trial 4	.926465	N/A	N/A
Trail 5	.842851	N/A	N/A
Average	.910358	.928779	.844764
Standard Deviation	.041081	.062681	.182436

Figure A5. Cell Viability data for 11.25, 15, and 20 wt% polymer **9** hydrogels in supplemented DMEM

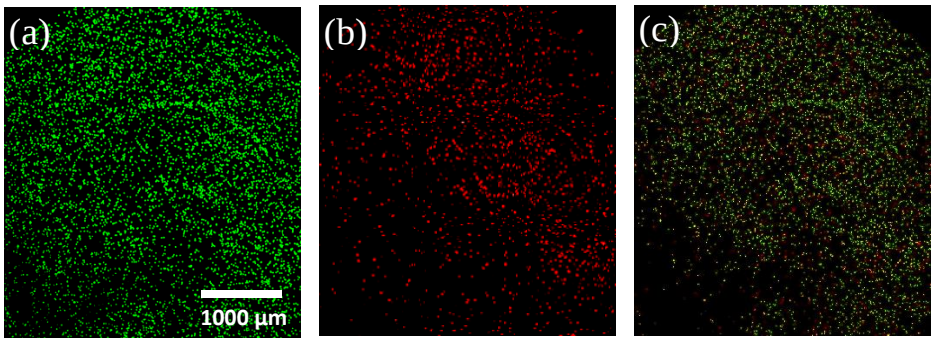

Figure A6. Confocal microscopy images of encapsulated HeLa cells in a 11.25 wt% formulation of polymer **9** in supplemented DMEM (a) green fluorescence channel indicating live cells (b) red fluorescence channel indicating dead cells (c) composite channel (scale bar: 1000 µm)

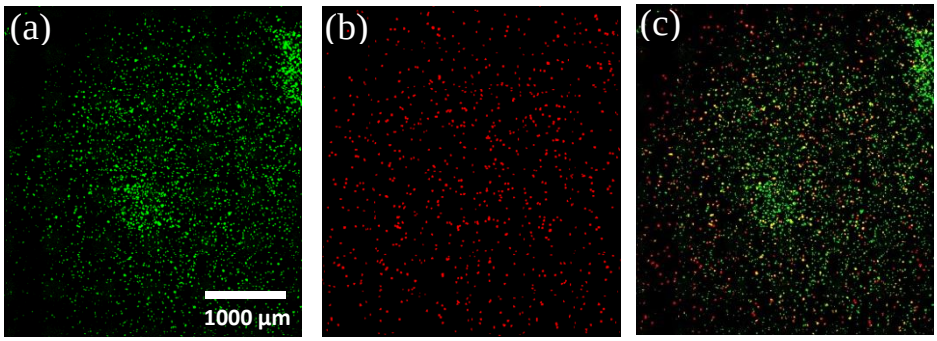

Figure A7. Confocal microscopy images of encapsulated HeLa cells in a 15.0 wt% formulation of polymer **9** in supplemented DMEM (a) green fluorescence channel indicating live cells (b) red fluorescence channel indicating dead cells (c) composite channel (scale bar: 1000 µm)

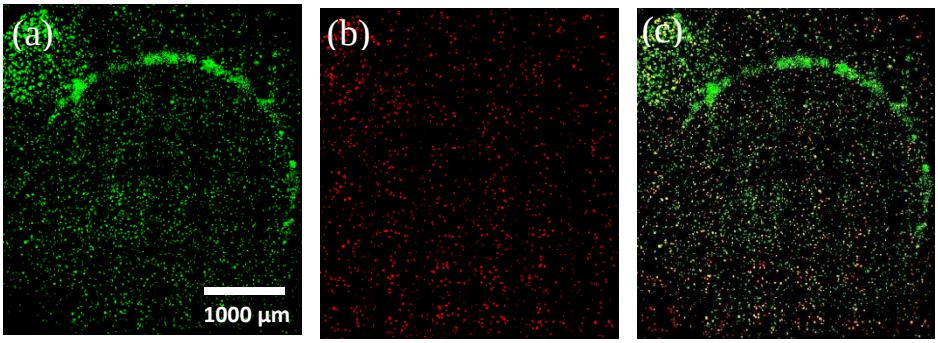

Figure A8. Confocal microscopy images of encapsulated HeLa cells in a 20.0 wt% formulation of polymer **9** in supplemented DMEM (a) green fluorescence channel indicating live cells (b) red fluorescence channel indicating dead cells (c) composite channel (scale bar: 1000 µm)

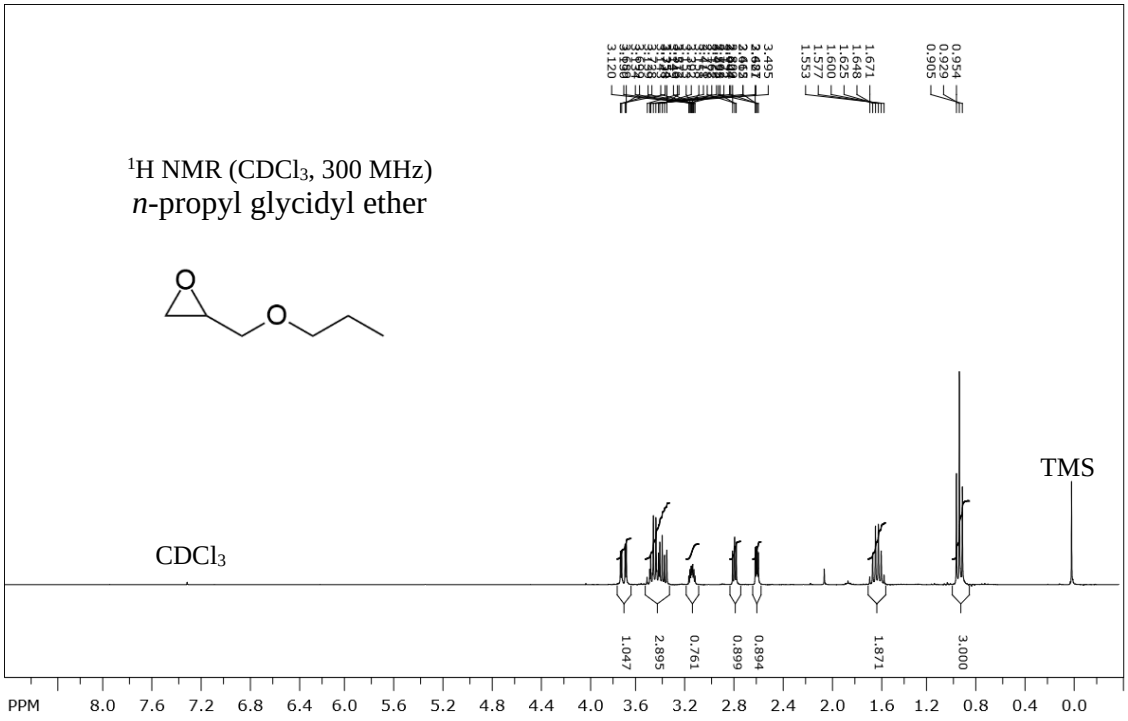

Figure A9. ^{1}H NMR of *n*-propyl glycidyl ether

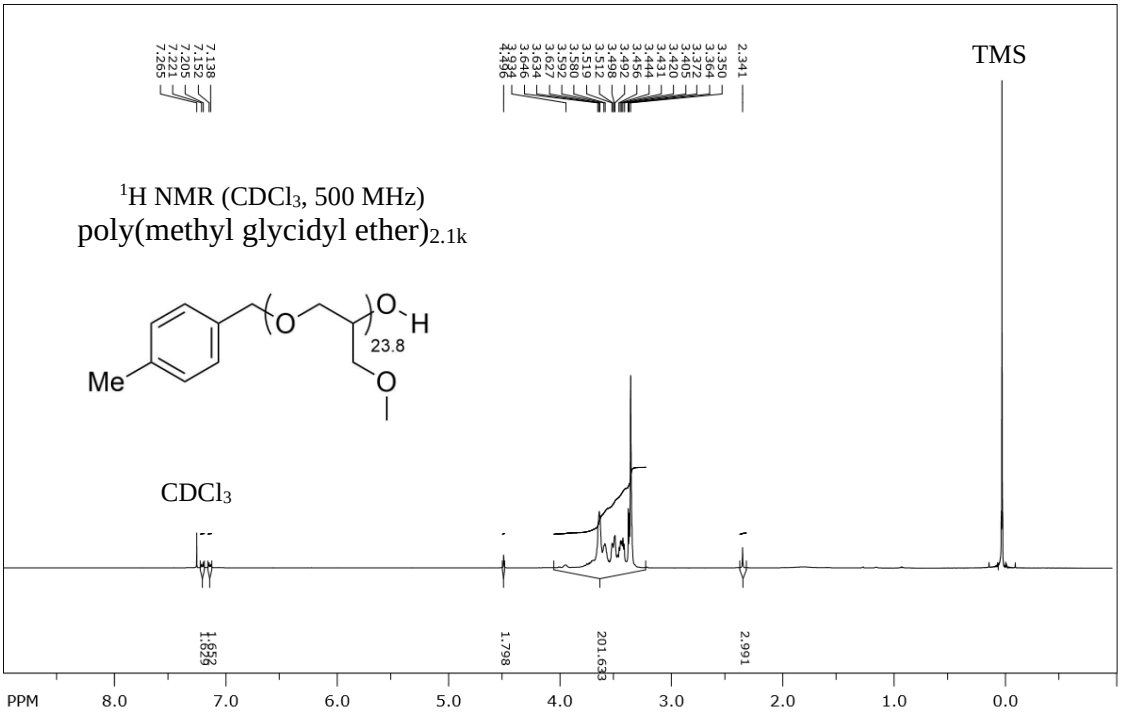

Figure A10. ^{1}H NMR of poly(methyl glycidyl ether)$_{2.1k}$

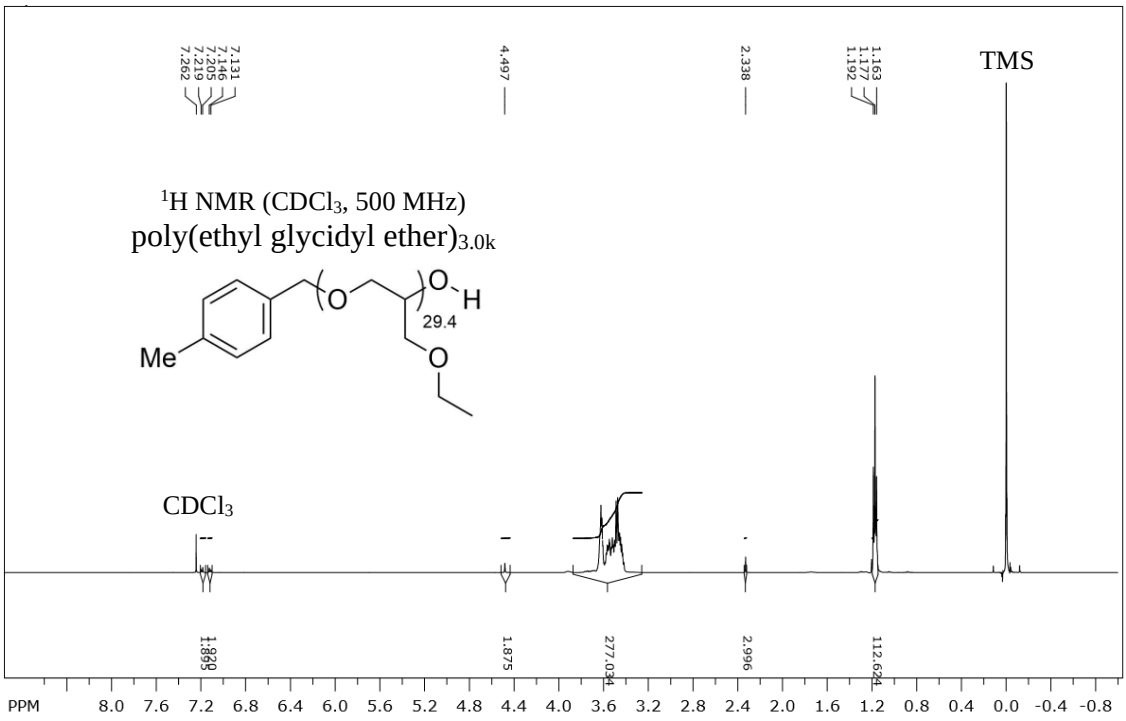

Figure A11. ^{1}H NMR of poly(ethyl glycidyl ether)$_{3.0k}$

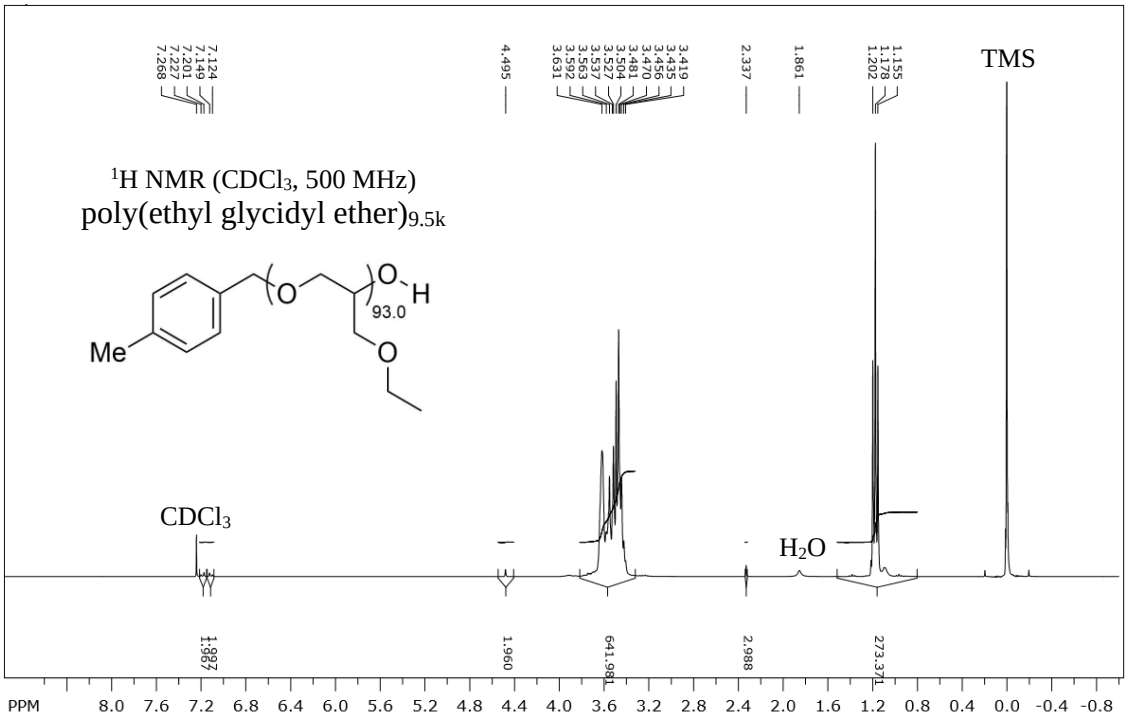

Figure A12. ^{1}H NMR of poly(ethyl glycidyl ether)$_{9.5k}$

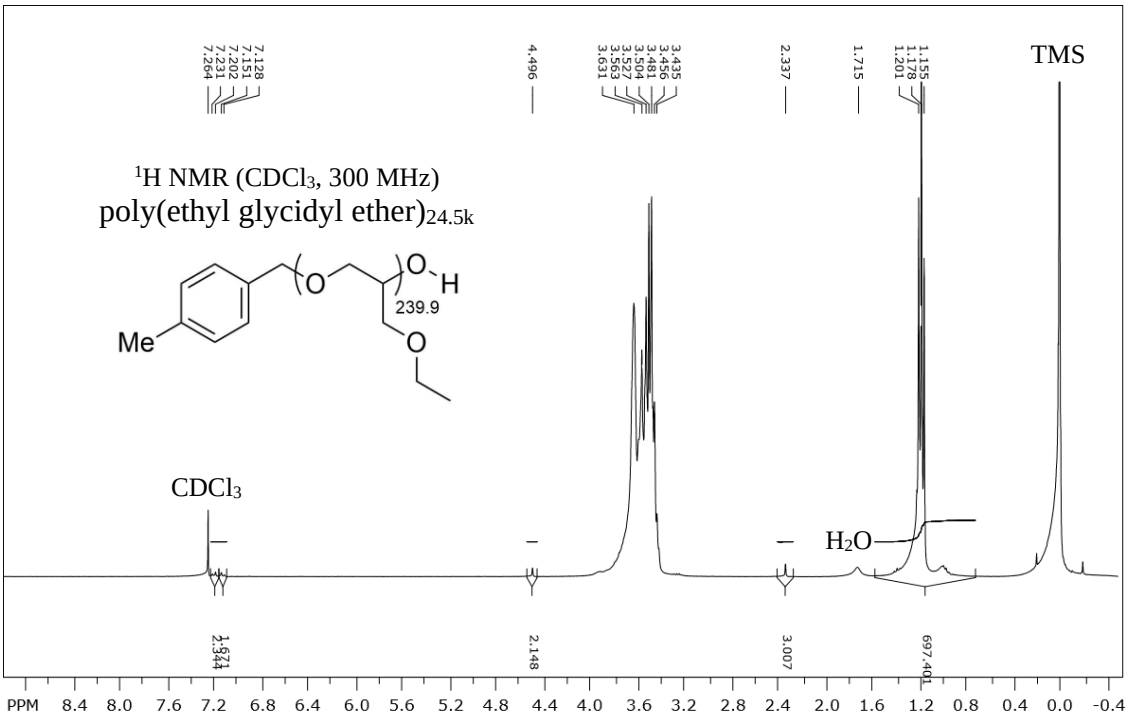

Figure A13. ^{1}H NMR of poly(ethyl glycidyl ether)$_{24.5k}$

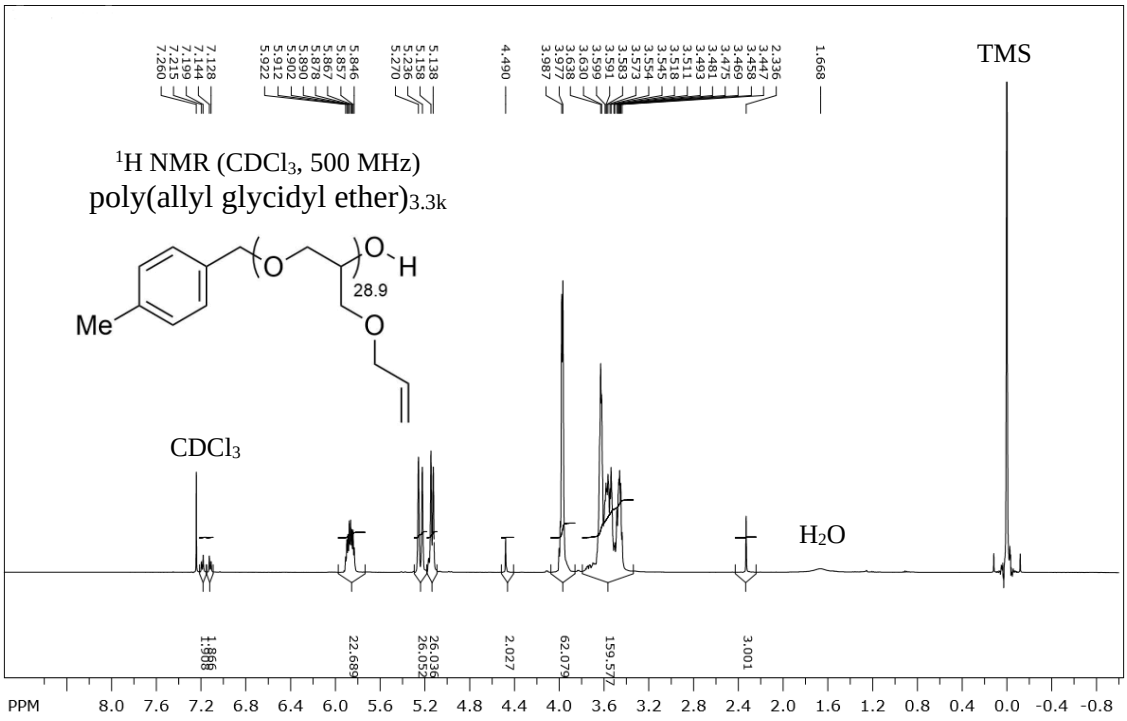

Figure A14. ^{1}H NMR of poly(allyl glycidyl ether)$_{3.3k}$

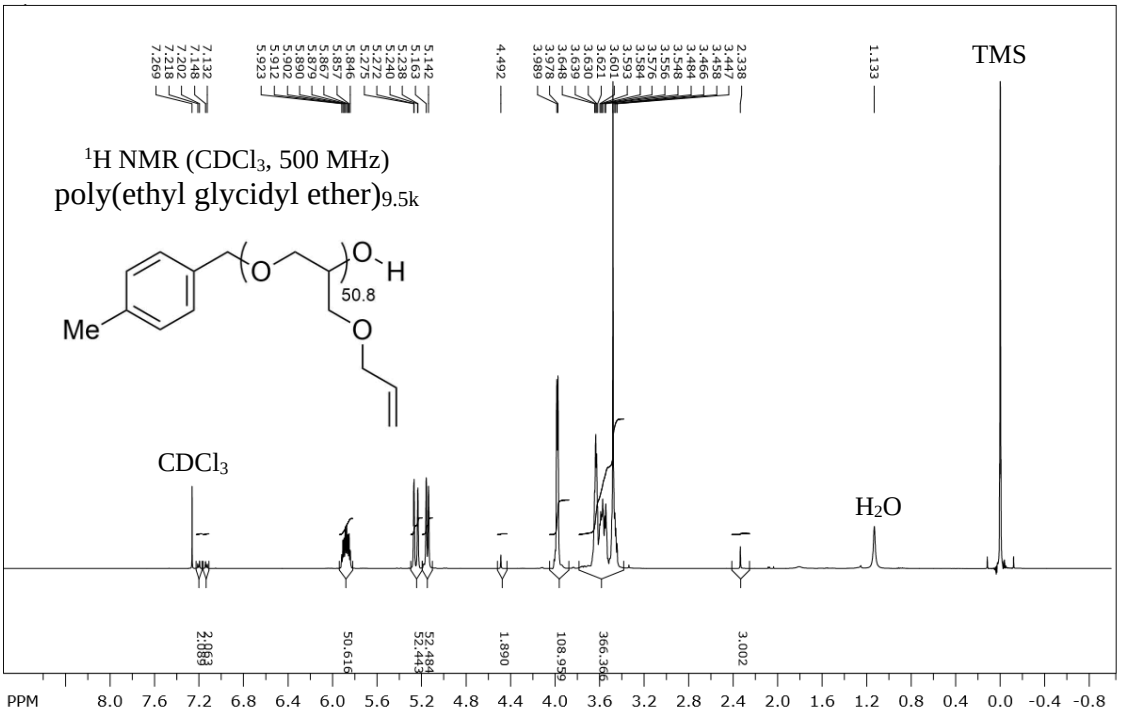

Figure A15. ^{1}H NMR of poly(allyl glycidyl ether)$_{5.8k}$

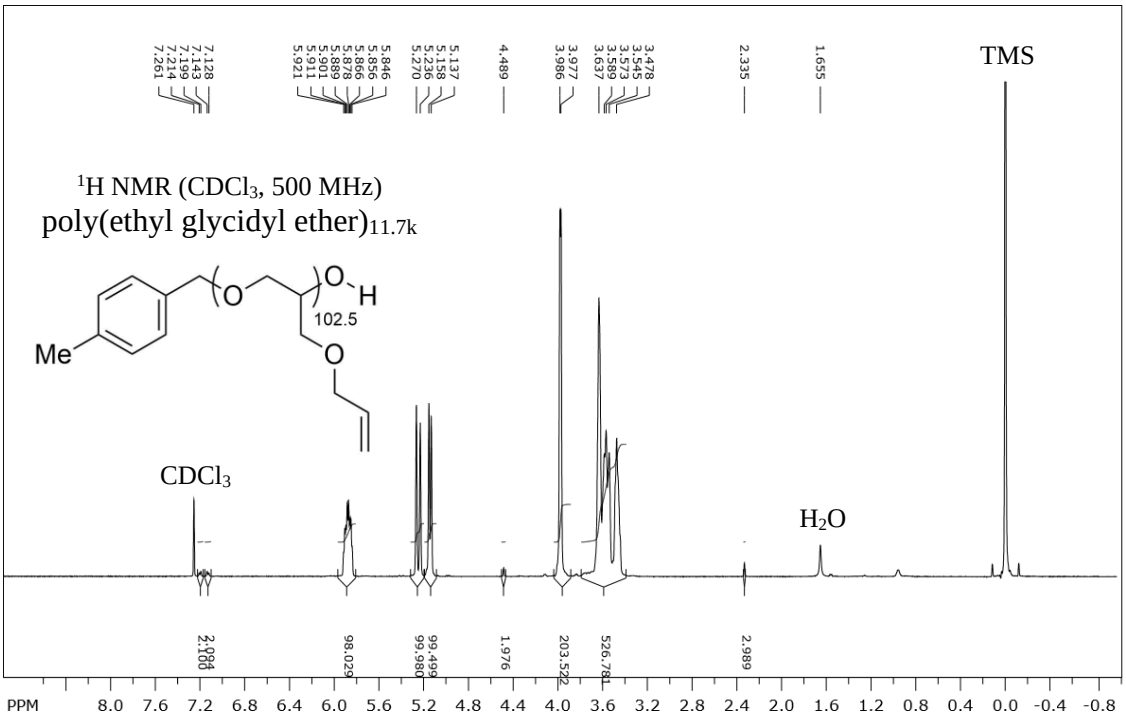

Figure A16. ^{1}H NMR of poly(allyl glycidyl ether)$_{11.7k}$

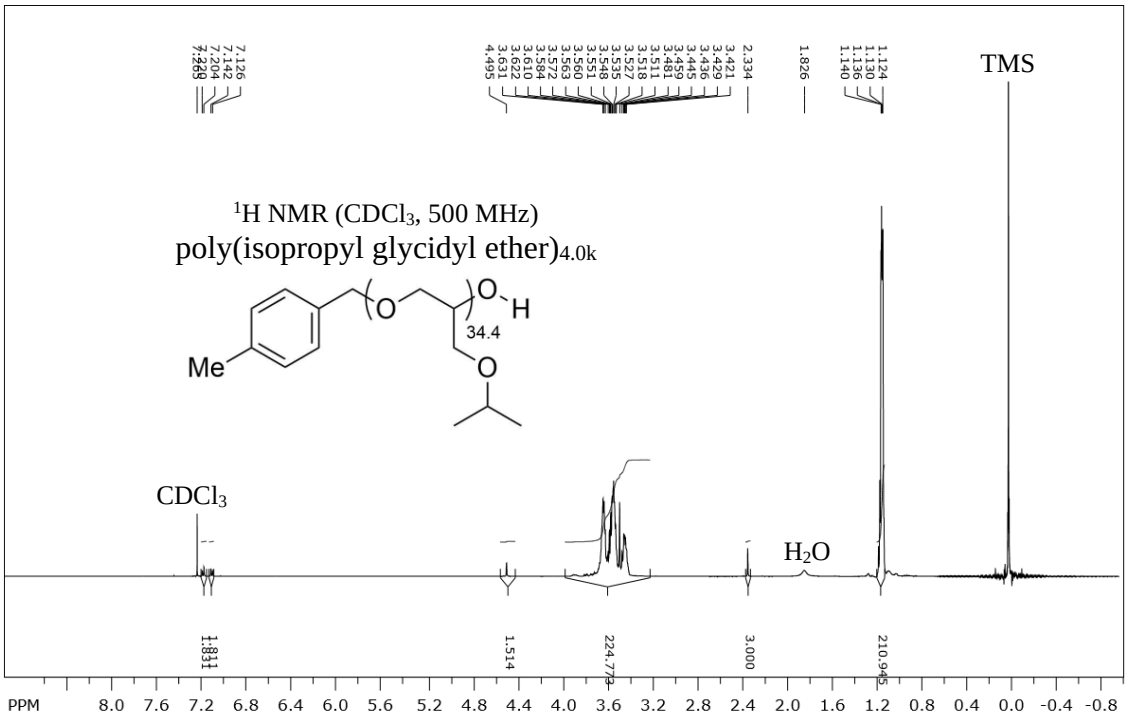

Figure A17. ^{1}H NMR of poly(isopropyl glycidyl ether)$_{4.0k}$

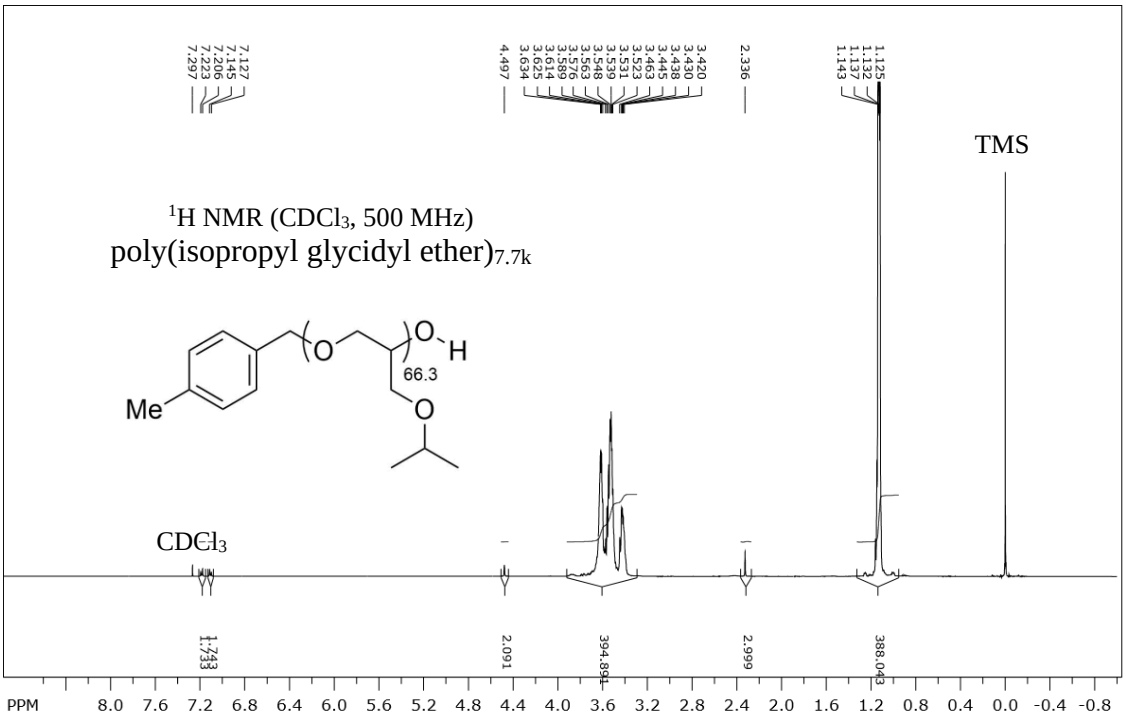

Figure A18. ^{1}H NMR of poly(isopropyl glycidyl ether)$_{7.7k}$

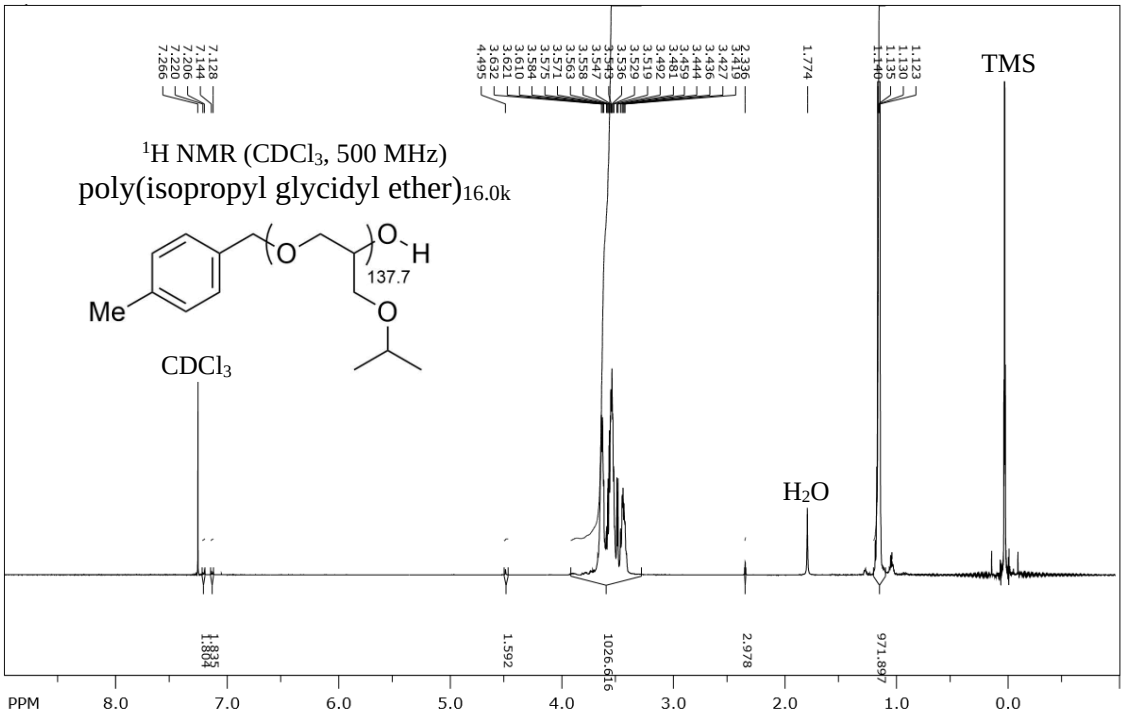

Figure A19. ^{1}H NMR of poly(isopropyl glycidyl ether)$_{16.0k}$

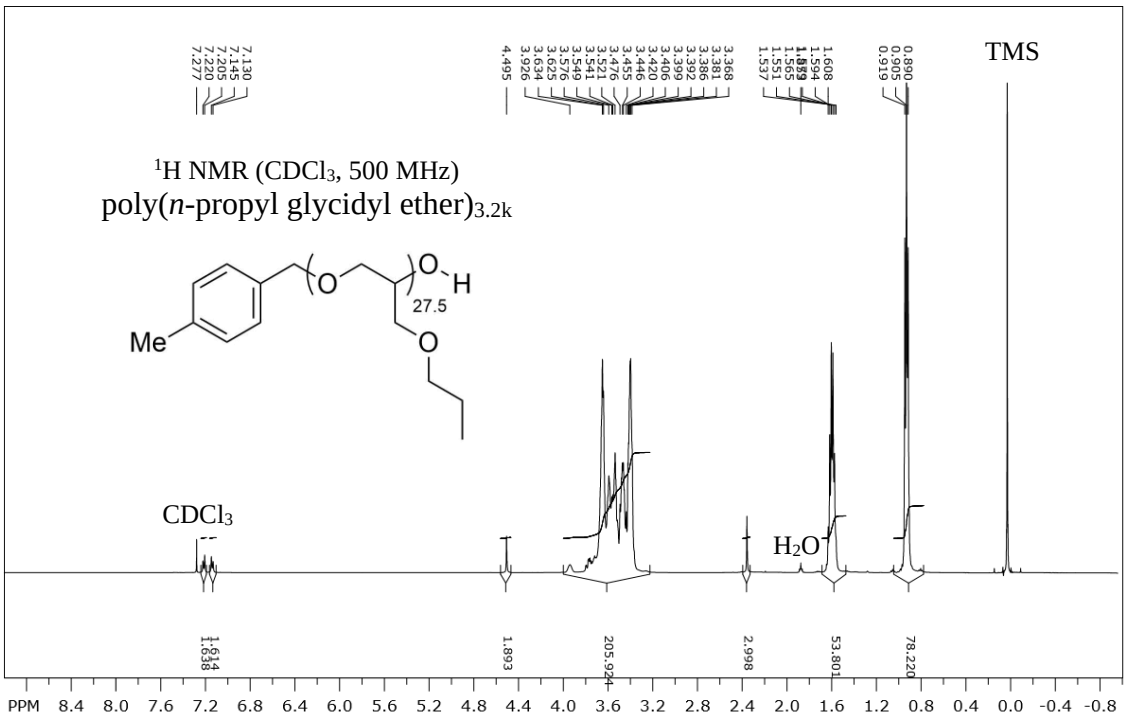

Figure A20. ^{1}H NMR of poly(*n*-propyl glycidyl ether)$_{3.2k}$

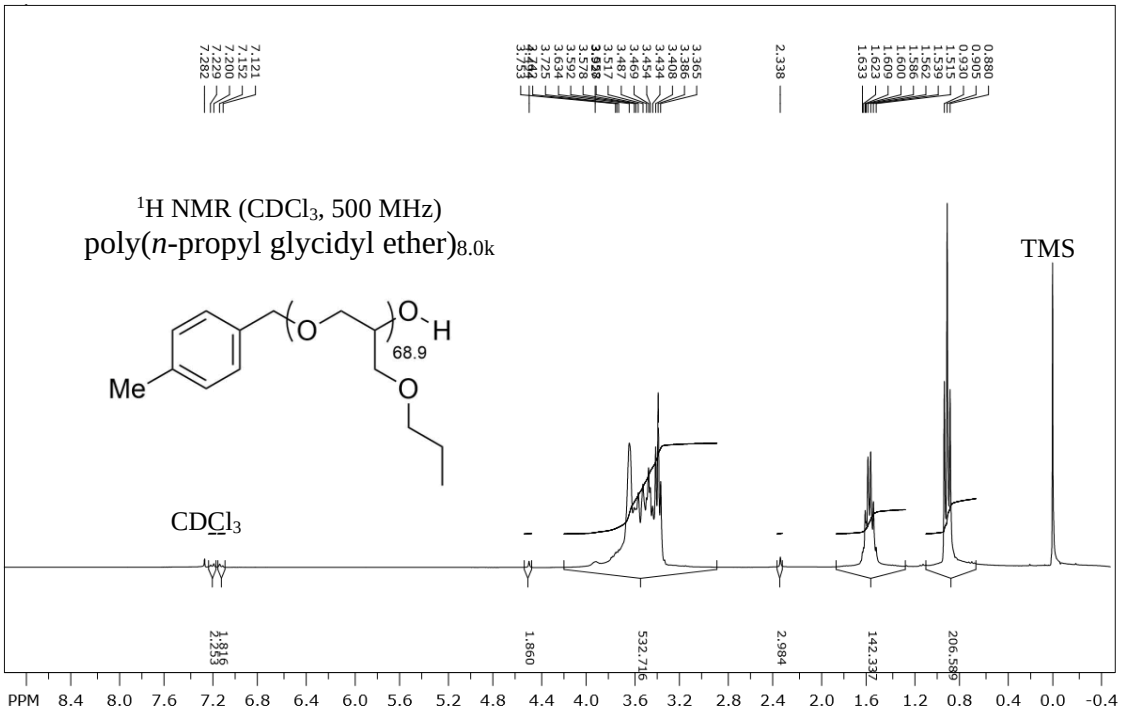

Figure A21. ^{1}H NMR of poly(*n*-propyl glycidyl ether)$_{8.0k}$

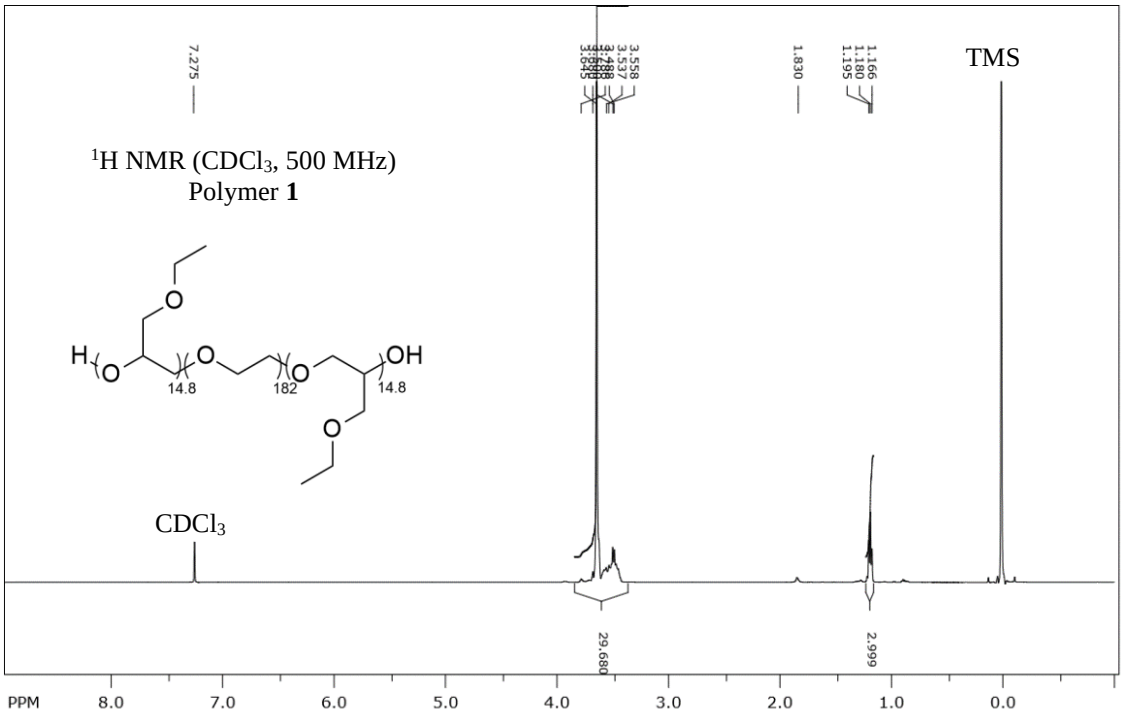

Figure A22. ^{1}H NMR of Polymer **1**

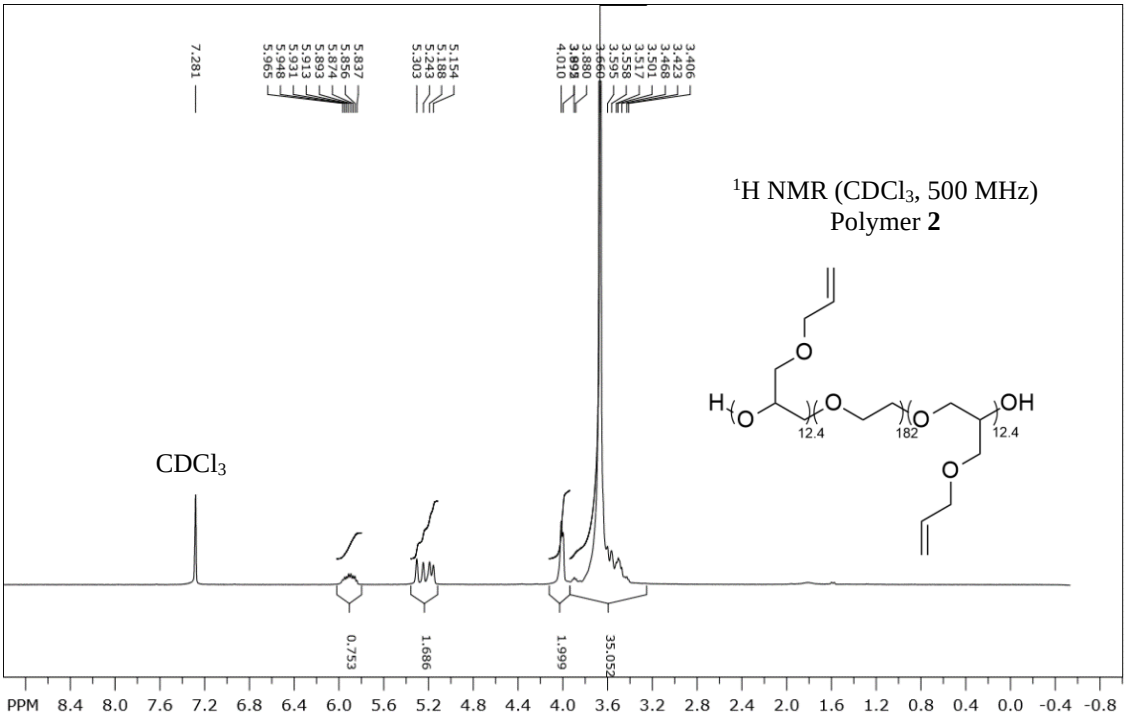

Figure A23. ^{1}H NMR of Polymer **2**

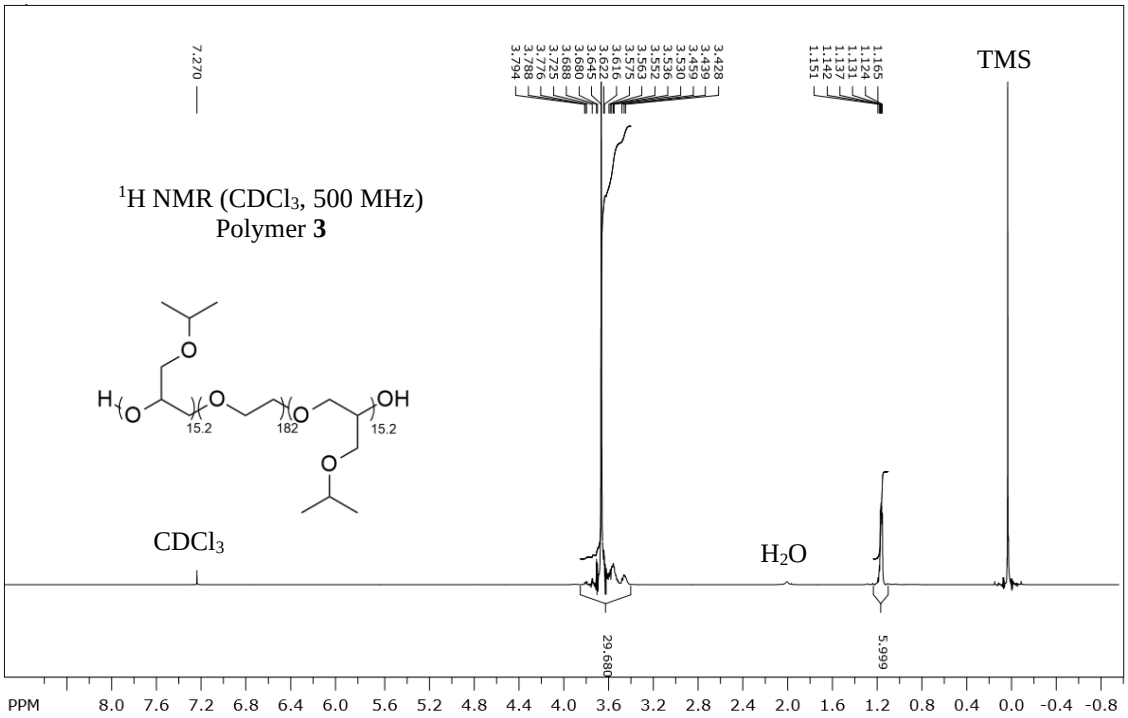

Figure A24. ^{1}H NMR of Polymer **3**

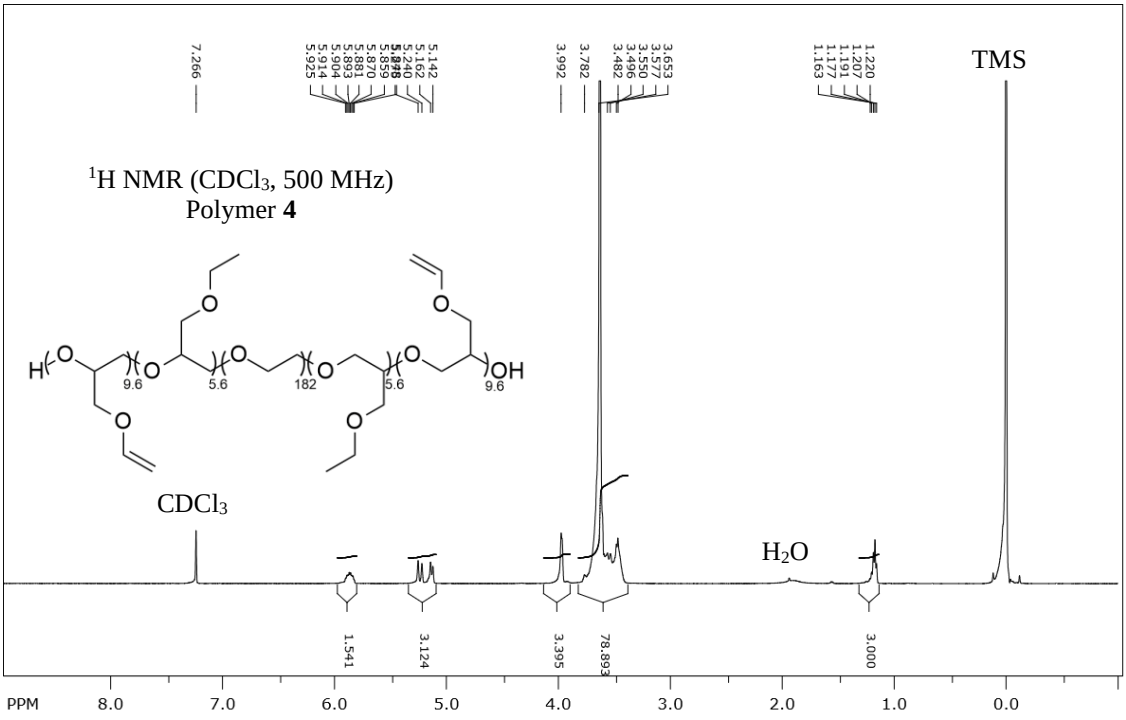

Figure A25. ^{1}H NMR of Polymer **4**

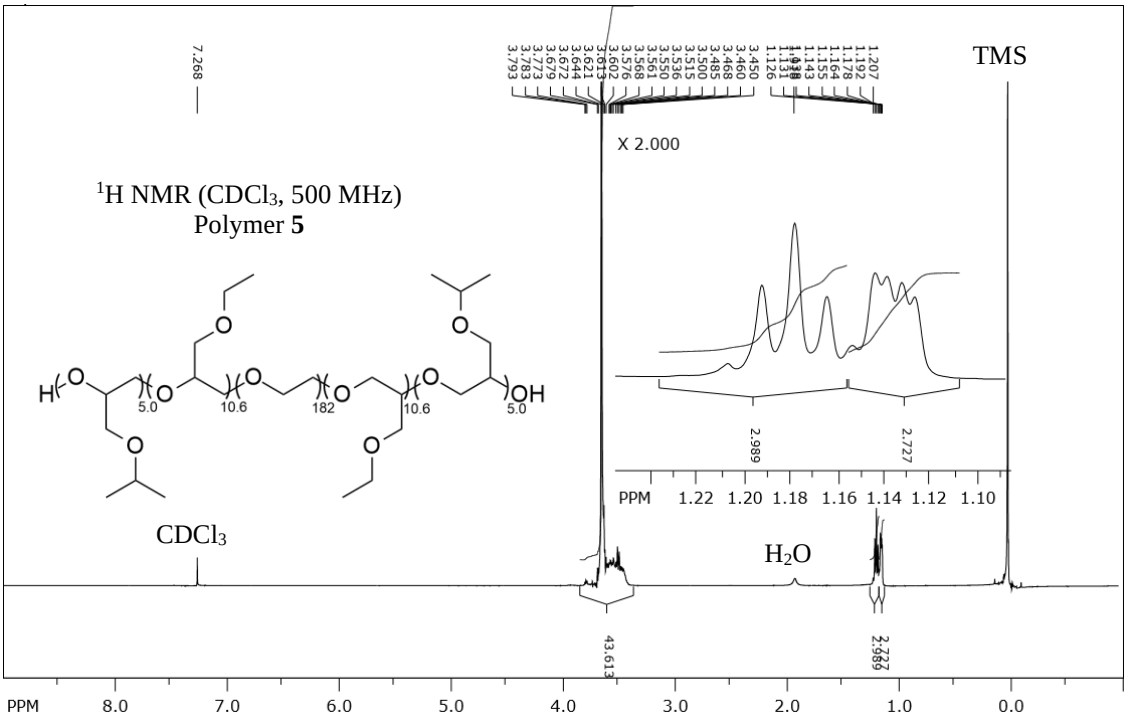

Figure A26. ^{1}H NMR of Polymer **5**

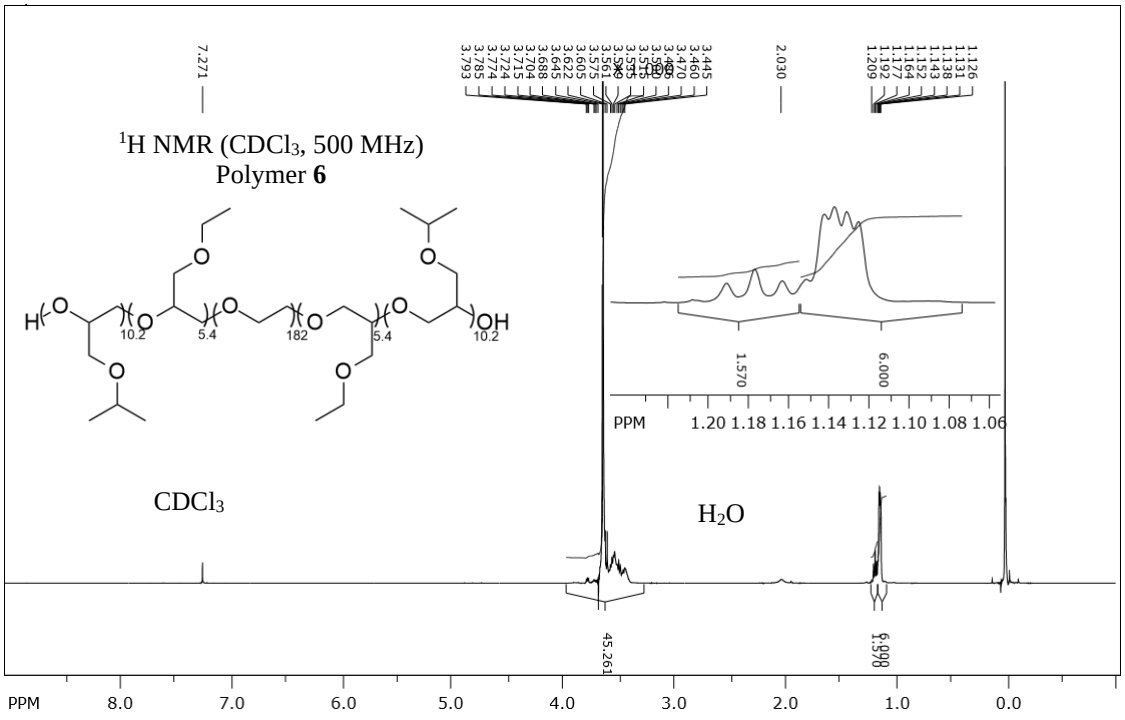

Figure A27. ^{1}H NMR of Polymer **6**

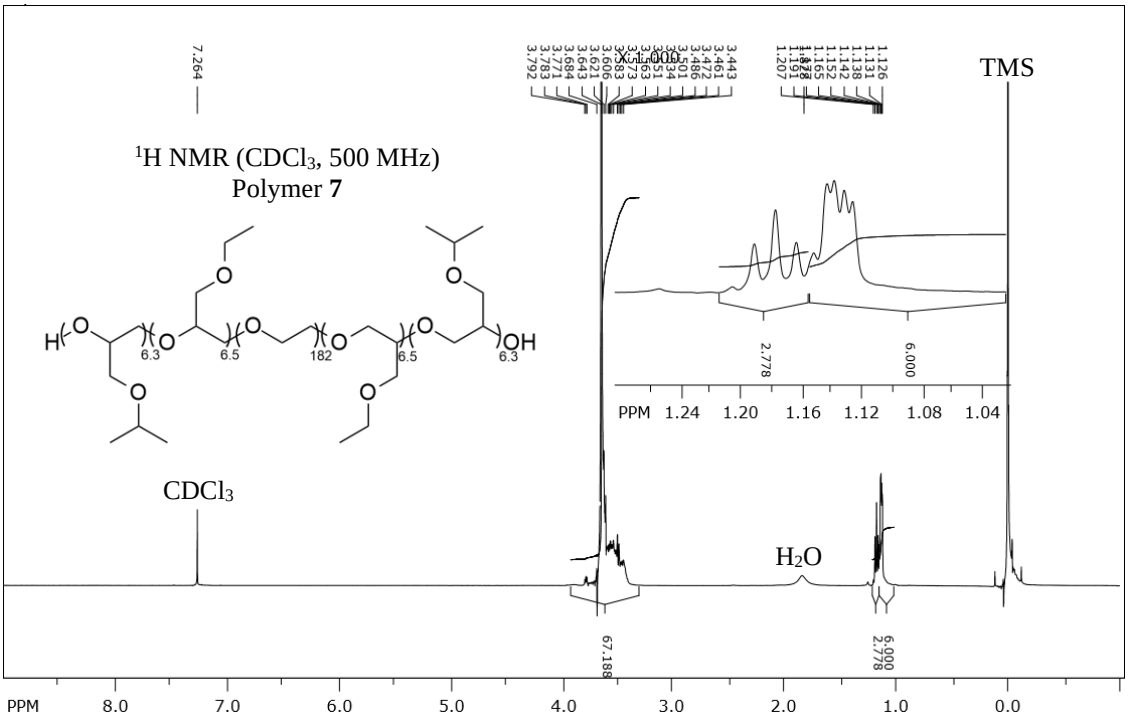

Figure A28. ^{1}H NMR of Polymer **7**

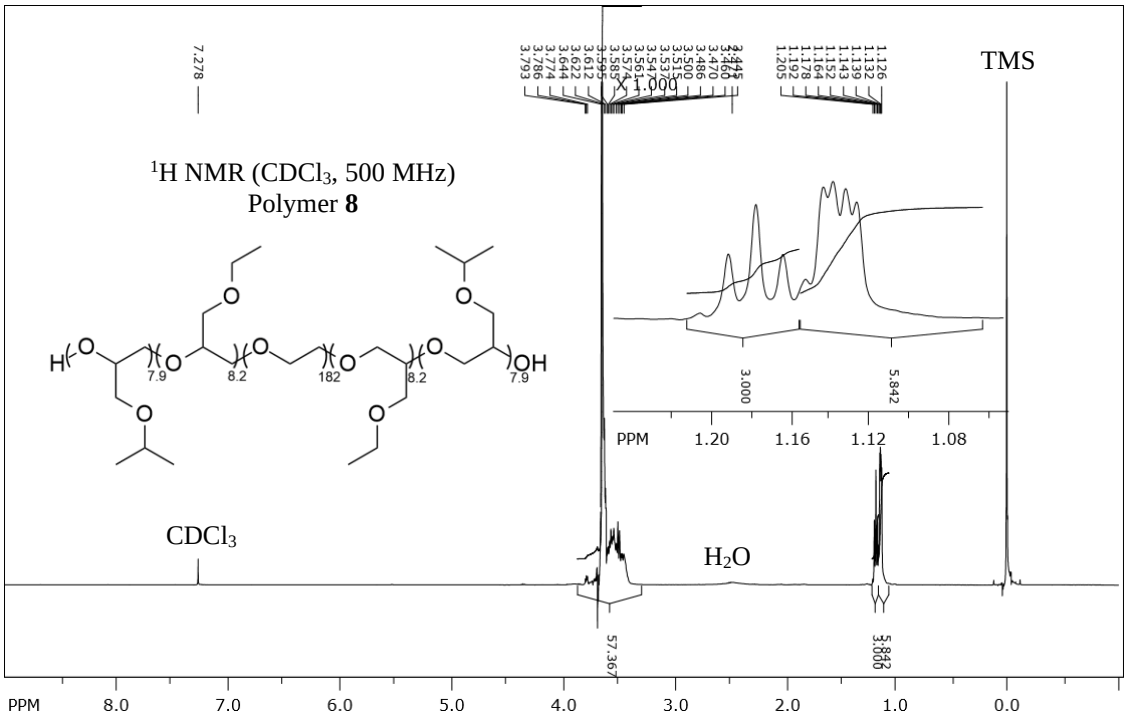

Figure A29. ^{1}H NMR of Polymer **8**

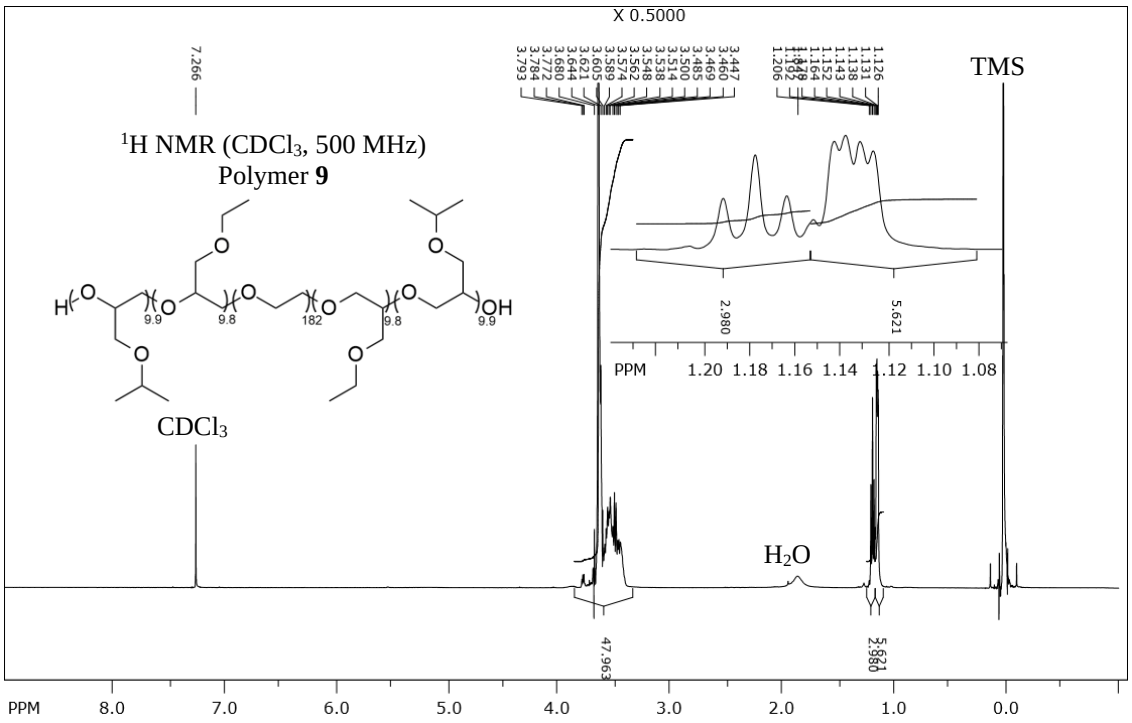

Figure A30. ^{1}H NMR of Polymer **9**

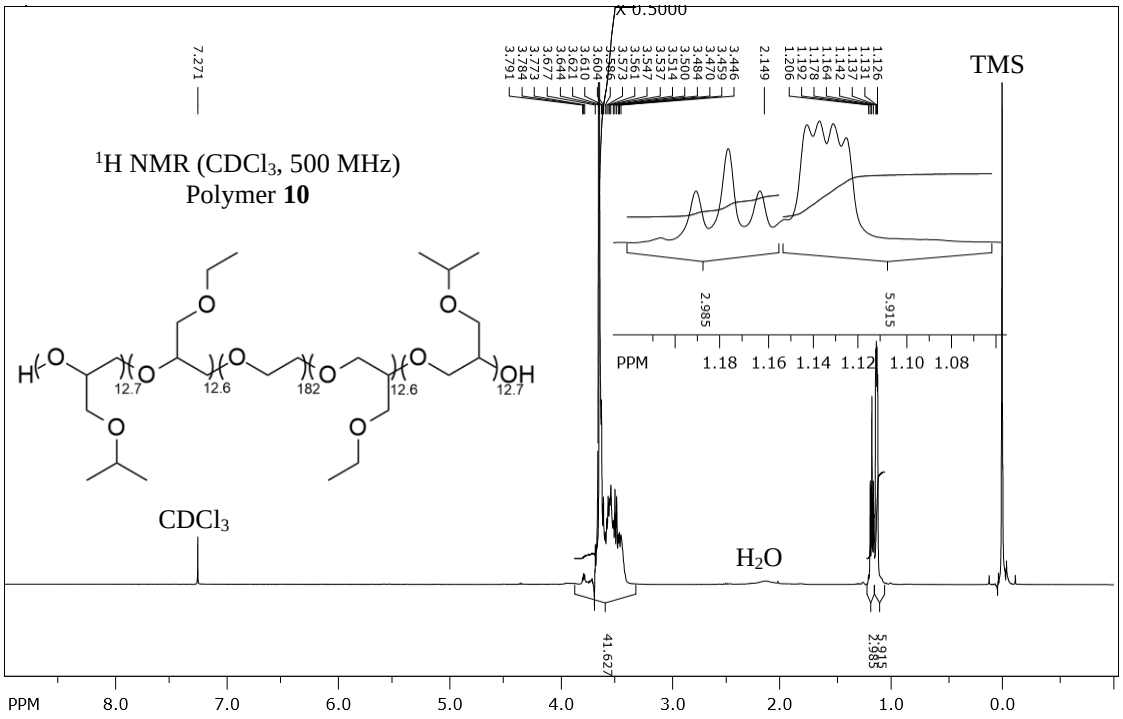

Figure A31. ^{1}H NMR of Polymer **10**

APPENDIX B

Poly(alkyl glycidyl ether) Hydrogels for Harnessing the Bioactivity of Engineered Microbes

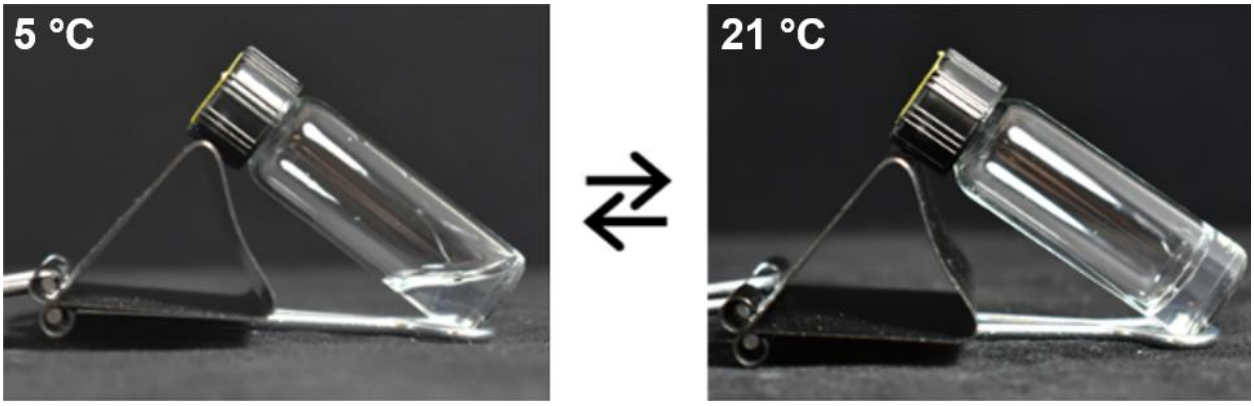

Figure B1. Graphical representation of the temperature induced sol-gel transition of polymer **2**.

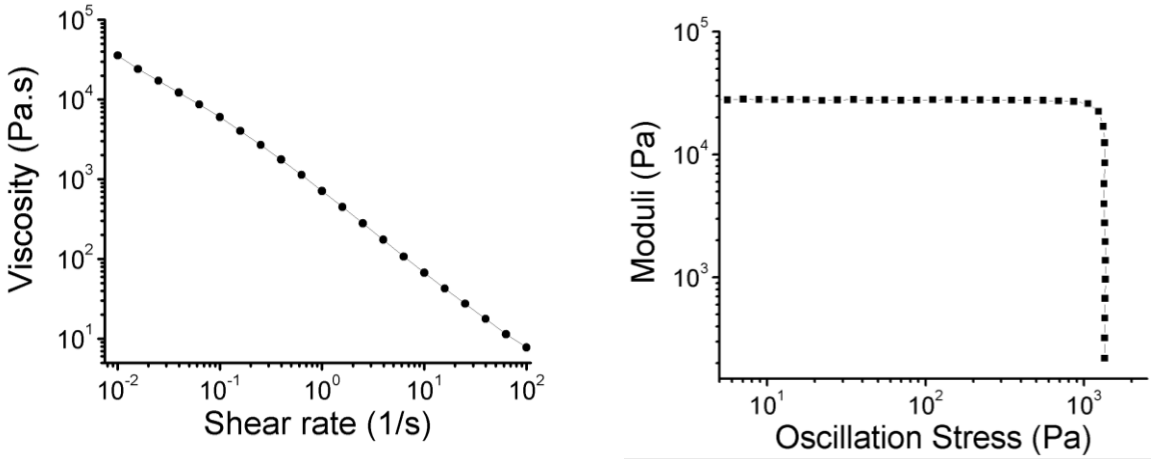

Figure B2-B3. Viscosity vs Shear Rate and Oscillatory Yield Stress experiments for a 20 wt % solution of Polymer 1

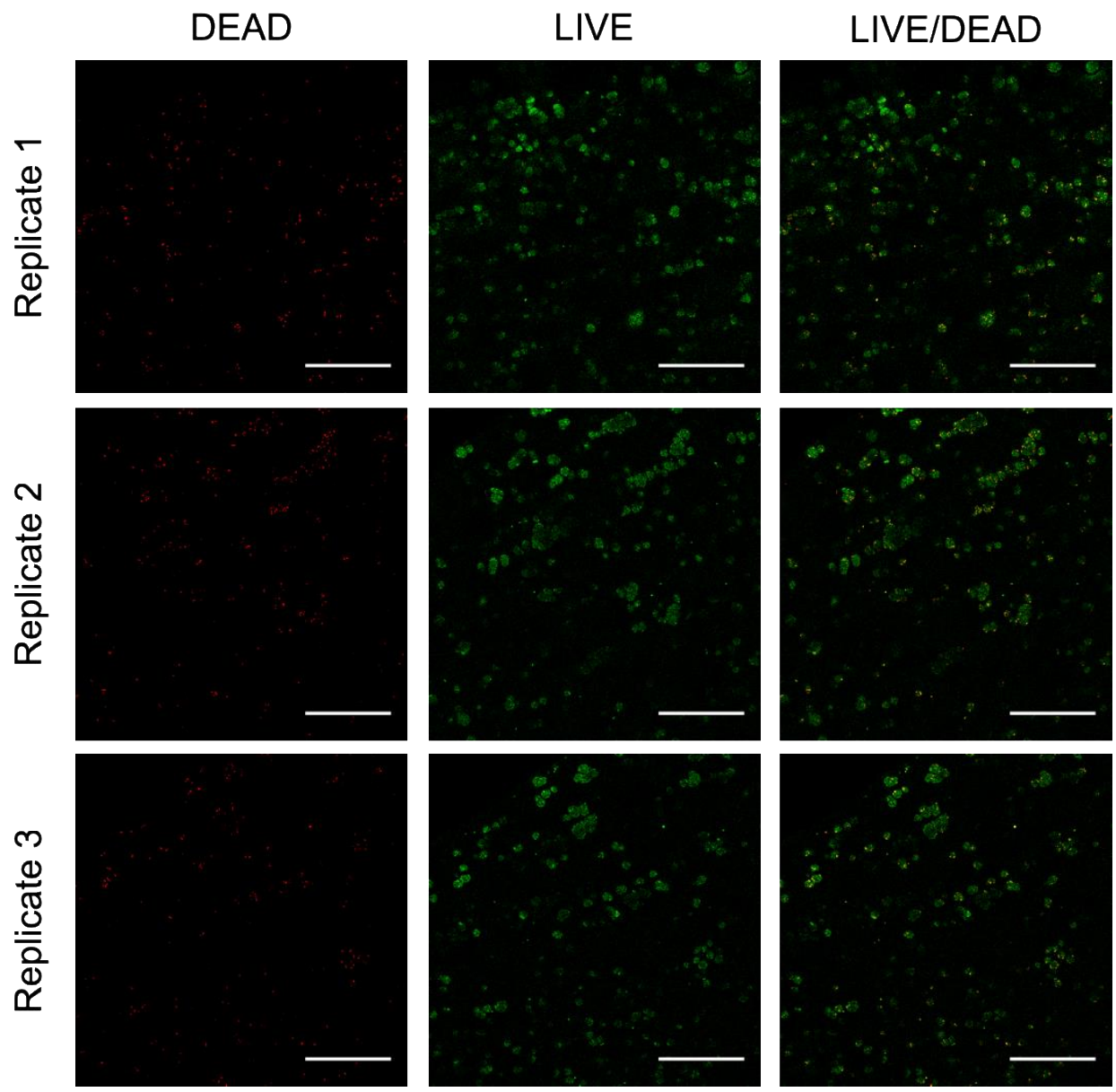

Figure B4. Confocal microscopy images of live/dead assay results at day 1 of incubation in SC media. The first column shows the dead cells (red channel), while the second column shows the live cells (green channel). The third column is an overlay of the live and dead cell channels.

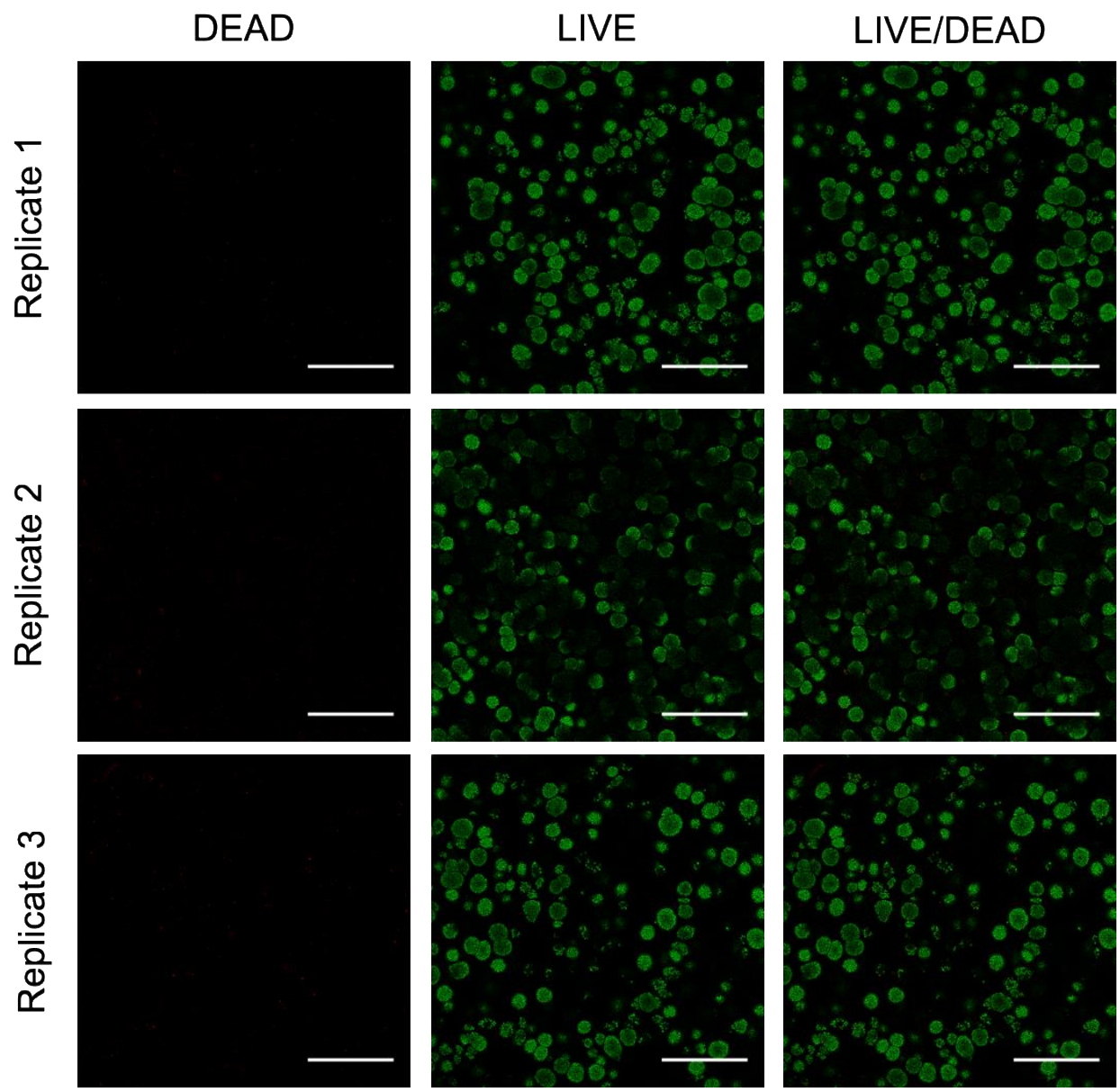

Figure B5. Confocal microscopy images of live/dead assay results at day 3 of incubation in SC media. The first column shows the dead cells (red channel), while the second column shows the live cells (green channel). The third column is an overlay of the live and dead cell channels.

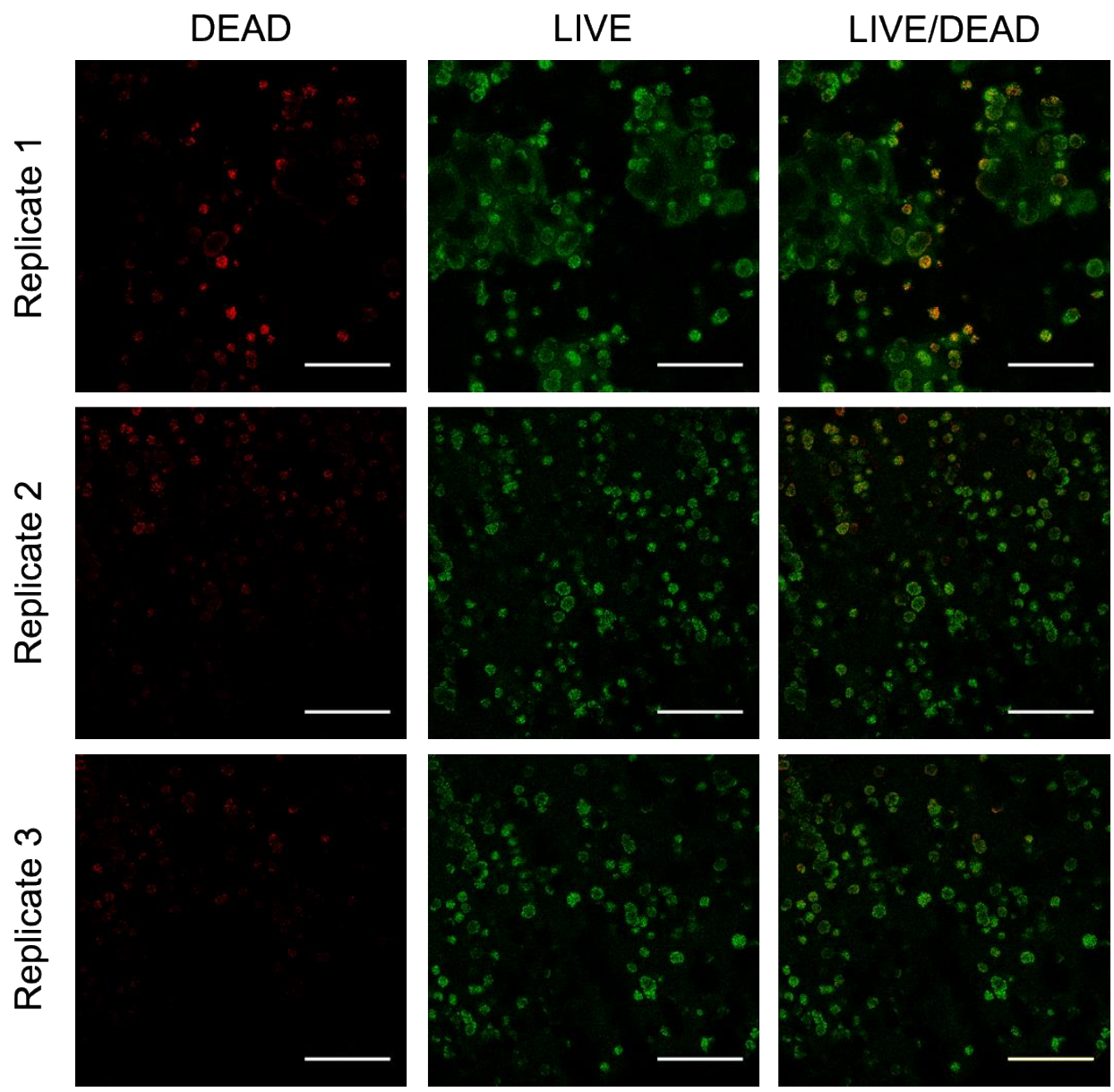

Figure B6. Confocal microscopy images of live/dead assay results at day 7 of incubation in SC media. The first column shows the dead cells (red channel), while the second column shows the live cells (green channel). The third column is an overlay of the live and dead cell channels.

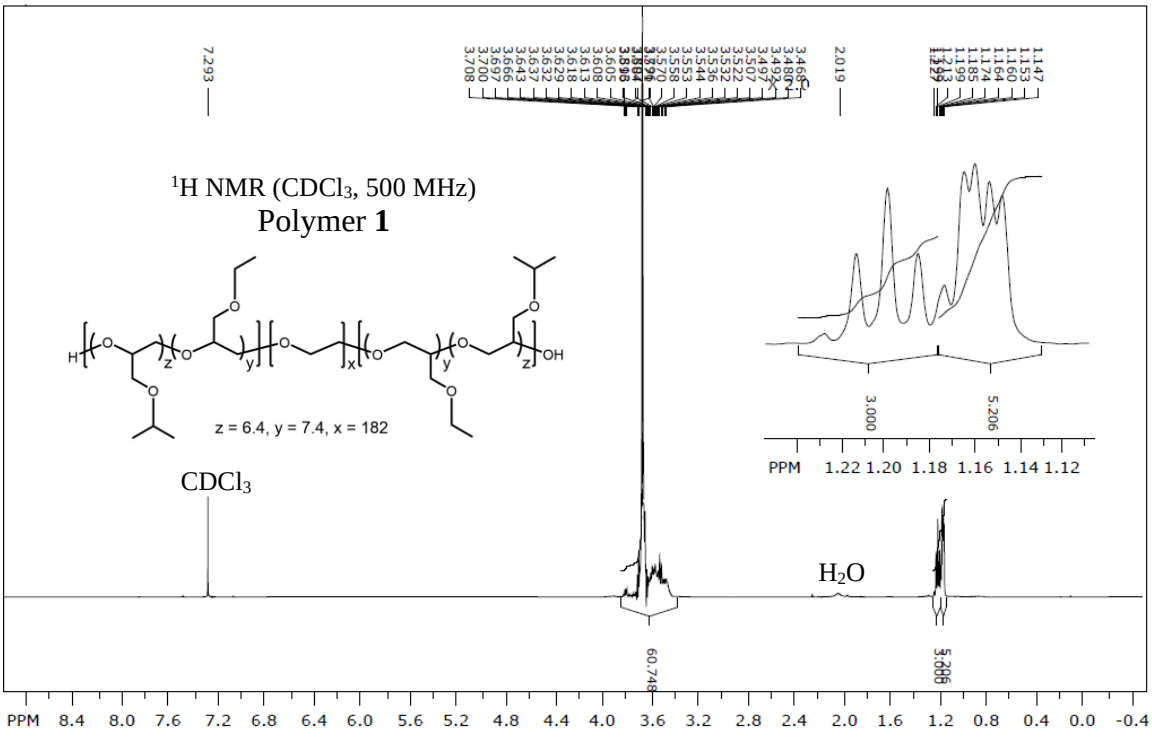

Figure A7. ^{1}H NMR of Polymer **1**

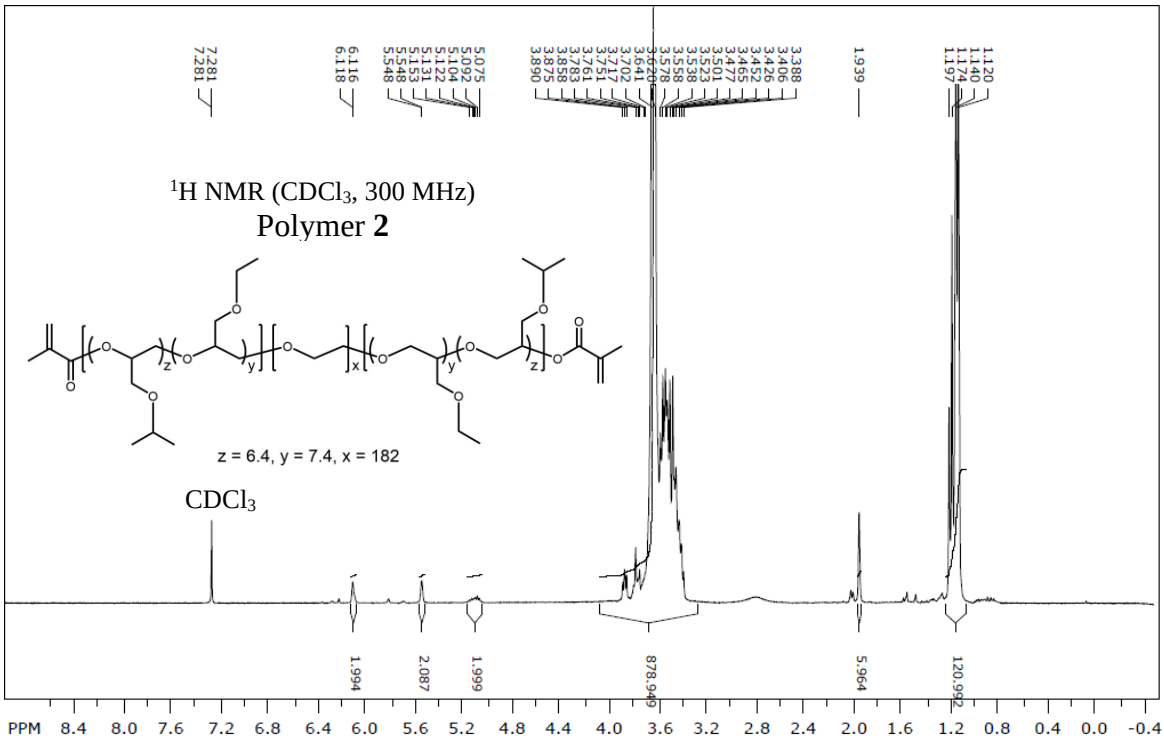

Figure B8. ^{1}H NMR of Polymer **2**

APPENDIX C

The Post-Functionalization of Multi-Stimuli-Responsive Hydrogels for Extrusion-Based Additive Manufacturing

Synthesis of PGE

The ABA triblock copolymer was synthesized via anionic ring-opening polymerization according to previous literature reports from our group. Briefly, PEO (Mn = 8,000 g mol-1, 10 g, 1.25 mmol) was added to the reaction vessel and dried under vacuum overnight. Dry THF (150 mL) was added under an Ar atmosphere and heated to 50 °C to facilitate dissolution of the macroinitiator. Once sufficiently dissolved, a potassium naphthalenide solution (1M in THF) was titrated into the flask until the solution remained a slight green color, indicating full deprotonation of PEO hydroxyl end groups. Isopropyl glycidyl ether (2.90 g, 25 mmol) and ethyl glycidyl ether (2.17 g, 21.25 mmol) were added to begin polymerization. The reaction continued for 24 h at 65 °C and was subsequently quenched with a degassed solution of 1% v/v AcOH in MeOH. The reaction mixture was then precipitated into cold hexane. The polymer was collected via centrifugation (4400 rpm, 10 min) and the supernatant decanted. The product was washed twice with additional hexane and collected again in the same manner. The isolated polymer solution was dried in a vacuum oven for at least 24 h to afford PGE as an off-white solid (14.14 g). 1H NMR (500 MHz, CDCl3): δ = 1.15-1.17 (m, -O-CH-(CH3)2), 1.17-1.23 (t, -O-CH2-CH3, J = 7.0 Hz), 3.47-3.81 (m -O-CH2-CH2-O- and -O-CH2-CH(CH2-O-CH2-CH3)-O- and -O-CH2-CH(CH2-O-CH-(CH3)2)-O-).

Synthesis of PGE-MA

PGE (7 g, 0.624 mmol) was dissolved in dry THF (50 mL) under a nitrogen atmosphere until complete dissolution of the polymer. Triethylamine (0.86 mL, 6.24 mmol) was added to increase the reactivity of the polymer hydroxyl chain ends and the mixture was heated at 65 °C for 30 min. Methacrylic anhydride (9.3 mL, 62.4 mmol) was then added and the reaction mixture was stirred for 24 h at 65 °C. After this time, the reaction was quenched with MeOH. The reaction mixture was then precipitated into cold ether. The polymer was collected via centrifugation (4400 rpm, 10 min) and the supernatant decanted. The product was dried in a vacuum oven for 24 h. The polymer was collected, redissolved in MeOH, and precipitated into ether once more. The isolated polymer was dried in a vacuum oven for 24 h to afford PGE-MA as an off-white solid (4.64 g). The degree of functionalization (fn) was determined by comparing the integrations of the methacrylate vinyl (6.12 and 5.55 ppm) and methyl (1.94 ppm) protons, as well as the PEO chain-end methylene protons (5.08-5.15 ppm), to their theoretical values. For example, 1.99 (vinyl, actual)/2 (vinyl, theoretical) X 100 ≈ 100% functionalization of chain ends. These integration values were referenced to the total alkyl glycidyl ether protons for each polymer chain (1.12-1.20 ppm, 121 H). 1H NMR (300 MHz, CDCl3): δ = 1.12-1.20 (m, -O-CH-(CH3)2) and -O-CH2-CH3), 1.94 (s, CH3C(CO2)=CH2), 3.39-3.89 (m, -O-CH2-CH2-O- and -O-CH2-CH(CH2-O-CH2-CH3)-O-, and -O-CH2-CH(CH2-O-CH-(CH3)2)-O-), 5.08-5.15 (m, -CH2-CH-O-(C=O)), 5.48 (s, H-CH=C), 6.18 (s, H-CH=C).

Rheological Measurements. Dynamic oscillatory rheological experiments were performed on a TA Instruments Discovery HR-2 rheometer equipped with a 20 mm parallel-plate geometry unless otherwise specified. Samples were equilibrated in an ice bath for at least 10 min, then carefully loaded onto the Peltier plate at 5 °C. A pre-shear experiment was applied to ensure bubbles were eliminated from the sample cell. The sample was equilibrated at 21 °C for 8 min. Strain sweep

experiments were performed, and all studies were conducted using a strain value in the linear viscoelastic regime. Temperature ramp experiments were performed at 1 Hz from 5 to 50 °C at 2 °C min^{-1}. Cyclic strain tests (frequency 1 Hz) were performed at 21 °C using alternating strains of 1% for 5 minutes and 100% for 3 minutes per cycle. Viscosity versus shear rate experiments were performed at 21 °C. The gel yield stress values were measured under oscillatory strain (frequency: 1 Hz, 21 °C) starting with an initial strain of 0.01% and converted to applied oscillatory stress.

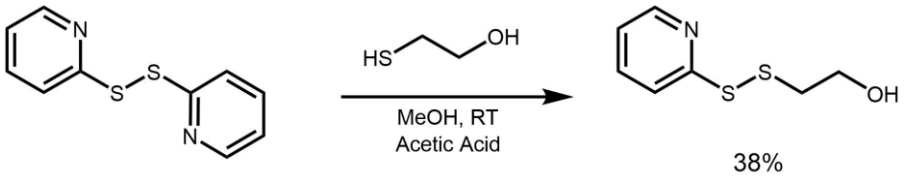

Scheme C1. Synthesis of hydroxyethyl pyridyl disulfide (HEPDS)

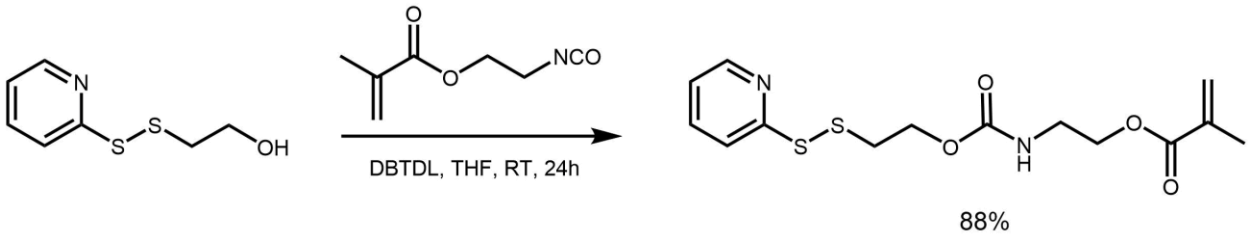

Scheme C2. Synthesis of pyridyl disulfide urethane methacrylate (PDS-UM)

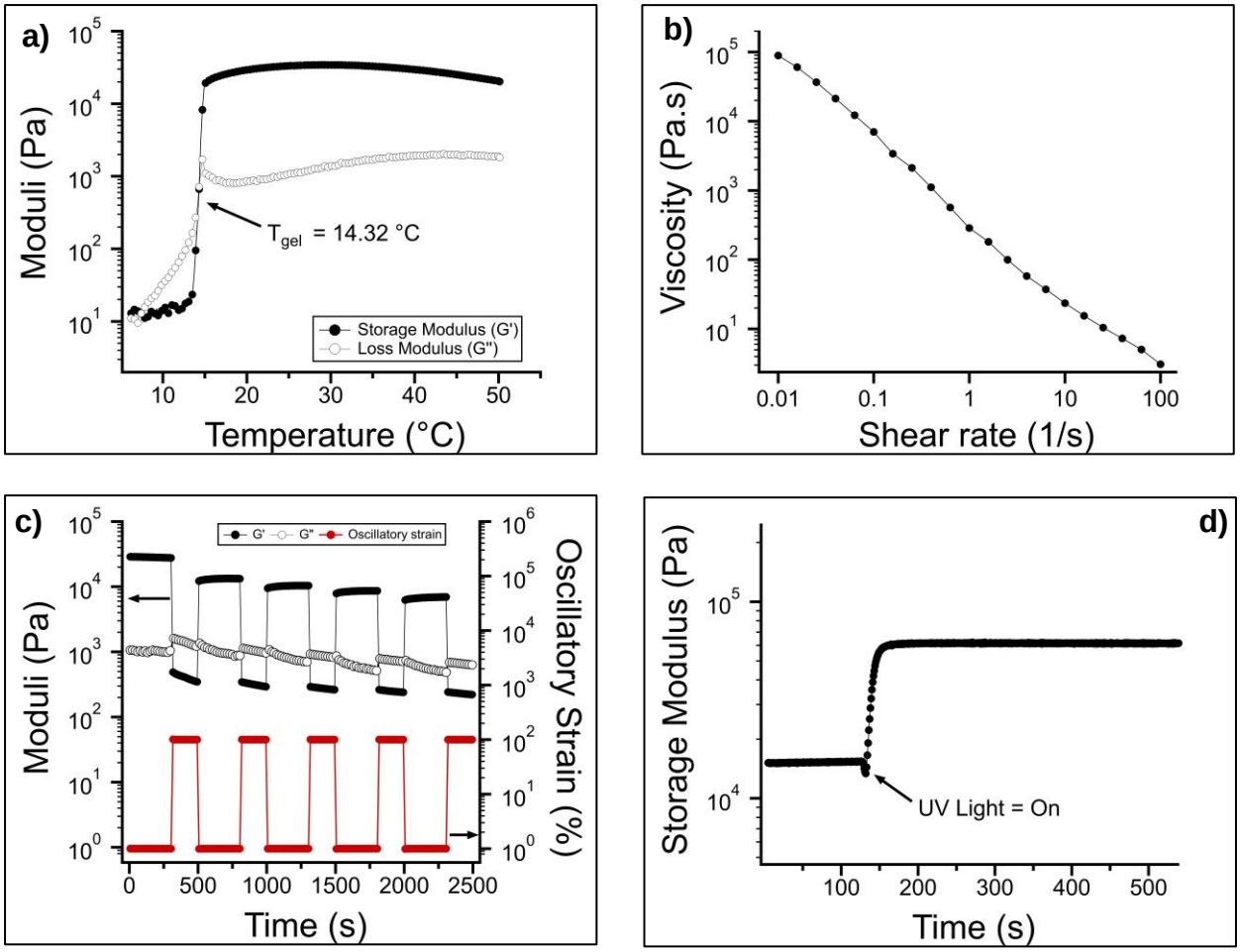

Figure C1. Rheological characterization of PGE-MA/PDS-UM hydrogels. (a) Dynamic oscillatory temperature ramp displaying storage (G', filled) and loss (G'', open) moduli. (b) Viscosity vs shear rate experiment depicting shear-thinning behavior (c) Cyclic strain experiment demonstrating rapid recovery of hydrogel storage modulus (black circles) from periods of high (100%) to low (1%) oscillatory strain (red circles). (d) Dynamic oscillatory UV-Cure experiment demonstrating photochemical crosslinking upon exposure to 365 nm UV light.

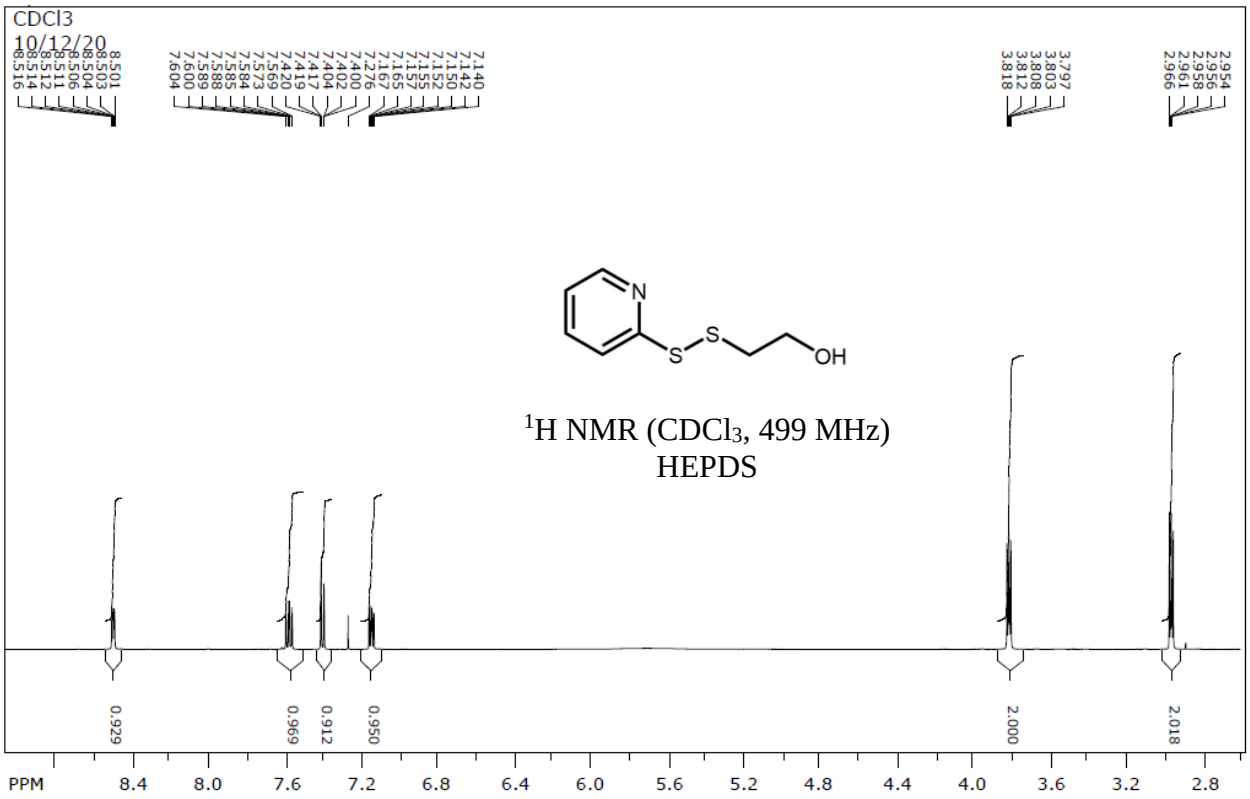

Figure C2. ^{1}H NMR of HEPDS ($CDCl_3$,499 MHz)

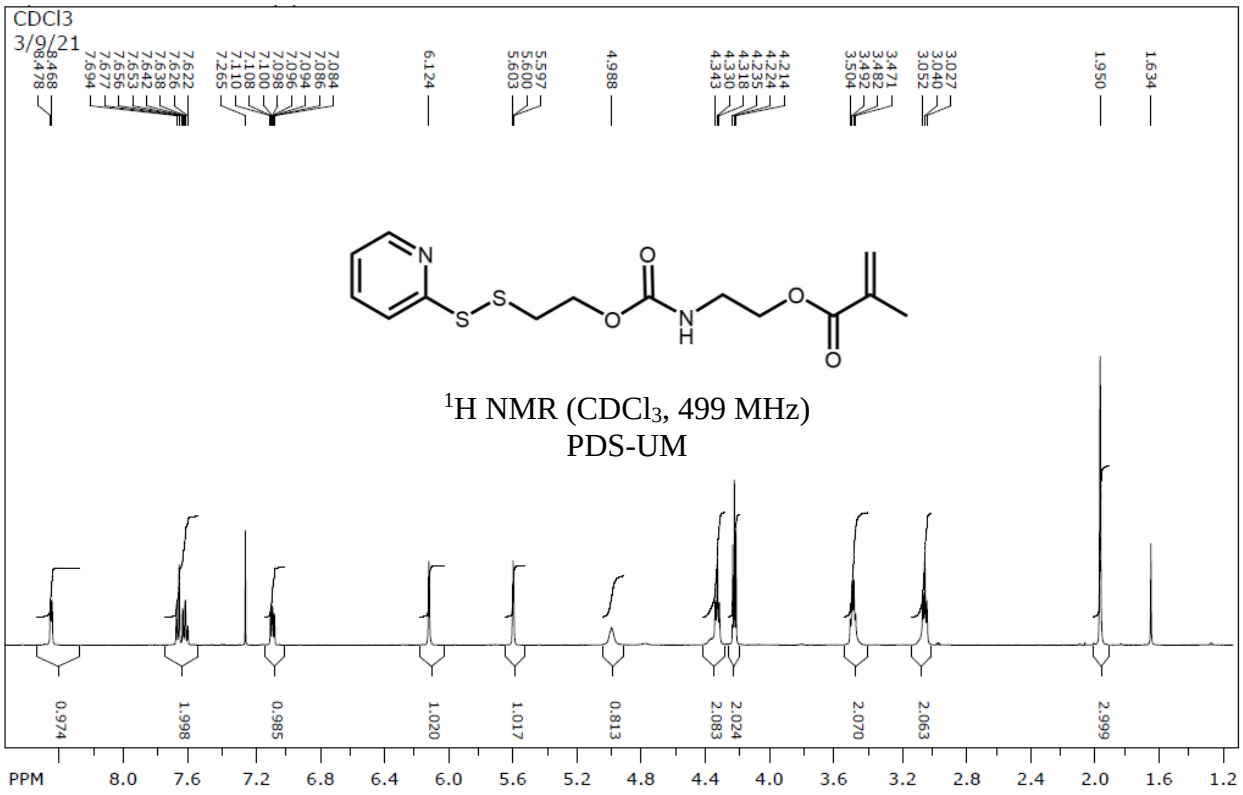

Figure C3. ^{1}H NMR of PDS-UM ($CDCl_3$,499 MHz)